



Title	Structural Health Monitoring by Vibration Measurement with Non-contact Laser Excitation
Author(s)	Huda, Feblil
Citation	北海道大学. 博士(工学) 甲第11568号
Issue Date	2014-09-25
DOI	10.14943/doctoral.k11568
Doc URL	http://hdl.handle.net/2115/57206
Type	theses (doctoral)
File Information	Feblil_Huda.pdf



[Instructions for use](#)

**STRUCTURAL HEALTH MONITORING
BY VIBRATION MEASUREMENT WITH
NON-CONTACT LASER EXCITATION**

DOCTORAL DISSERTATION

FEBLIL HUDA

DIVISION OF HUMAN MECHANICAL SYSTEM AND DESIGN

GRADUATE SCHOOL OF ENGINEERING

HOKKAIDO UNIVERSITY

SEPTEMBER, 2014

**Structural Health Monitoring by Vibration
Measurement with Non-contact Laser Excitation**

FEBLIL HUDA

A Dissertation submitted to
the Division of Human Mechanical System and Design of
the Graduate School of Engineering of

Hokkaido University

In partial fulfillment of the requirements for the degree of

Doctor of Engineering

Sapporo, September 2014

Supervisor:

Professor

Itsuro KAJIWARA

Acknowledgement

First and Foremost, I would like to express my deep gratitude to my supervisor Prof. Itsuro Kajiwara for his support, encouragement, and guidance during my study in Hokkaido University.

Secondly, I would like to thank to Prof. Yukinori Kobayashi, Prof. Shigeru Tadano, and Prof. Takeshi Nakamura for reviewing my works and giving their suggestions for this dissertation improvement in the dissertation defense on Wednesday, 23rd July, 2014. I also would like to thank to The Directorate General of Higher Education, Ministry of Education and Culture of the Republic of Indonesia (DIKTI) for all the financial support, and to staffs in Faculty of Engineering and English Engineering Education (e3) program of Hokkaido University for helping me in many things about administrative matter.

I am so happy to express my sincere gratitude to Associate Prof. Hiroyuki Harada, Associate professor in smart mechanism Laboratory, Ms. Yamaguchi, laboratory secretary, and all lab members for being good friends, and for helping me in daily activities in laboratory of smart mechanism. Moreover, I would like to express my deep appreciation to all Indonesian friends for giving support, help and happiness in my daily life.

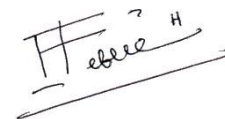
I would like to express my special thanks to my beloved wife Siska for her patience, loves, and supports and for her sacrifices to take care our children during my study. To my children, Fathiyyah and Fathurrahman for their smiles that always make me keep in spirit to complete my study in Hokkaido University. Thank you for all their love.

And finally, I would like to dedicate in humble gratitude to my Mama and Papa who have been giving us loves, making great sacrifice for the sake of their children education. May Allah, The Almighty, always bless them in every second of their lives.

Claims of Originality

This doctoral dissertation contains no material which has been accepted for the award of any degree or diploma in any University. Base on the author's knowledge and belief, it contains no material previously published or written by another person, except where due reference is made in the text.

Signature: *Febil Huda*

A handwritten signature in black ink, consisting of a stylized 'F' followed by 'e', 'b', 'e', 'e', and 'H'. The signature is written on a horizontal line that extends to the right.

September 2014

Abstract

Damage identification as a part of structural health monitoring plays a significant role to ensure the current condition of structures. In general, there are two main steps constituting a diagnostic procedure in damage identification: the experimental measurement and the data processing. It is evident that, for each measurement technique, a dedicated signal processing strategy should be designed and employed. In this dissertation author proposes new damage identification in structural health monitoring using non-contact laser excitation vibration test in the title “Structural health monitoring by vibration measurement with non-contact laser excitation”.

This dissertation consists of five chapters. The first chapter “Introduction” presents the background, motivation, and objectives of this research. In the second chapter “Laser excitation” author intends to find appropriate non-contact excitation method for damage identification as the basic idea of research in this dissertation. For this purposes, two methods of laser excitation that proposed by some researchers are explored to investigate the reliability of these methods to be combined in structural health monitoring. Two methods of laser excitation are laser ablation and laser-induced breakdown. Excitation by laser ablation to metal structure occurs when laser beam focused and directed to metal and then absorbed by metal generates high-temperature plasma, and large quantities of particles are then released (in the form of a plume) from the metal. Releasing the particle at a velocity from the metal represents the laser induced impulse. Excitation by laser-induced breakdown (LIB) occurs when laser beam focused, plasma is then generated, and a portion of this plasma energy is transformed to a shock wave, which is the source of the sound generated by LIB. This sound can be used as a source of acoustic excitation. Based on the review, author find that these two laser excitation method are eligible to be applied and combined in structural health monitoring. Excitation by laser ablation generates ideal impulse force on metal structure, has high reproducibility, works well in high and low frequencies measurement, so it is applicable to structural health monitoring on metal structure, like detecting bolt loosening in bolted structure. Acoustic excitation by LIB generates ideal point source of sound for ideal acoustic excitation, totally non-contact method, has high reproducibility, so it is suitable for structural health monitoring in light and flexible structure, like membrane.

In the third chapter, a vibration testing and health monitoring system based on an impulse response excited by laser ablation to detect bolted joint loosening is presented. A high power Nd: YAG pulse laser is used to generate an ideal impulse on a structural surface which offers the potential to measure high frequency vibration responses on the structure. A health monitoring apparatus is developed with this vibration testing system and a damage detecting algorithm. The joint loosening can be estimated by detecting fluctuations of the high frequency response with the health monitoring system. Additionally, a finite element model of bolted joints is proposed by using three-dimensional elements with a pretension force applied and with contact between components taken into account to support the bolt loosening detection method. Frequency responses obtained from the finite element analysis and the experiments using the laser excitation, are in good agreement. The bolt loosening can be detected and identified by introducing a damage index by statistical evaluations of the frequency response data using the Recognition-Taguchi method. The effectiveness of the present approach is verified by simulations and experimental results, which are able to detect and identify loose bolt positions in a six-bolt joint cantilever.

In the fourth chapter, a vibration testing and health monitoring system based on an impulse response excited by laser to detect damage in membrane structures is presented. A high power Nd: YAG pulse laser is used to supply an ideal impulse to a membrane structure by generating shock waves via LIB in air. A health monitoring apparatus is developed with this vibration testing system and a damage detecting algorithm which only requires the vibration mode shape of the damaged membrane. Artificial damage is induced in membrane structure by cutting and tearing the membrane. The vibration mode shapes of the membrane structure extracted from vibration testing by using the LIB and laser Doppler vibrometer are then analyzed by 2-D continuous wavelet transformation. The location of damage is determined by the dominant peak of the wavelet coefficient which can be seen clearly by applying a boundary treatment and the concept of an iso-surface to the 2-D wavelet coefficient. The applicability of the present approach is verified by finite element analysis and experimental results, demonstrating the ability of the method to detect and identify the positions of damage induced on the membrane structure.

Finally, in the last part, the fifth chapter presents the conclusion of the overall research that has been conducted and some suggestion to further research.

List of Figures

Fig. 2.1	Process of the laser ablation [14]	11
Fig. 2.2	Experimental set-up of vibration test using pulsed high power laser [14] (a) general set-up of system, (b) attachment of load cell and accelerometer	12
Fig. 2.3	Auto-FRF H_{11} by laser excitation and impulse hammer [14]	13
Fig. 2.4	Auto-FRF H_{22} by laser excitation and impulse hammer [14]	14
Fig. 2.5	Cross-FRF H_{31} by laser excitation and impulse hammer [14]	14
Fig. 2.6	Input characteristics of laser excitation and impulse hammer [14]	15
Fig. 2.7	Different characteristics between laser excitation and impulse hammer [14]	15
Fig. 2.8	Process to achieve acoustic excitation by LIB	18
Fig. 2.9	Time responses of sound pressure generated by LIB [17]	19
Fig. 2.10	Galilean laser beam expander [17]	20
Fig. 2.11	Layout of microphone in the anechoic box for directional test (overhead view) [17]	21
Fig. 2.12	Measured power spectra at each point [17]	22
Fig. 2.13	Star plot of the sound pressure levels and measurement positions in each frequency [17]	22
Fig. 3.1	Vibration testing arrangement using the high power pulse laser	28
Fig. 3.2	One-bolt joint model	29
Fig. 3.3	Procedure to determine the benchmark for bonded area	32
Fig. 3.4	Stress distribution between flanges in contact for determining bonded contact condition	33
Fig. 3.5	Six-bolt joint model	34

Fig. 3.6	Excitation and measurement points for verification of the model (a) vertical of the one-bolt joint, (b) horizontal of the one-bolt joint, (c) vertical of the six-bolt joint	35
Fig. 3.7	Frequency response of the one-bolt joint in the normal condition (a) in the vertical direction, (b) in the horizontal direction	36
Fig. 3.8	Frequency response of the one-bolt joint in the vertical direction with the loose condition of tightening torques (a) 20 Nm, (b) 18 Nm, (c) 15 Nm, (d) 10 Nm	37
Fig. 3.9	Frequency response of the one-bolt joint in the horizontal direction with the loose condition of tightening torques (a) 20 Nm, (b) 18 Nm, (c) 15 Nm, (d) 10 Nm	38
Fig. 3.10	Frequency response of the one-bolt joint by the experiments (a) in the vertical direction, (b) in the horizontal direction	39
Fig. 3.11	Principal vibration mode shapes of the one-bolt joint model in the normal condition	39
Fig. 3.12	Frequency response of the six-bolt joint in the normal condition	40
Fig. 3.13	Frequency response of the six-bolt joint in loose condition based on damage cases in Table 2 (a) damage 1, (b) damage 5	41
Fig. 3.14	Frequency responses of the six-bolt joint by the experiments	41
Fig. 3.15	Excitation and measurement point positions used in bolt loosening detection	46
Fig. 4.1	Acoustic excitation of a membrane structure by LIB	53
Fig. 4.2	Vibration testing apparatus and arrangement for the membrane structure	53
Fig. 4.3	Finite element model of the membrane structure (with forces and meshing elements)	58
Fig. 4.4	Simulation results of the normal membrane vibration (a) first principal mode shape (41.8 Hz), (b) interpolated first principal mode shape, (c) wavelet coefficient, (d) wavelet coefficient with boundary treatments	60
Fig. 4.5	Finite element model of membrane with damage scenarios detailed in Table 4.1	61

Fig. 4.6	Simulation results for detecting the L-cut damage (A in Table 4.1) on the membrane (a) first principal mode shape (41.78 Hz), (b) interpolated first principal mode shape, (c) wavelet coefficient, (d) wavelet coefficient with boundary treatment, (e) 3-D view of iso-surface, (f) top view of iso-surface	63
Fig. 4.7	Iso-surface view of the detected L-tear damage (B in Table 4.1) on the membrane by simulation data (a) 3-D view of iso-surface, (b) top view of iso-surface	64
Fig. 4.8	Simulation results of first principal mode shape for detecting the I-cut damage (C in Table 4.1) on the membrane (a) first principal mode shape (41.79 Hz), (b) wavelet coefficient with boundary treatment	65
Fig. 4.9	Simulation results of higher order mode shape for detecting the I-cut damage (C in Table 4.1) on the membrane (a) mode shape (851 Hz), (b) wavelet coefficient with boundary treatment, (c) 3-D view of iso-surface, (d) top view of iso-surface	66
Fig. 4.10	Frequency response of the membrane in the normal condition at centre of membrane	67
Fig. 4.11	Experimental results for detecting the L-cut damage (A in Table 4.1) on the membrane (a) first principal mode shape (40.63 Hz), (b) interpolated first principal mode shape, (c) wavelet coefficient, (d) wavelet coefficient with boundary treatment, (e) 3-D view of iso-surface, (f) top view of iso-surface	68
Fig. 4.12	Iso-surface view of the detected L-tear damage (B in Table 4.1) on the membrane by experimental data (a) 3-D view of iso-surface, (b) top view of iso-surface	69
Fig. 4.13	Experimental results of higher order mode shape for detecting the I-cut damage (C in Table 4.1) on the membrane (a) mode shape (843.8 Hz), (b) wavelet coefficient with boundary treatment, (c) 3-D view of iso-surface, (d) top view of iso-surface	70
Fig. 4.14	Membrane with I-cut and square-hole damage	71

Fig. 4.15	Experimental results for detecting I-cut and square-hole damage on the membrane (a) mode shape (799.1 Hz), (b) wavelet coefficient with boundary treatment, (c) 3-D view of iso-surface, (d) top view of iso-surface	72
Fig. 4.16	Frequency response of membrane without induced damage and condition with damage in two places	73
Fig. 4.17	Plots of the two mode shapes (a) mode shape w/o induced damage (801.6 Hz), (b) mode shape with damage in two places (799.1 Hz)	74
Fig. A.1	Membrane structure L-cut damage	86
Fig. A.2	First principal mode shape of membrane (a) basic mode shape, (b) interpolated mode shape	87
Fig. A.3	Wavelet coefficient by Mexican hat	87
Fig. A.4	Wavelet coefficient by Pet hat	87
Fig. A.5	Wavelet coefficient by DOG	88
Fig. A.6	Wavelet coefficient by Dergauss	88
Fig. A.7	L-cut damage detection by DerGauss wavelet (a) damage position, (b) 3-D iso-surface view, (c) 2-D iso-surface view	89
Fig. A.8	Rectangle damage detection by DerGauss wavelet (a) damage position, (b) 3-D iso-surface view, (c) 2-D iso-surface view	90

List of Tables

Table 2.1	Configurations of the three convex lenses used to focus the laser beam [17]	19
Table 3.1	Relationship between tightening torques and pretension forces	31
Table 3.2	List of torques applied in damage cases for the six-bolt joint model	35
Table 3.3	Variables of members in a unit space	43
Table 3.4	η and β of the members in a unit space	44
Table 3.5	Y of the members in a unit space	44
Table 3.6	Damage index based on simulation	48
Table 3.7	Damage index based on experiments	48
Table 4.1	Details of the damage induced on the membrane	61

Contents

Acknowledgement	ii
Claim of originality	iii
Abstract	iv
List of figures	vi
List of tables	x
1 Introduction	1
1.1 Background and motivation	1
1.2 Objectives and outline	5
2 Laser excitation	8
2.1 Introduction	8
2.2 Laser ablation	10
2.2.1 Proseses of laser ablation	10
2.2.2 Vibration test by laser ablation	11
2.3 Laser-induced breakdown	17
2.3.1 Proseses of laser-induced breakdown	17
2.3.2 Acoustic excitation system using LIB	18
2.4 Non-contact laser excitation and damage identification	23
2.5 Concluding remarks	23
3 Bolt loosening analysis and diagnosis by non-contact laser excitation vibration test.	25
3.1 Introduction	25
3.2 Vibration test system using laser ablation	27
3.2.1 Pulse laser	27
3.2.2 Measurement and analysis of output	28
3.3 Finite element analysis of bolted joint	28
3.3.1 Model description	29
3.3.2 Determining contact condition between flanges	30
3.3.3 Frequency response analysis	32
3.3.4 Finite element model of generalize complex bolted joint	33
3.4 Validation of laser excitation vibration measurements by the finite element model	35
3.4.1 Frequency response on the one-bolt joint model	36
3.4.2 Frequency response on the six-bolt joint model	40

3.5 Bolt loosening detection approach	42
3.5.1 Recognition-Taguchi method	42
3.5.2 The location of excitation and measurement points	46
3.6 Diagnosis results	47
3.6.1 Diagnosis process	47
3.6.2 Results and discussion	48
3.7 Concluding remarks	49
4 Damage Detection in Membrane Structures Using Non-contact Laser	
Excitation and Wavelet Transformation	50
4.1 Introduction	50
4.2 Vibration testing system using LIB	52
4.2.1 Acoustic excitation by LIB	52
4.2.2 Measurement and analysis of the output	53
4.2.3 Membrane structure setup	54
4.2.4 Mode shape estimation	54
4.3 2-D CWT for damage detection in membrane structure	55
4.3.1 2-D CWT derivative Gauss	55
4.3.2 The procedure for damage detection on the membrane	57
4.4 FEA investigation of damage detection on the membrane structure	58
4.4.1 Model description	58
4.4.2 Analysis of the normal condition by simulation	59
4.4.3 Application of damage detection	61
4.5 Damage detection in membrane structure by experiment	66
4.5.1 Damage detection for single damage on membrane	66
4.5.2 Damage detection for two damages on membrane	71
4.6 Concluding remarks	74
5 Conclusions and future work	76
5.1 Conclusions	76
5.2 Future works	78
List of publications	79
Bibliography	80
Appendix	84

Chapter 1

Introduction

1.1 Background and motivation

The process of implementing a damage identification strategy for mechanical engineering infrastructure, aerospace, and civil structures is referred to as structural health monitoring [1]. Because of the large impact that safety and reliability has on many fields, especially on mechanical engineering infrastructure, structural health monitoring (SHM) has become one of the most important subjects in mechanical engineering to ensure that the structures are safe and reliable to be operated.

In the SHM, in order to know the condition of structure, the process involves the observation of a structure or mechanical system using periodically spaced measurements, the extraction of damage-sensitive features from these measurements and the statistical analysis of these features to determine the current state of system health and safety. For long-term SHM, the output of this process is periodically updated to obtain the information about structure's ability to continue performing its proper function in the inevitable aging and the damage accumulation resulting from the operational environments. Under an extreme event, such as an earthquake or unanticipated blast loading, SHM is used for rapid condition screening. This screening is intended to provide reliable information about system performance during such extreme events and the subsequent integrity of the system [1].

Damage identification as a part of SHM plays an important role to make sure the current condition of structures. In general, there are two main steps of diagnostic procedure in damage identification: the experimental measurement and the data processing. The selection of measurement method has raised some issues in damage detection research area which have been widely investigated in recent years. Several of the issues are the requirements that an experimental technique must satisfy: it must be non-destructive, easy to be used, rapid enough for monitoring and with clear and of accessible interpretation.

Various non-destructive test (NDT) methods have been applied for damage detection. As the examples, like on fatigue crack detection methods, these include ultrasonic test [2,3], radiographic techniques [4], acoustic emission techniques, magnetic flux leakage inspection methods, eddy current methods [5], penetrant methods and thermography-based methods [6,7]. In particular, the methods are feasible, but depending on the specific response parameters and methods used for sensing, the methods may require many sensors be directly installed and contacted to the surface of the objective structure, sometimes using magnetic base stand. Such installation can cause changes in the electromagnetic fields within targeted materials, can contaminate tested structure, and this condition may influence and skew the measurement results.

The diagnostic methods largely studied and applied are those based on vibration measurements, since they allow non-destructive evaluation on investigated structures. Some problems and inconvenient are also found in these methods, that usually involving part directly mounted and contacted to the surface of tested parts for applying excitation force, can possibly contaminate tested structure and add safety constraints such as the need for additional inspection, endanger measurement operators if the measurements last on narrow operational area and even do not give the possibility of conducting the measurement in narrow area. These conditions make non-contact method become important.

The usual approach in damage detection based on vibration measurement consists in the determination of dynamic characteristics changes due to the presence of the

damage. The dynamic characteristics of a structure can be assessed from the frequency response functions (FRFs) which are obtained by applying an excitation force to the structure and measuring the input and output using load cell and accelerometer, respectively. The excitation force is generally applied using an impulse hammer or a vibration exciter; in particular, the impact testing using an impulse hammer is used widely for vibration testing due to the simplicity of the apparatus. However, the impact testing relies significantly on the skill and experience of the experimenter; additionally, it does not allow application of an ideal impulse excitation, limiting its use to measurements of low- and mid-frequency regions of under several kilohertz. For this reason, it is difficult to conduct accurate FRF measurements on structures that have natural frequencies in the high frequency region of tens of kilohertz. Evaluation of the high frequency vibration is becoming very important for various mechanical systems, because specifically, it has been reported that changes in natural frequencies and mode shapes are more prominent in modes at higher frequencies when damage occurs within a structure [8]. A hammer gun [9], an automatic impact excitation apparatus [10] have been examined for the purpose of improving the accuracy of FRF measurements that use the impact testing which relies significantly on the skill and experience of the experimenter, but these are not methods for achieving FRF measurement in the high frequency region, and these instruments need to be installed close to the target structures.

In order to solve the problems in vibration excitation for damage detection, an integrated non-contact damage detection system based on vibration is important to be developed. The measurements must be employing of non-contact structural excitation testing with high reproducibility, enable to extract measurement in high frequency and enable working in small area. Non-contact vibration excitation is known well using laser system which may fulfill the requirements.

The vibration testing based on impulse response excited by laser has been developed by some researchers. Koss and Tobin investigated laser-induced structural vibration [11], where the investigation was conducted in the range of frequency until 100 Hz. Philp et.al studied about single pulse laser excitation of structural vibration using power densities below the surface ablation threshold [12], where the vibration

response was investigated in the range of frequency until 2500 Hz. Those researches used cantilever beam as target structures, and did not show the comparison between vibration measurement result excited by laser and the other commonly used excitation method (like impulse hammer). Kajiwara et al. investigated an innovative vibration testing method based on impulse response excited by laser ablation [13,14]. A pulsed high power laser was used in this study for producing an ideal impulse force on a structural surface. Illuminating a point on a metal with the well-focused laser, laser ablation is caused by generation of plasma on the metal. As a result, an ideal impulse excitation force generated by laser ablation is applied to the point on the structure from the distance. Therefore, it is possible to measure high frequency FRFs due to the laser excitation. The validity of the method is verified by comparing the FRFs of the block obtained by the laser excitation, impulse hammer, and finite element analysis.

Excitation by laser ablation realizes the ideal impulse excitation force by instantly causing laser ablation by pulse-irradiating a metal surface with a high power YAG laser with its pulse duration of 5 ns. It can also be used for vibration testing of devices during actual operation since excitation can be performed without contact. Laser ablation is a process where high power laser is focused and irradiated on a solid, thereby rapidly increasing the surface temperature of the solid, explosively releasing atoms, molecules, and their ions, etc. [15]. In this method, a pulsed high power laser is used to trigger instantaneous laser ablation on an irradiated surface in order to obtain an ideal impulse excitation input. Vibration measurement in the high frequency region is thus made possible.

From what mentioned above, to employ non-contact structural excitation for damage detection in a structure is really possible. Because of that, in this dissertation, methods to identify structural damage by using non-contact laser excitation system are proposed to find the best and convenient solution in structural health monitoring using vibration approach.

1.2 Objectives and outline

As the continuation of the trends and facts described above, in this dissertation, vibration testing and health monitoring system based on an impulse response excited by laser is proposed to detect damage on structures. This idea is built based on the applicability of laser in giving excitation to structures and the needs to have high reproducibility non-contact excitation system on structure. The source of excitations is proposed in two methods: laser ablation and laser-induced breakdown.

In this dissertation, vibration testing and health monitoring system based on an impulse response excited by laser ablation is proposed to detect bolted joint loosening, and vibration testing and health monitoring system based on an impulse response excited by laser-induced breakdown is proposed to detect damage on membrane structures. Besides that, finite element analysis which describe condition of normal, loose bolt and damage membrane are proposed to evaluate laser excitation measurements and damage detection method.

In the aspect of structural analysis, damage in structures will change the natural frequency and mode shape of structures. Damages on metal structures are usually in form of loosening, crack, and so on. Bolt loosening is one of frequently cases on mechanical structures. In this dissertation, a vibration testing and health monitoring system based on an impulse response excited by laser ablation is proposed to detect bolted joint loosening. A high power Nd: YAG pulse laser is used to generate an ideal impulse on a structural surface which offers the potential to measure high frequency vibration responses on the structure. A health monitoring apparatus is developed with this vibration testing system and a damage detecting algorithm. The joint loosening can be estimated by detecting fluctuations of the high frequency response with the health monitoring system. Additionally, a finite element model of bolted joints is proposed by using three-dimensional elements with a pretension force applied and with contact between components taken into account to evaluate and support the bolt loosening detection method. The bolt loosening is detected and identified by introducing a damage index by statistical evaluations of the frequency response data using the Recognition-Taguchi method. This part hopefully will

contribute on structural health monitoring on bolted structure, where non-contact excitation is employed to give the high accuracy and the easiness of measurement.

In this dissertation, a vibration testing and health monitoring system based on an impulse response excited by laser is also proposed to detect damage in membrane structures. A high power Nd: YAG pulse laser is used to supply an ideal impulse to a membrane structure by generating shock waves via laser-induced breakdown in air. A health monitoring apparatus is developed with this vibration testing system and a damage detecting algorithm which only requires the vibration mode shape of the damaged membrane. Artificial damage is induced in membrane structure by cutting and tearing the membrane. The vibration mode shapes of the membrane structure extracted from vibration testing by using the laser-induced breakdown and laser Doppler vibrometer are then analyzed by 2-D continuous wavelet transformation. The location of damage is determined by the dominant peak of the wavelet coefficient which can be seen clearly by applying a boundary treatment and the concept of an iso-surface to the 2-D wavelet coefficient. The applicability of the present approach is verified by finite element analysis. The proposed method is expected to contribute on non-contact measurement and structural health monitoring in membrane structures.

This dissertation is organized in five chapters. Chapter 1 presents the background, motivation, and the objectives of this study. The next is chapter 2 that presents an overview of non-contact laser excitation; the mechanism of generation, and the ways of giving the excitation to the structures. This includes the components which involved generating the excitation to structure in the forms of vibration test by laser ablation and vibration test by laser-induced breakdown.

Chapter 3 explains a vibration testing and health monitoring system based on an impulse response excited by laser ablation to detect bolted joint loosening. The idea to detect loose bolt position by proposing vibration testing system and a damage detecting algorithm is presented in this chapter. The joint loosening is estimated by detecting fluctuations of the high frequency response with the health monitoring system, and the position of loose bolt is detected and identified by introducing a

damage index by statistical evaluations of the frequency response data using the Recognition-Taguchi method.

Chapter 4 presents vibration testing and health monitoring system based on an impulse response excited by laser to detect damage in membrane structures. The vibration mode shapes of the membrane structure extracted from vibration testing by using the laser-induced breakdown and laser Doppler vibrometer are analyzed by 2-D continuous wavelet transformation. The location of damage is determined by the dominant peak of the wavelet coefficient which can be seen clearly by applying a boundary treatment and the concept of an iso-surface to the 2-D wavelet coefficient.

Chapter 5 as the last chapter of this dissertation contains the conclusions and some possible future works as the continuation of this research.

Chapter 2

Laser Excitation

This chapter is intended to elaborate the high power laser effects that can be used to generate impulse excitation to structure which can be combined with damage feature detection to construct structural health monitoring system. For this purpose, two methods of excitation using laser that have been proposed by some researchers are explored and evaluated briefly. Some components and their rules are explained in this chapter. Based on the exploration, author finds the appropriate excitation methods by laser that can be implemented to propose structural health monitoring (SHM) on mechanical structure. At the end of this chapter, author explains briefly in which field and structure types that the laser excitation method can be implemented as SHM.

2.1 Introduction

Lasers offer a type of high power light source, capable of producing interesting and useful effects [16]. Investigations of the effects of laser beams have multiplied, and the works on laser effects represent an important technology within the growing laser field. The main properties that are different in laser radiation as compared to radiation from conventional light sources are the intensity, directionality, monochromaticity, and coherence of the laser radiation. The laser properties are explained briefly in this dissertation based on explanation by Ready [16].

First important property of lasers is the intensity. This is the point by which lasers are most known. The ability to produce very high power beam is the aspect of lasers that well known by the public imagination. The shower of sparks and flash of light from a metallic surface struck by a laser beam has become familiar. With simple systems it is possible to generate short-duration pulses of red or infrared laser light with powers of the order of millions of watts. Several billions to trillions of watts have been obtained in a pulse in more sophisticated systems. Such high power pulses of laser radiation can vaporize metallic and refractory surfaces in a fraction of a second.

The second important property of laser radiation is the directionality of the beam. Laser radiation is confined to a narrow cone of angles. Typically, for a gas laser system, the spreading angle is of the order of a few tenths of a milliradian, and for solid state lasers it is of the order of a few milliradians. Because of the narrow divergence angle of the laser radiation, it is easy to collect all the radiation with a simple lens system. The narrow beam angle also allows focusing of the laser light to a small spot. Therefore, the directionality of the radiation is an important factor in the ability of lasers to deliver high irradiances to a target and therefore to produce interesting effects.

The third property is the monochromaticity of laser radiation. This simply means that the laser light does not cover a wide range of frequencies as ordinary light does. To be sure, the frequency spread is not infinitesimally small, but in a gas laser it is fairly simple to obtain a frequency stability of one part in 10^{10} . In specialized models even higher frequency stabilities have been obtained. For solid state lasers, the frequency spreads are typically of the order of several megahertz. This is not as good as with a gas laser, but it is still very impressive.

The monochromaticity as such generally plays very little role in producing laser effects. For vaporization of a metal surface, for example, it makes little difference whether the radiation is monochromatic or covers a broad band so long as a specified number of watts per square centimeter are brought to the surface. Monochromaticity makes focusing easier in that chromatic aberration of the lens.

The last important property of laser is coherence. Coherence is related to the narrowness of the beam divergence angle. An incoherent source can be focused to a small area only with a large sacrifice in the total power of the source, so that coherence properties are indirectly related to the ability of the laser to produce high irradiance. However, the coherence of the laser beam is not of primary concern. Generally, once a certain number of watts per square centimeter is delivered to a surface, the effect will be much the same whether the radiation is coherent or not.

By the properties mentioned above, lasers have the potential to be implemented in various fields of engineering and science. In the field of structural health monitoring and damage identification using vibration approach, an excitation to generate vibration on structure is needed to know the change of modal parameters of the structure. The excitation method could require: non-contact excitation, ideal impulse excitation, high reproducibility, possibility of conducting excitation in narrow area, and in kind of non-destructive test. Based on the properties of laser, it has the potential to give the excitation to measured structure and to be combined with damage identification. The possible methods of excitation are laser ablation [13,14] and laser-induced breakdown [17].

2.2 Laser ablation

2.2.1 Proseses of laser ablation

The process of the laser ablation is presented in Fig. 2.1. When a laser beam is irradiated on a metal surface, it will be absorbed by the metal, and the atoms absorbing the laser light release ions. The absorption of the energy in the laser beam by metal will also generate high temperature plasma, and large quantities of particles are then released (in the form of a plume) from the metal (Fig. 2.1(a)). Momentum is then generated when a mass Δm released at a velocity v from the metal, represented by Δmv , and this expresses the laser-induced impulse.

To generate a larger excitation force on the structure, a water droplet is placed on the metal surface during laser ablation as shown in Fig. 2.1(b). The laser ablation occurs on the metal surface when the laser passes through the water droplet and reaches the

metal surface. In addition to the release of particles from the metal surface, the water droplet evaporates with the rapid increase in the temperature of the metal surface, releasing the mass ΔM of the water droplet at a velocity V . The total resulting momentum is $\Delta mv + \Delta MV$, resulting in a larger impulse with than without the water droplet (Fig. 2.1(b)). The particles and water vapor are released radially from the metal surface, and the direction of the impulse only comprises the element that is normal to the metal surface. This impulse constitutes the excitation force on the structure.

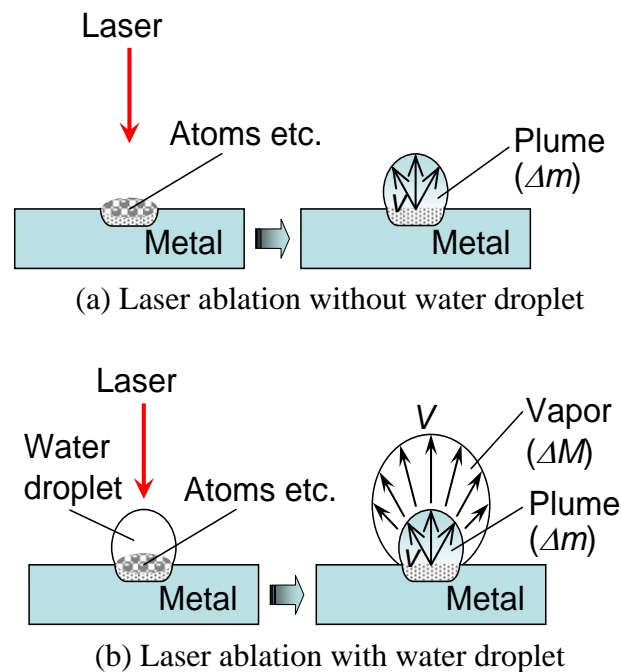


Fig. 2.1 Process of the laser ablation [14]

2.2.2 *Vibration test by laser ablation*

In order to proof the applicability of laser ablation in applying non-contact excitation to mechanical structure, Kajiwara et.al conducted vibration testing based on impulse response excited by laser ablation [13,14]. A vibration testing system using pulsed high power laser is shown in Fig. 2.2.

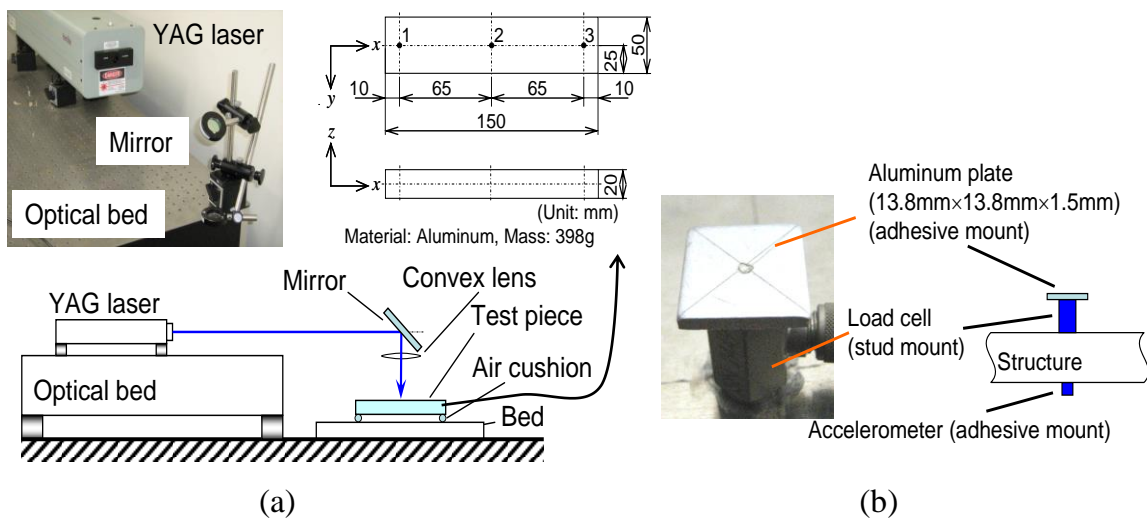


Fig. 2.2 Experimental set-up of vibration test using pulsed high power laser [14]
 (a) general set-up of system, (b) attachment of load cell and accelerometer

A YAG laser (Continuum Surelite II) with a wavelength of 1064 nm, output of 650 mJ, and a pulse width of 5 ns was installed on an optical table. In order to enable vibration testing using free support and fixed support on structures of various shapes and sizes, the optical axis of the laser beam was first deflected using a mirror, after which the beam was focused to a spot with a diameter of 2 mm using a convex lens to cause laser ablation. The objective structure was an aluminum block (Fig. 2.2(a)). As shown in Fig. 2.2(b), the excitation force generated by laser ablation is measured by fixing a load cell to the input point of the structure using a stud mount. In order to prevent the load cell from being damaged by laser ablation, an aluminum flat plate of size 13.8 mm × 13.8 mm, thickness 1.5 mm, and mass 0.7 g was attached to the top surface of the load cell using an adhesive, and laser ablation was triggered on the aluminum plate. For the response, an accelerometer was attached to the measuring point of the structure using an adhesive. A spectral analyzer was used for measuring the excitation forces and acceleration responses, and analyzing the frequency responses of the object structure. The maximum measurement frequency is set to 40 kHz in this study.

Using the block shown in Fig. 2.2(a), auto-FRFs H_{11} and H_{22} and a cross-FRF H_{31} were measured where points 1 and 2 are the excitation points and points 1, 2, and 3 are the measurement points. H_{ij} is FRF between an input point j and output point i . The aluminum plate was mounted, using an adhesive, on the load cell, which was in

turn fixed to the top surface of the block using screws, and the accelerometer was fixed to the bottom surface of the block using an adhesive. The measurements were conducted by using laser excitation and impulse hammer. The FRF measurements results can be seen in Fig 2.3 for auto-FRF H_{11} , Fig 2.4 for auto-FRF H_{22} and Fig 2.5 for cross FRF H_{31} .

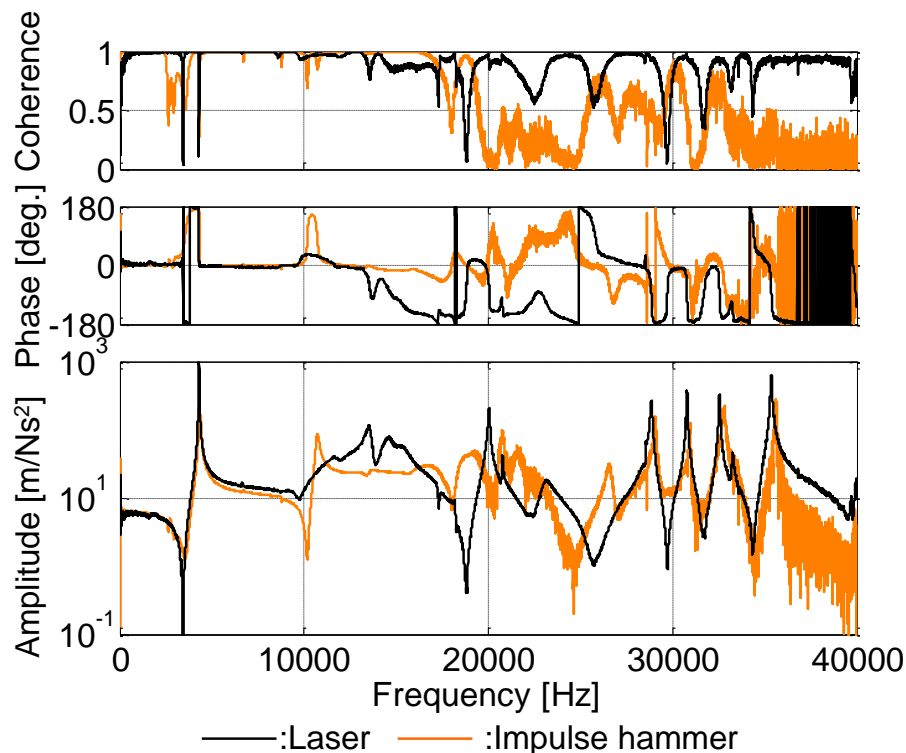


Fig. 2.3 Auto-FRF H_{11} by laser excitation and impulse hammer [14]

Fig. 2.3 to Fig. 2.5 show that the FRFs using both methods are in close agreement in the frequency region of fewer than 10 kHz. However, it can be seen that the coherence of the FRF via the impact testing drops considerably in the frequency region of over 20 kHz. It also can be seen in high frequency that impulse hammer gave the noisy response. Fig. 2.6 shows input characteristics of the laser and impulse hammer excitations. It is observed from Fig. 2.6 that the power spectrum with the impulse hammer also drops considerably over 20 kHz, resulting in the degradation of the accuracy of FRF.

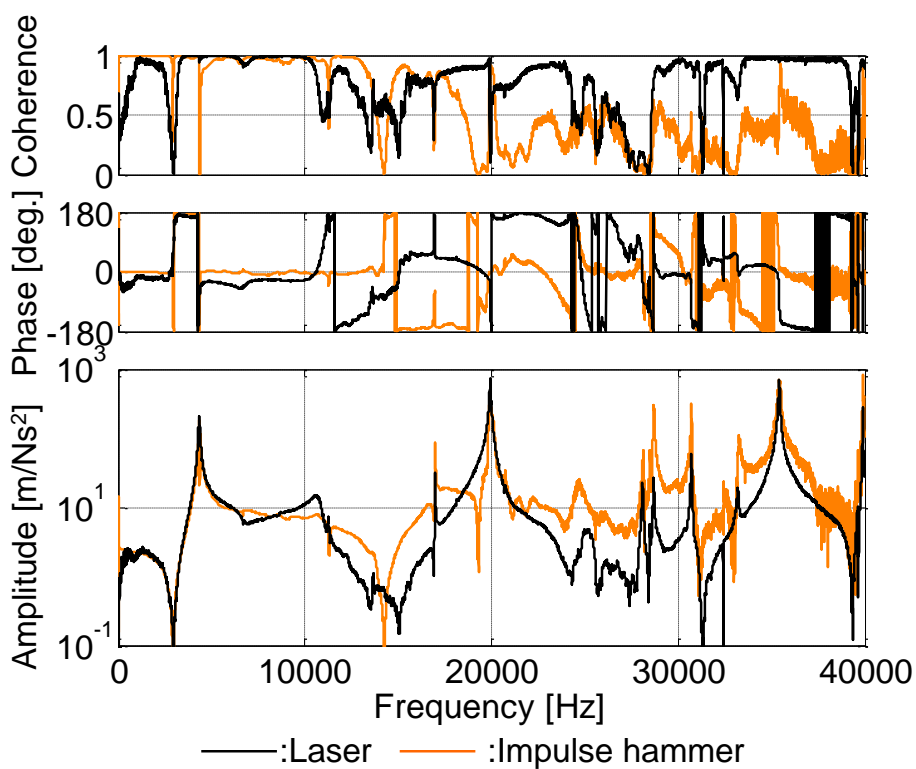


Fig. 2.4 Auto-FRF H_{22} by laser excitation and impulse hammer [14]

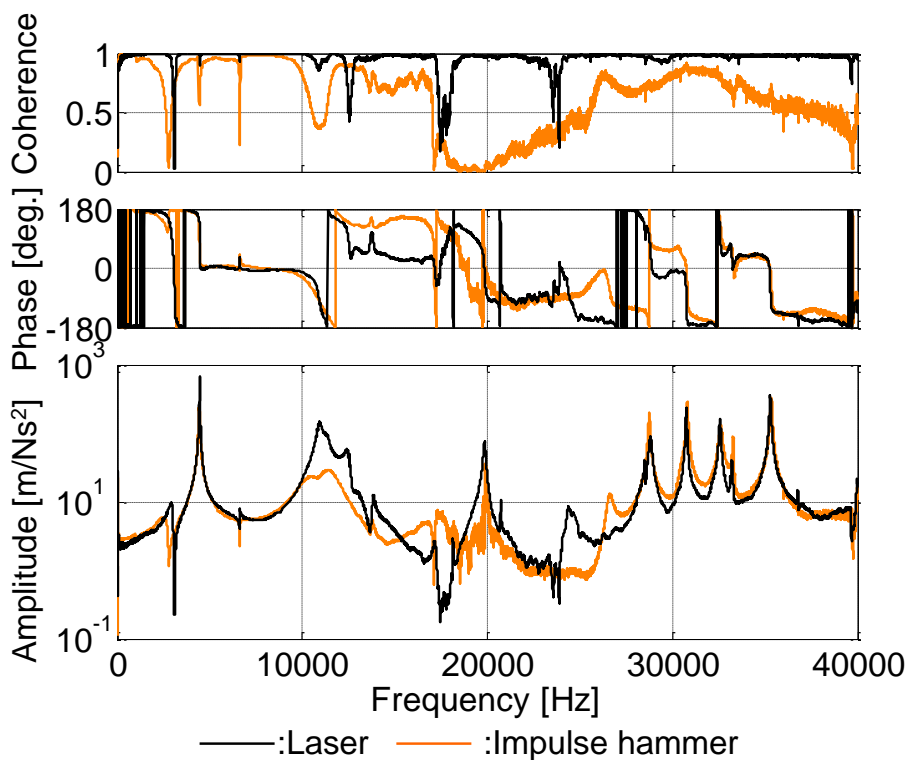


Fig. 2.5 Cross-FRF H_{31} by laser excitation and impulse hammer [14]

The input characteristics different between laser excitation and impulse hammer can also be investigated by minimizing time scale. Fig. 2.7 shows the different characteristics between laser excitation and impulse hammer, where the time scale is minimized. The excitation by laser occurred in really short time, while the excitation by impulse hammer shows curvy excitation force. This is a fact that ideal impulse force to metal structure could be sourced from non-contact excitation by laser ablation.

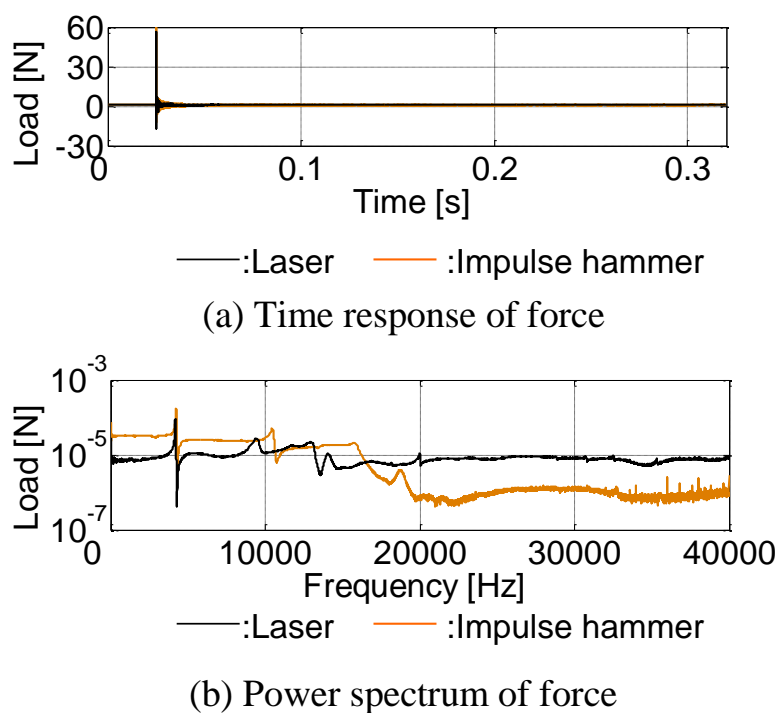


Fig. 2.6 Input characteristics of laser excitation and impulse hammer [14]

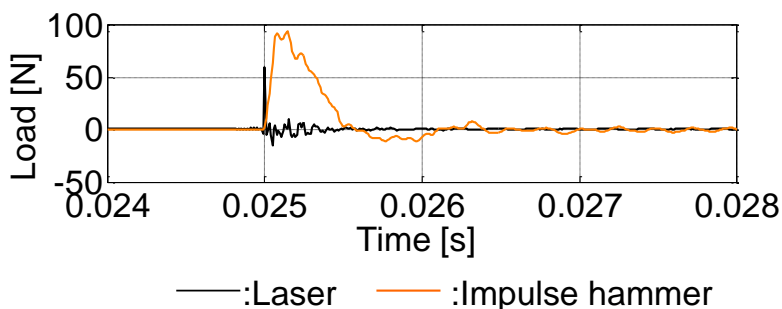


Fig. 2.7 Different characteristics between laser excitation and impulse hammer [14]

From what mentioned above, the strength points of non-contact laser excitation to structure can be established. It works well in low and high frequencies, has the ability in applying excitation force in really short time, showing a promising potency of a new non-contact excitation.

In applying non-contact laser excitation by laser ablation in the field and next experiment of vibration, if using laser excitation in vibration test requires attaching load cell on the objective structure, the experiment would not be involving non-contact excitation. This term will be a weak point of the laser ablation application in vibration test. To solve this problem, Hosoya et.al proposed FRF measurement method using pulsed-laser ablation [18] and it does not require detection of the input force.

This method was proven by conducting vibration testing. On the testing, a frequency-domain acceleration spectrum was obtained from an accelerometer attached to a test object due to a pulsed-laser-ablation excitation force, applied at various excitation points on the object. The Fourier transform of the obtained time-domain acceleration yields the complex acceleration frequency spectrum, which is divided by the previously calibrated pulsed-laser-ablation force. Furthermore, it was confirmed that the phase of the output-frequency spectrum can be properly adjusted by accounting for the response dead time, with the result being the FRF of the test object. Because the laser pulse can be measured without contact with the test object and it constitutes an ideal point impulse, it is possible to use this technique to excite micro devices.

The laser excitation can apply an ideal impulse excitation, making it possible to use the Fourier transform of the output response for the evaluation of the vibration characteristics of the system as the frequency response function. The Fourier transforms of time histories of an input force $f(t)$ and output response $x(t)$ into the frequency domain are described by

$$F(\omega) = \int_{-\infty}^{\infty} f(t) e^{-j\omega t} dt \quad (2.1)$$

$$X(\omega) = \int_{-\infty}^{\infty} x(t) e^{-j\omega t} dt \quad (2.2)$$

The output response $x(t)$ can be expressed by the convolution integral with an impulse response function $h(t)$ of the system:

$$x(t) = \int_{-\infty}^{\infty} h(t - \tau) f(\tau) d\tau \quad (2.3)$$

The Fourier transform of Eq.(2.3) results in

$$X(\omega) = H(\omega) F(\omega) \quad (2.4)$$

where, $H(\omega)$ is the frequency response function of the system. When $f(t)$ is an impulse force, ideally the Dirac delta function, the Fourier transform of $f(t)$ becomes $F(\omega) = 1$, and Eq.(2.4) is expressed by

$$X(\omega) = H(\omega) \quad (2.5)$$

The result is that the Fourier transform of the response $x(t)$ becomes the frequency response function.

2.3 Laser-induced breakdown

2.3.1 *Proseses of laser-induced breakdown*

The laser-induced breakdown (LIB) refers to the formation of plasma through the cascade process caused by electrons emitted from atoms and molecules that have absorbed multiple photons through a multi-photon process when a laser beam is focused in a gas. A portion of this plasma energy is transformed to a shock wave, which is the source of the sound generated by LIB, which has the potency to be acoustic excitation force. This is one of the high power laser effects.

The local intensity I [W/m^2] required for LIB is given by [19]:

$$I = \frac{E}{S\Delta t} \quad (2.6)$$

where E is the laser pulse energy [J], Δt is the duration of the laser pulse [s], and S is the area on which the laser is focused [m^2].

The LIB threshold in air is $I \geq 10^{15}$ W/m^2 . When the laser's local intensity is smaller than this threshold, a convex lens can be used for focusing the laser beam, thereby reducing the spot radius. By passing the laser beam through the convex lens which focuses the beam, the local intensity of the laser beam reaches to or above the

minimum LIB threshold of 10^{15} W/m^2 [19-21].

The process to achieve acoustic excitation by LIB is presented in Fig. 2.8. From the figure, it can be seen that Nd: YAG pulse laser is used to produce laser beam, and laser beam is then passed to convex lens. The LIB occurs in the distance of focal length of the convex lens from the convex lens position.

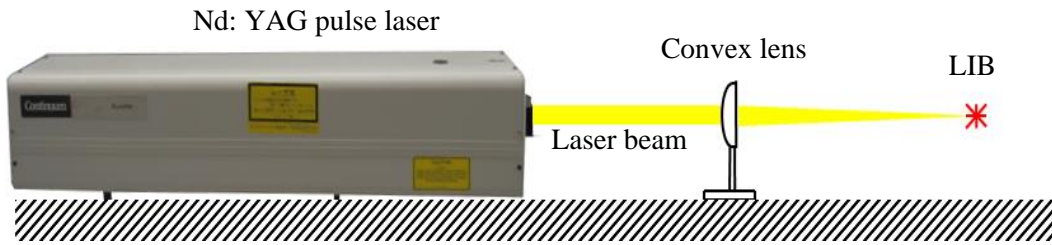


Fig. 2.8 Process to achieve acoustic excitation by LIB

2.3.2 Acoustic excitation system using LIB

Hosoya et.al proposed acoustic testing in a very small space based on a point sound source generated by LIB [17], using the same scheme set-up as Fig. 2.8 to illustrate the acoustic excitation system that uses the point sound source generated by LIB. The system uses an Nd: YAG pulse laser (Surelite III-10, Continuum Inc., wavelength: 1064 nm, laser beam radius: 4.75 mm, pulse width: 5ns, maximum output: 1J, radial divergence angle: 0.25 mrad), and a convex lens placed on the optical table to focus the laser beam and generate the point sound source LIB. The spot radius of sound source is increased as the focal length increases, causing the LIB threshold to vary, as well. Table 2.1 shows the configuration of three convex lenses used to focus laser beam.

The spot radius of LIB is expressed by

$$r = f \frac{\lambda}{\pi W_0} = f \Delta\theta \quad (2.7)$$

Therefore,

$$\Delta\theta = \frac{\lambda}{\pi W_0} \quad (2.8)$$

The spot radius r [m] is given by Eq. (2.7) using the focal length of the convex lens f [m], the laser's wavelength λ [m], the laser beam radius W_0 [m], and the radial divergence angle $\Delta\theta$ [rad] [22].

The effectiveness of the point sound source generated by LIB as an acoustic excitation source is shown by examining the sound pressure and frequency band at which excitation is possible. The directionality of this point sound source was also examined and the relationship between the sound pressure of the point source, and the spot radius as well as the laser pulse energy was investigated.

Table 2.1 Configurations of the three convex lenses used to focus the laser beam [17]

Lens	Focal length	Spot radius	Area
	f [mm]	r [μm]	S [mm^2]
Lens L1 (BK7 SLB-30-100P)	100	25	0.0020
Lens L2 (BK7 SLB-30-200P)	200	50	0.0079
Lens L3 (BK7 SLB-30-300P)	300	75	0.0177

Fig. 2.9 shows times response sound pressure generated by LIB. The ten measured waveforms of the sound pressure are plotted, and the experiments were conducted using convex lens with focal length of $f = 100 \text{ mm}$ and energy of $E = 990.09 \text{ mJ}$. It is shown on the figure that the point sound source generated by LIB on that configuration has high reproducibility.

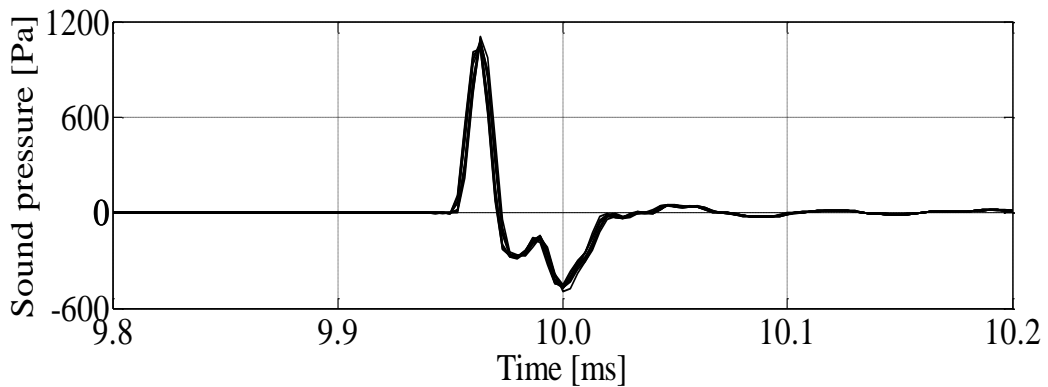


Fig. 2.9 Time responses of sound pressure generated by LIB [17]

Hosoya et.al [17] found that the reproducibility of the point sound source generated by LIB decreases as the focal length (using convex lens with longer focal length) increases because a longer focal length makes the spot radius larger, causing fluctuations in the location at which LIB takes place. The reproducibility of the sound pressure of the point sound source generated by LIB was improved by reducing the spot radius of the convex lens with a long focal length using Galilean laser beam expander. Thus, convex lenses of various focal lengths can be used with this method.

Reducing the spot radius is effective for improving reproducibility. Therefore, by introducing a beam expander, the spot radii can be reduced when using convex lenses of long focal lengths. As in Eq. (2.8), when W_0 is multiplied by α because of the beam expander, r is divided by α . Fig. 2.10 illustrates the Galilean laser beam expander used in this experiment. The beam expander increases the radius of the unfocused laser beam by a factor of 4.3: from 4.75 mm to 20.43 mm; by focusing this beam through the convex lens, the spot radius can be reduced by a factor of 0.23. Thus, by using this beam expander, a spot radius through a convex lens of focal length 300 mm (lens L3) can be reduced to 17 μm .

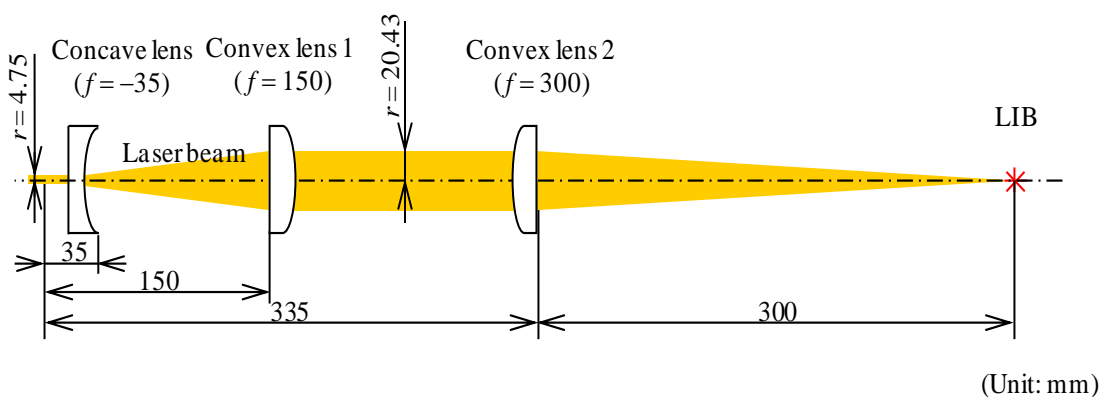


Fig. 2.10 Galilean laser beam expander [17]

To verify that the point sound source generated by LIB is non-directional, the experiment was conducted by measuring sound pressure on the point sound source generated by LIB in the anechoic box, and twelve microphones were placed 80 mm from the sound source as shown in Fig. 2.11. A laser pulse energy of 197.4 mJ and

lens with focal length 100 mm and spot radius 25 μm were used. Fig. 2.12 shows the average power spectra of the sound pressure measured at each point when superimposed. Fig. 2.13 shows the sound pressure level at each point for frequencies 10, 30, 50, and 70 kHz. For asymmetric pair of measurement points (e.g., i and xii) in the anechoic box, the time responses of sound pressure, as well as their power spectra, were confirmed to be almost the same. In Figs. 2.12 and 2.13, the power spectra of the sound pressure within the measured frequency range were very similar for each measurement point. The difference in sound pressure level at each frequency was approximately 4 dB; this is assumed to be due to errors in the locations of the LIB and/or the microphones, which were the measurement points. Therefore, if the distance between the sound source and measurement point is the same, the measured sound pressure level is also the same at any location, which means the point sound source generated by LIB can be considered non-directional.

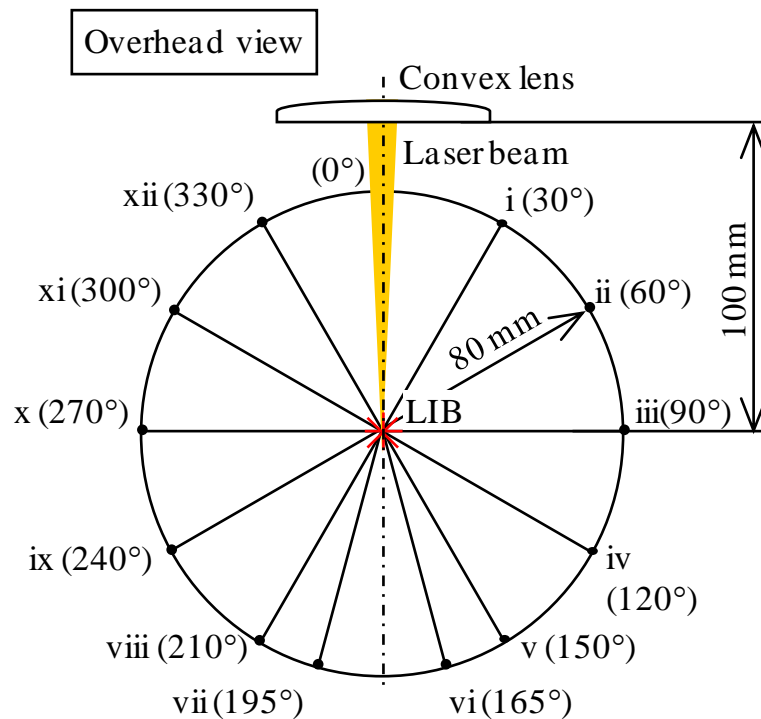


Fig. 2.11 Layout of microphone in the anechoic box for directional test
(overhead view)[17]

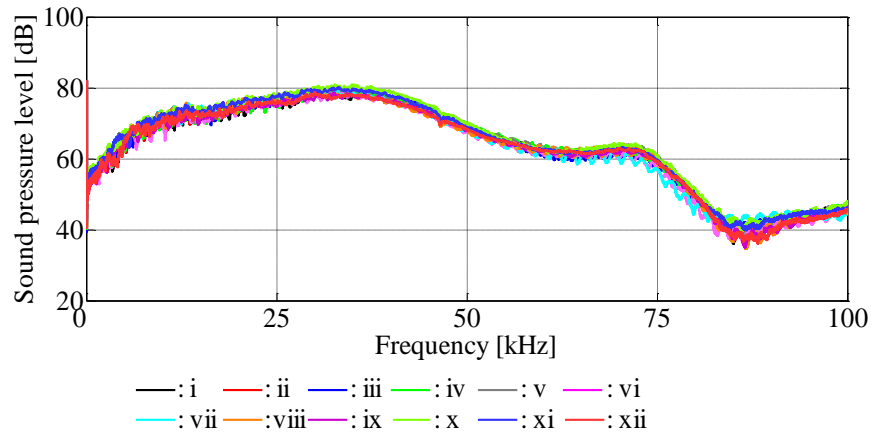


Fig. 2.12 Measured power spectra at each point [17]

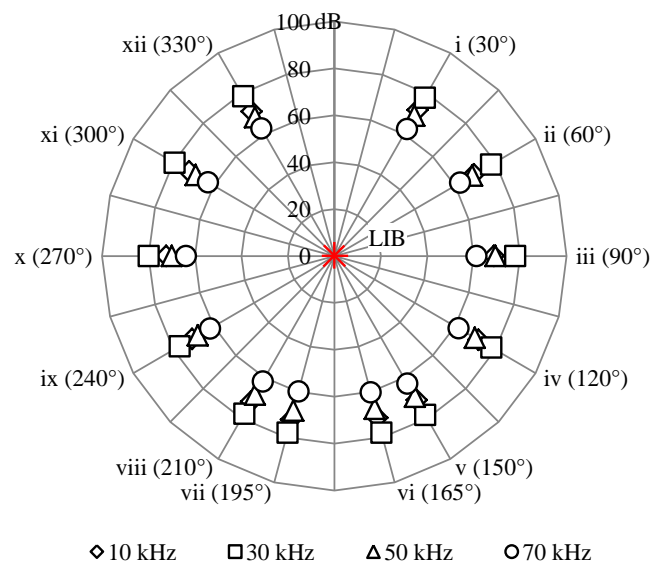


Fig. 2.13 Star plot of the sound pressure levels and measurement positions in each frequency [17]

From what mentioned above, the acoustic excitation method based on a point sound source generated by LIB is promising the future excitation method on structure. By some properties like high reproducibility, non-directional, as one of non-contact excitations, ideal acoustic excitation, make this excitation method one candidate which answers the problem of non-contact acoustic excitation method.

2.4 Non-contact laser excitation and damage identification

As mentioned in chapter 1 that, in damage identification using vibration approach, the ideal excitation method is required to ensure the accuracy, reliability and easiness of measurement. In applying non-contact laser excitation to damage identification, the mechanism of laser excitation needs to be carefully considered, so that the excitation method not only gives the easiness in measurement, but also enhances the quality of measurement.

Non-contact laser excitation by laser ablation is a type of excitation that is usually applied to metal structures. Besides giving ideal impulse excitation, this excitation method has strength point in measuring high frequencies vibration, but laser ablation causes a small damage on measured structure, so this excitation method will be appropriate to be applied to metal structures that have no problem with the effect of small damage caused by ablation. It will be suitable to be combined with damage identification on bolted joint structure. In chapter 3, author proposed bolt loosening detection using non-contact laser excitation by laser ablation.

Acoustic excitation by LIB was applied in the experiment to determine natural frequency of aluminum pipe [17]. Besides non-contact excitation which gives possibility to conduct measurement in really narrow area, this kind of excitation causes no damage. So, this kind excitation is suitable to be combined with damage detection on extremely light and flexible structure, which requires completely non-contact excitation and non-destructive measurement. In chapter 4 of this dissertation, author proposes damage detection in membrane structures using non-contact laser excitation. Acoustic excitation by LIB will be applied and combined with damage identification method to detect damage in membrane structures.

2.5 Concluding remarks

It is explained in this chapter that there are two mechanism of high power laser effect that can be used as excitation to structure to generate vibration; laser ablation

and laser-induced breakdown (LIB). Excitation by laser ablation to metal structure occurs when laser beam focused and directed to metal and then absorbed by metal generates high temperature plasma, and large quantities of particles are then released (in the form of a plume) from the metal. Releasing the particle at a velocity from the metal represents the laser-induced impulse. The impulse causes the vibration of structure. Excitation by LIB occurs when laser beam is focused, and plasma is then generated, and a portion of this plasma energy is transformed to a shock wave, which is the source of the sound generated by LIB. This sound can be used as a source of acoustic excitation.

Therefore, in this dissertation, high power laser effects became the basic idea to explore vibration test using non-contact excitation. A short explanation about excitation that occurs by laser has been done using force and sound intensity measurement for both of the methods. Vibration measurements by laser excitation have high reproducibility, enabled high frequency measurement, and give the easiness of measurement since it is non-contact and really possible to be conducted in narrow area. It is also described how these laser excitations can be implemented to vibration testing without measuring the input.

Chapter 3

Bolt Loosening Analysis and Diagnosis by Non-contact Laser Excitation Vibration Test

Excitation force plays an important role in vibration testing to generate vibration on measured structures. Besides requiring of having high reproducibility, the excitation method in structural health monitoring (SHM) also needs to perform the ability of measuring in wide range of frequency, and convenient in operation. Non-contact excitation by laser excitation is a candidate which could fulfill the requirement of vibration test for damage detection and structural health monitoring. In this chapter, author proposes new method of the application of vibration test with non-contact laser ablation excitation in bolt loosening analysis and diagnosis.

3.1 Introduction

Bolted joints are widely employed when joining two or more parts together in mechanical products and structures due to the ease of disassembly for maintenance. However, bolted joint failures, including self-loosening, shaking apart, slippage, stress cracking due to fatigue, and breaking due to corrosion [23], are frequent, and it has been suggested that most failures of bolted joint are caused by loosening [24]. For this reason, bolt loosening has become an important research area in mechanical engineering in efforts to prevent failures in a variety of mechanical applications.

Several methods of bolt modeling have been studied by previous researchers. Kim proposed four kinds of finite element models to model structures with bolted joints [25]. Ahmadian developed a non-linear generic element formulation for modeling bolted lap joints [26]. Bograd gave an overview of different approaches to modeling the dynamics of mechanical joints in assembled structures where the finite element method is based on three different approaches: node-to-node contact using the Jenkins frictional model, thin layer elements, and zero thickness elements [27]. That research has been concerned with the bolted joint modeling in commonly occurring conditions only. However, modeling of bolted joints that undergo loosening is necessary to underpin bolt loosening detection methods.

Detecting the loosening of bolted joints is important to ensure the proper functioning of structures or subassemblies. The process to implement a method of damage detection is generally referred to as structural health monitoring [28]. Several approaches have been investigated in regard to the detection of loosening in bolted joints, especially those using impedance [29,30], electrical conductivity [31], and vibration measurements [32]. Vibration based approaches have commonly involved contact excitation, using piezoelectric materials or impulse hammers to excite a structure to determine the frequency response. However, using piezoelectric components require these to be firmly attached to structures and larger sized piezoelectric components may need to be bolted to a structure. Hammering methods require specially trained technicians and are time consuming. Further, the reproducibility of input characteristics with hammering is poor, while measurements of dynamics characteristics require high reproducibility to be optimally useful. These issues have led to research into non-contact excitation methods with better reproducibility. Vibration measurement systems using non-contact laser excitation can guarantee a very high degree of measurement reproducibility [13,14,17].

Lasers are used in a variety of applied technologies due to their high coherence and energy density. There are two reasons for employing lasers as the source of the excitation in this study. Besides providing a high degree of measurement reproducibility, laser excitation also allows measurement of vibrations at high frequencies. Specifically, it has been reported that changes in natural frequencies

and mode shapes are more prominent in modes at higher frequencies when damage occurs within a structure [8]. This would make it a suitable excitation method for bolt loosening detection.

In this study, a finite element modeling method for bolted structures is proposed and a laser health monitoring technique for detecting bolt loosening in joint structures is developed. Vibration testing based on non-contact impulse excitation using laser ablation is conducted. A high power Nd: YAG pulse laser is used for producing an ideal impulse on the structural surface. The high frequency response of the structure is then measured. Loose bolt conditions are simulated by reducing the torque used to tighten a bolted joint assembly. The change in vibration characteristics due to the bolt loosening affected in this manner in the high frequency region can be extracted by the laser excitation vibration measurement. The research approach is supported by a finite element model of bolted joints that undergo loosening, which is verified by vibration testing based on non-contact impulse excitation using laser ablation. Finally, a method for loose bolt detection is proposed by applying a statistical evaluation of the Recognition-Taguchi (RT) method to a six-bolt joint cantilever with a loose bolt.

3.2 Vibration testing system using laser ablation

3.2.1 Pulse laser

High frequency vibration measurement of structures with natural frequencies in the high frequency range may be conducted by laser excitation vibration testing. A vibration testing arrangement using a high power pulse laser is shown in Fig. 3.1. An Nd: YAG laser (Continuum Surelite III) with a wavelength of 1064nm, maximum output of 1 J, and a pulse width of 5ns is installed on an optical table. The beam is focused at a spot on the structure, and has a diameter of 25 μ m using a convex lens with the focal length 100mm to cause the laser ablation.

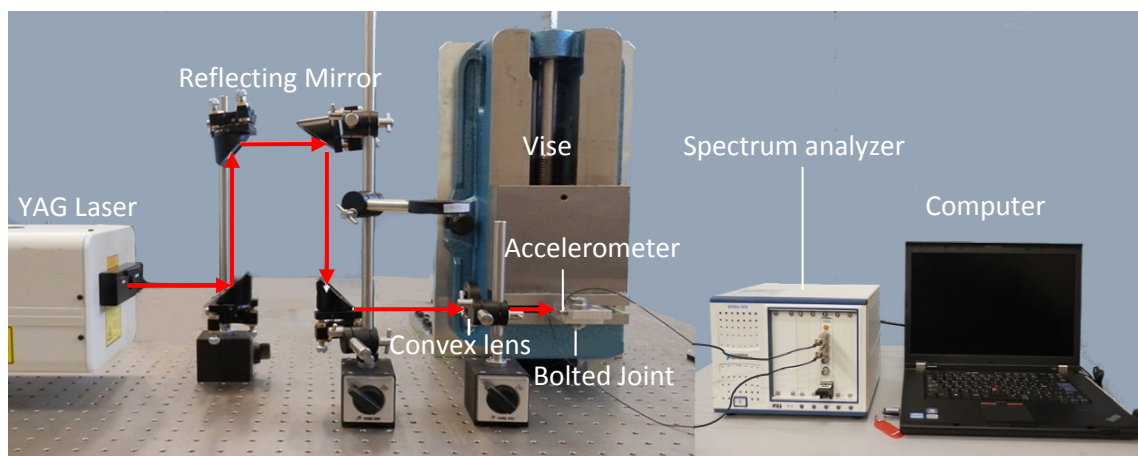


Fig. 3.1 Vibration testing arrangement using the high power pulse laser

3.2.2 Measurement and analysis of output

To measure the output response, accelerometers are attached to the measuring points of the structure with an adhesive. A spectrum analyzer (A/D; NI-4472B, Software; Catec CAT-System) is used for measuring the acceleration response and analysing the Fourier spectrum of the structure. The maximum measurement frequency is set to 40 kHz in this study. Based on the specifications, the natural frequency of the accelerometers used in this experiment is above 50 kHz, and experiments verified that the natural frequency of the accelerometers is sufficiently higher than the maximum measurement frequency of 40 kHz.

The laser excitation realizes an ideal impulse excitation, making it possible to use the Fourier transform of the output response for the evaluation of the vibration characteristics of the system as the frequency response function. When *excitation force* is an impulse force, ideally the Dirac delta function, the Fourier transform of force $f(t)$ becomes $F(\omega)=1$, as mentioned in chapter 2. The result is that the Fourier transform of the response $x(t)$ becomes the frequency response function.

3.3 Finite element analysis of bolted joint

With the aim of developing the finite element model of bolted joints, a simple three-dimensional finite element model of a bolted joint with solid element formed by one bolt-nut and two flanges was used in the bolted joint modeling. This model allowed

an independent study of the normal and loose conditions to be considered for the model. The normal condition represents the bolt with standard tightening torque, and loose condition occurred when the bolt get lower tightening torque than standard. A more complex bolted joint was next modeled for the application of the proposed method to more complex structures.

3.3.1 Model description

The finite element analysis software ANSYS 14.0 has been used to model bolted joint with pretension force and mating part contact. The one-bolt joint model is constructed in form of cantilever, where one of the flanges is fixed, as shown in Fig. 3.2. The SOLID186 element of ANSYS which is defined by twenty nodes, having three degrees of freedom at each node is used to construct physical model of bolted joint. The total number of nodes and elements are 29635 and 5412, respectively.

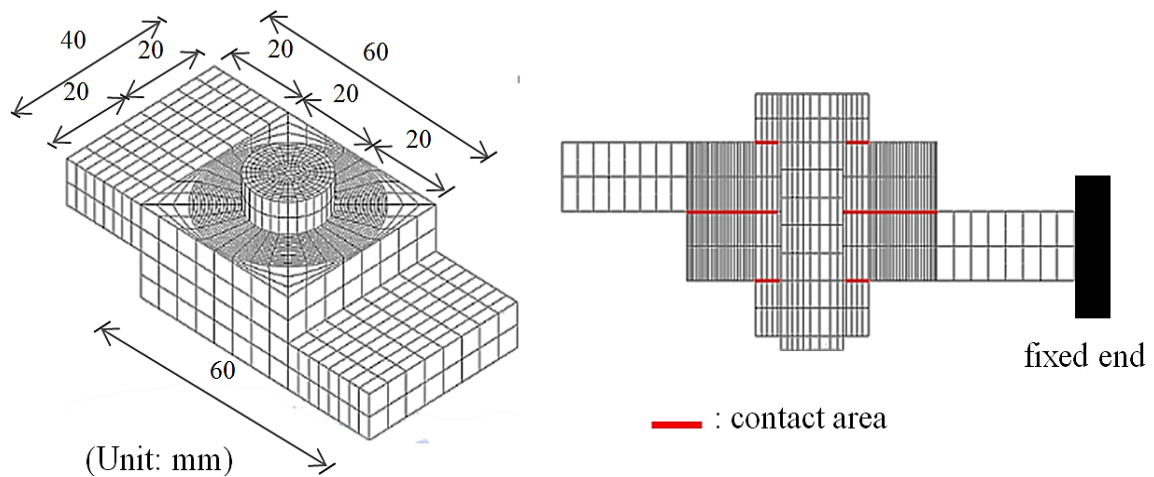


Fig. 3.2 One-bolt joint model

In the model, the tightening torque applied to the bolt is converted to a pretension force. The relationship between the given tightening torque and the arising pretension force is described by

$$F = \frac{T}{K \times d} \quad (3.1)$$

where F , T , K , and d are the pretension force, the tightening torque, torque coefficient, and the nominal diameter of bolt, respectively.

The pretension force is applied by using pretension element PRETS179 in ANSYS, where the value of the pretension force can be applied directly to the bolt. The pretensions of the bolt will be varied from standard pretension which represents normal condition to lower ones which represent loosening conditions. The contact modeling is presented by surface-surface contact elements, which is a pair, the contact element CONTA174 and the target element TARGE170. The contact elements are applied to the interfaces between bolt head and upper flange, nut and lower flange, and between upper flange and lower flange. There are three types contact used in this model:

- a) Bonded, where no sliding or separation between interfaces or edges is allowed.
- b) Frictional, where two contacting interfaces may be subject to shear stresses up to a specified magnitude across the interface before sliding occurs.
- c) No separation, where separation of the interfaces in contact is not allowed, but where small amounts of frictionless sliding may occur along the contacting interfaces.

The simple bolted joint connection used in this study is composed of two aluminum flanges, each 10 mm thick and joined with a stainless steel M10 bolt. The material of the bolt and the flanges are assumed to exhibit linear elastic behaviors during clamping. The mechanical properties of the material used in the linear elastic finite element analysis for the bolt are a Young's modulus of 193 GPa, a Poisson ratio of 0.31, and a mass density of 7750 kg/m³, for the flanges the Young's modulus is 68 GPa, the Poisson ratio 0.33, and the mass density 2700 kg/m³.

3.3.2 Determining contact condition between flanges

The static structural analysis with a given pretension force applied to the bolt was conducted to determine the contact type between the flanges which are subject to the pretension force. This analysis is also used to establish the initial conditions for the following analysis, the pre-stressed modal analysis.

To determine the contact type between the flanges, the region where the stresses due to the pretension that produced the clamping force are predominant is set so they

may be considered to be bonded to each other. That region forms a conical shape and covers a range of $25^\circ \leq \alpha \leq 33^\circ$, as suggested by Osgood [33]. The bolt head and the nut are also assumed to be glued to the flanges due to the clamping force. A pretension force for the normal and loosened condition will be applied to the bolt. Table 3.1 shows the relationship between the given tightening torques and pretension forces arising in model.

Table 3.1 Relationship between tightening torques and pretension forces

Tightening Torque (Nm)	Pretension Force (N)	State
24.5	12260	Normal
20.0	10000	Loose
18.0	9000	Loose
15.0	7500	Loose
10.0	5000	Loose

The static structural analysis is then conducted with ideal conditions, where the entire contact area between the components of the bolted joint is assumed to be bonded. The stress and elastic strain data on the contact between the flanges are then obtained. By applying the conical shape suggested by Osgood, the values of the stress on the outer radius of the conical shape due to the normal pretension force are considered the basic values (benchmark) and the limits for the bonded area. The contact region with the value of stresses greater than or equal to the values of the benchmark becomes the bonded contact area, and the other contact areas will be frictional and no separation. This process is suggested in Fig. 3.3, which also shows that in the case of a loose condition, the contact arrangement will change with the benchmark values of the stress.

Fig. 3.4 shows stress distribution between flanges in contact used for determining the state of the bonded contact, and how to determine the limit of the contact area for bounded areas graphically when the benchmark values for stress is already established using the Osgood cone. By drawing a horizontal straight line based on the benchmark value which then crosses the curves of stress for every pretension

force, the limits for bonded contact is determined by as the point directly below the point where the horizontal line touches the stress curve. In this way the bonded area between flanges with a pretension force of 12260 N is 5.5 cm to 15 cm, and it is 5.5 cm to 13.5 cm, 5.5 cm to 13 cm, 5.5 cm to 12 cm, and 5.5 cm to 9.5 cm for pretension forces of 10000 N, 9000 N, 7500 N, and 5000 N, respectively. Using the elastic strain curve with the same procedure, will yield similar results as those for stress.

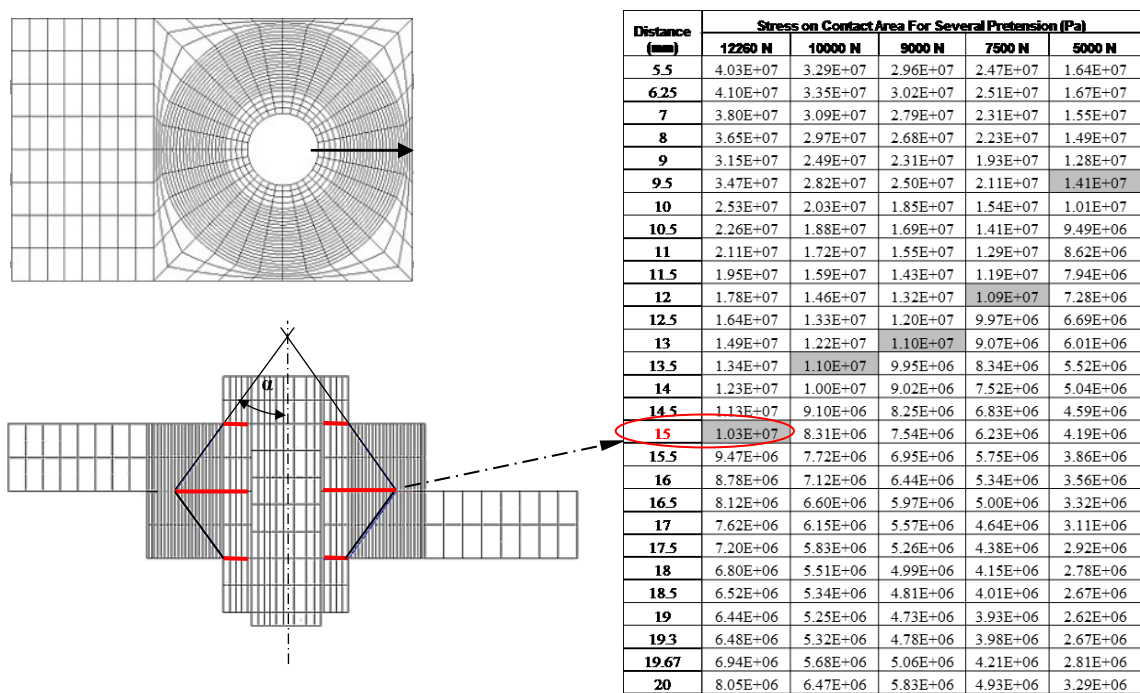


Fig. 3.3 Procedure to determine the benchmark for bonded area

3.3.3 Frequency response analysis

To utilize the bolted joint model proposed in this study for a dynamic analysis, a series of frequency response analysis tests using the finite element method were carried out. The frequency response analysis was executed by applying pre-stressed modal analysis with initial conditions given by the results of the static structural analysis.

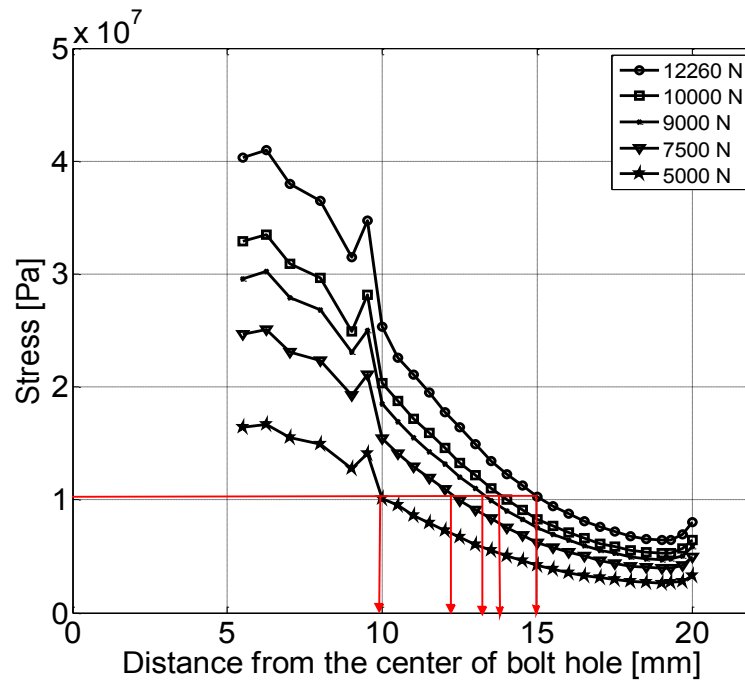


Fig. 3.4 Stress distribution between flanges in contact for determining bonded contact condition

Some reports have found that nonlinear features like frictional contact elements cannot be counted in a modal analysis [25,34], and this has caused other research to employ linear contact for the modal analysis. In this study, the effects of the frictional contact are taken into account in dynamic analysis as pre-stressed modal analysis, in which the static structural analysis with contact element results in the stress and elastic strain which are maintained as initial condition of next analysis, modal analysis. Even though there is no direct effect of frictional contact in the modal analysis, using frictional contact will affect the static structural analysis as the initial condition of the pre-stressed modal analysis.

Several pre-stressed modal analysis are carried out for normal and loose conditions. The loose conditions are given by changing the value of the pretension force and the type of contact area.

3.3.4 *Finite element model of generalized complex bolted joint*

To further evaluate the modeling method of the finite element analysis that has been developed above for a simple one-bolt joint, a more complex bolted joint model was

used to show the applicability of the method of the analysis. Here, a three-dimensional finite element model of a bolted joint which consists of two flanges and six bolts is built. The six-bolt joint is modeled as a cantilever with the same materials as the simple one. The dimensions in mm and the bolt numbering of the six-bolt joint model are shown in Fig.3.5.

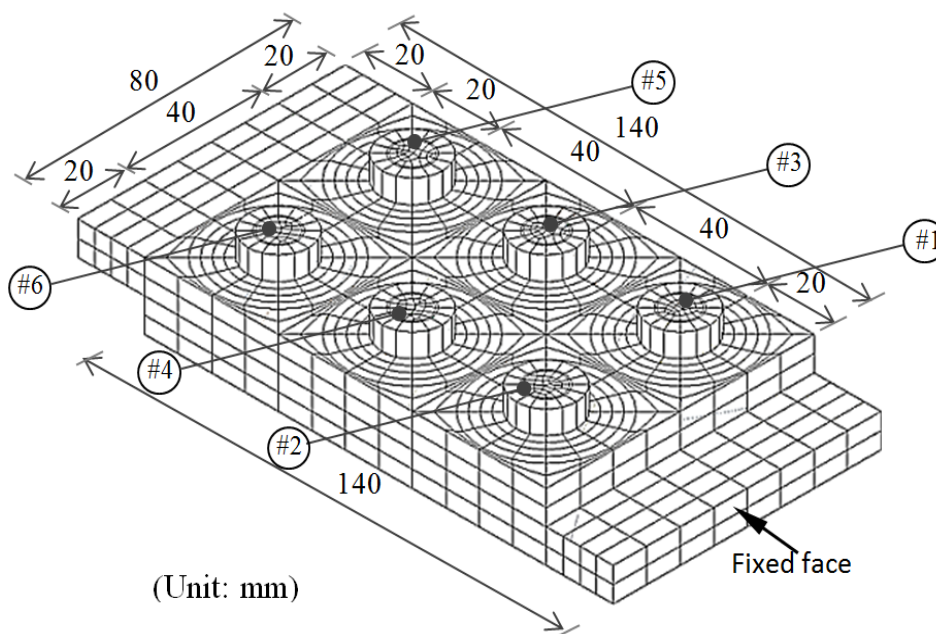


Fig. 3.5 Six-bolt joint model

Using the method applied to the simple one-bolt joint, a static analysis to determine contact area and a frequency response analysis were conducted. The normal condition was set by applying a tightening torque of 24.5 Nm to accord with a pretension force of 12260 N, and the loosening condition is adjusted by applying tightening torques of 20 Nm or 16.5 Nm for pretension forces of 10000 N or 8250 N, respectively. The list of damage cases considered here for the six-bolt model is provided in Table 3.2, where the applied tightening torque on each bolt is detailed for damage case.

Table 3.2 List of torques applied in damage cases for the six-bolt joint model

Condition	Tightening Torque (Nm)					
	Bolt 1	Bolt 2	Bolt 3	Bolt 4	Bolt 5	Bolt 6
Normal	24.5	24.5	24.5	24.5	24.5	24.5
Damage 1	20.0	24.5	24.5	24.5	24.5	24.5
Damage 2	24.5	24.5	24.5	20.0	24.5	24.5
Damage 3	24.5	24.5	24.5	24.5	20.0	24.5
Damage 4	16.5	24.5	24.5	24.5	24.5	24.5
Damage 5	24.5	24.5	24.5	16.5	24.5	24.5
Damage 6	24.5	24.5	24.5	24.5	16.5	24.5

3.4 Validation of laser excitation vibration measurements by the finite element model

In the laser excitation vibration tests, points for excitation and measurements were selected first, to ensure these points excite and measure most natural modes of excited structure. To validate laser excitation vibration measurements by finite element model analysis, the excitation and measurement points for the one-bolt joint and a six-bolt joint are chosen, resulting in excitation points and measurement points as shown in Fig. 3.6.

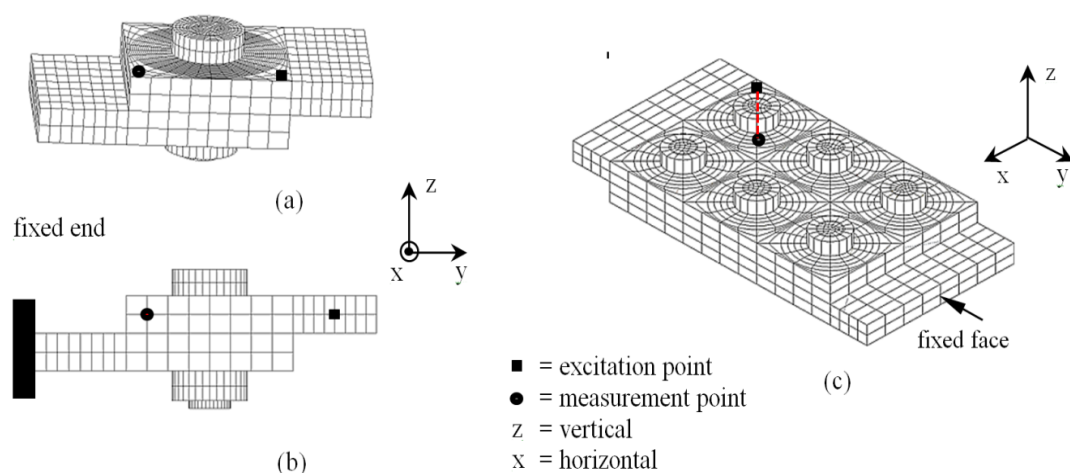


Fig. 3.6 Excitation and measurement points for verification of the model (a) vertical of the one-bolt joint, (b) horizontal of the one-bolt joint, (c) vertical of the six-bolt joint

For the simple one-bolt joint, the tests are to be conducted in the vertical and horizontal directions, as suggested in Fig. 3.6(a) and Fig. 3.6(b), respectively. Since on a complex structure, it is unusual to conduct the vibration test in the horizontal direction of a joint, the test for the six-bolt joint will be carried out in the vertical direction only, as suggested in Fig. 3.6(c). The measurement point of the six-bolt joint model is directly behind the excitation point.

3.4.1 Frequency response on the one-bolt joint model

A vibration test by using the laser excitation without a water droplet was conducted for the one-bolt joint model. The tightening torques is applied by a digital torque wrench for normal condition and loose conditions. The variation conditions to the one-bolt joint model are explained in Table 3.1. In order to compare simulations and experimental results, the frequency response graphs of the two sets of results will be plotted together, to show the degree of agreement between the results and enable an evaluation of the adequacy of the proposed method in modeling bolted joint with one-bolt. The frequency responses of the one-bolt joint in the normal condition are shown in Fig. 3.7.

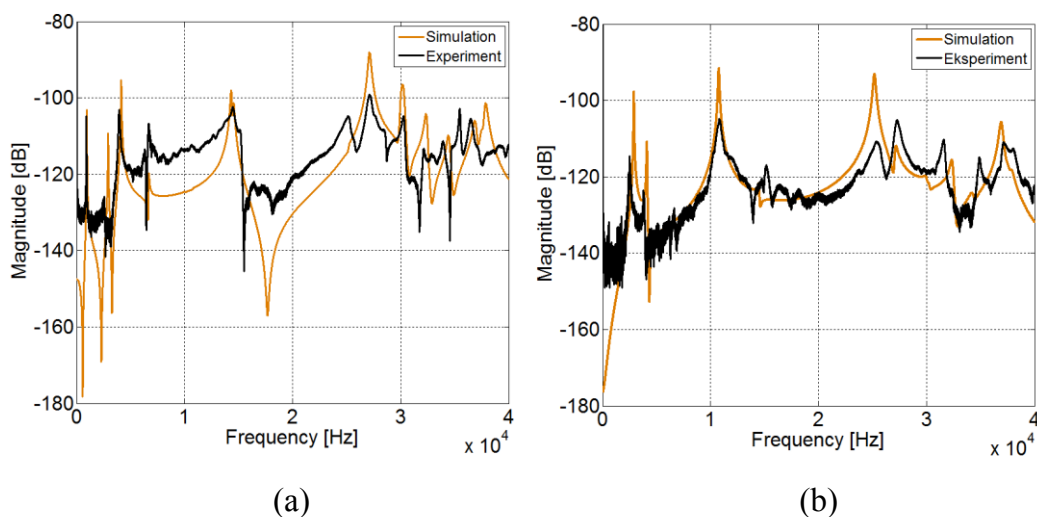


Fig. 3.7 Frequency response of the one-bolt joint in the normal condition (a) in the vertical direction, (b) in the horizontal direction

The frequency responses in the normal condition by simulation and experiment show good agreement, they have similar peaks and tendency over the whole

frequency range. This good agreement can be seen both in the vertical and horizontal directions of tests.

Fig. 3.8 shows the frequency response of the one-bolt joint with loose conditions in the vertical direction, and Fig. 3.9 shows that in the horizontal direction. When the tightening torque is reduced, the resonance peaks in the frequency response shift to lower frequencies. This shift is significant at high frequencies, but it is not clear in lower frequencies. This is seen clearly when all frequency responses with different tightening torque from normal condition to loosening conditions are plotted together. The frequency responses with different tightening torques obtained from the experiments in vertical and horizontal direction are shown in Fig. 3.10.

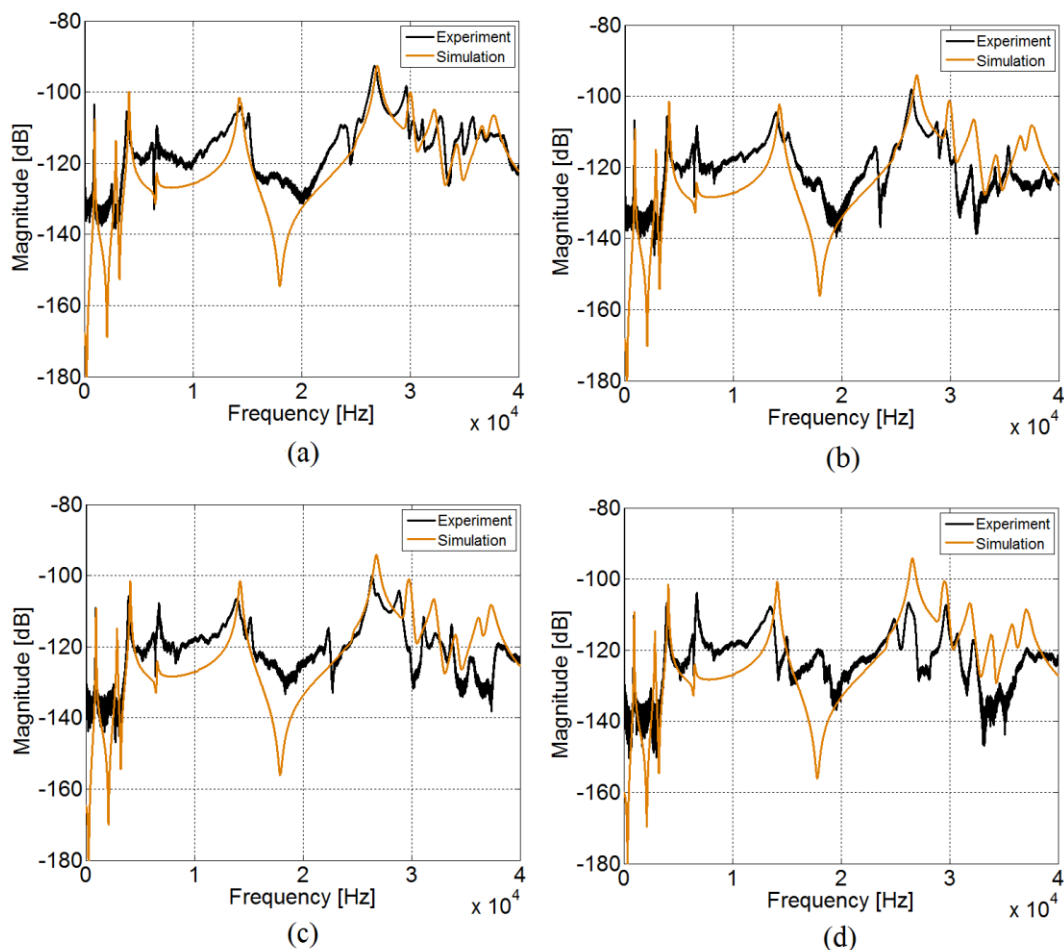


Fig. 3.8 Frequency response of the one-bolt joint in the vertical direction with the loose condition of tightening torques (a) 20 Nm, (b) 18 Nm, (c) 15 Nm, (d) 10 Nm

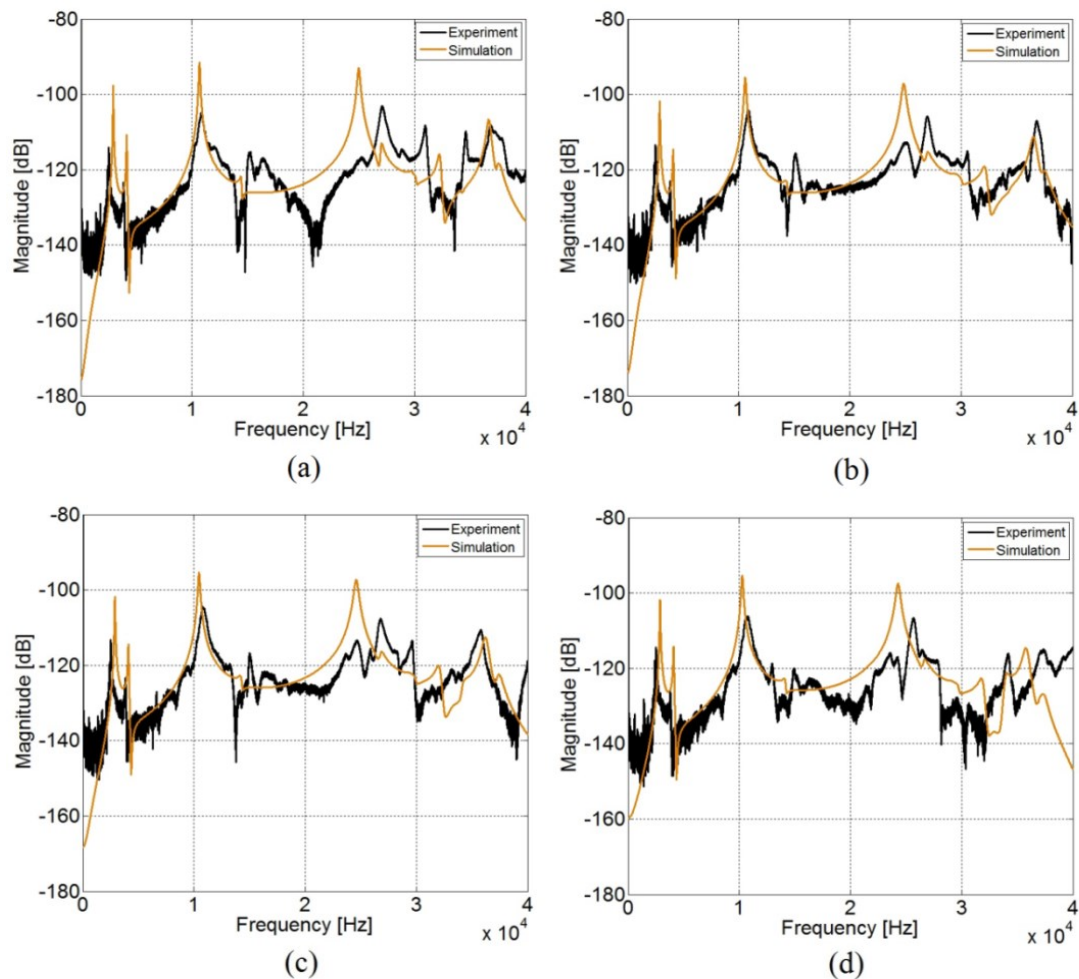


Fig. 3.9 Frequency response of the one-bolt joint in the horizontal direction with the loose condition of tightening torques (a) 20 Nm, (b) 18 Nm, (c) 15 Nm, (d) 10 Nm

Fig. 3.10 shows that the change of natural frequency is more significant at high frequencies than at low frequencies. This is clearly shown when a bolted joint undergoes loosening, the stiffness of the joint is reduced, and the stiffness reduction leads the significant shift of the high frequency resonance peaks to lower frequencies.

The resonance peak shifts at high frequencies can also be considered from the vibration mode shapes. The principal vibration mode shapes of the one-bolt joint model in normal condition are shown in Fig. 3.11. At low frequencies including the modes 1, 3, and 4, the deformation around the bolt is not large. At high frequencies including modes 10, 14, and 16, the mode shapes are complicated, the bolt and the nut undergo the significant elastic deformation. This mode deformation of the bolt

which has different pretension forces in each case of the loosening contribute more to the resonance peak shifts. This explains why the resonance peaks show significant changes at high frequencies rather than at low frequencies.

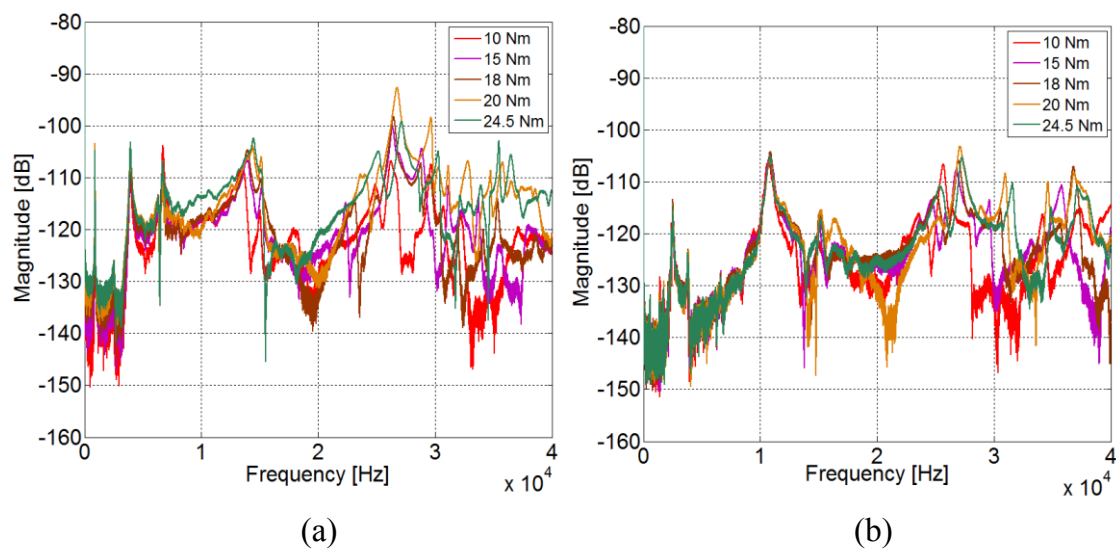


Fig. 3.10 Frequency response of the one-bolt joint by the experiments
(a) in the vertical direction, (b) in the horizontal direction

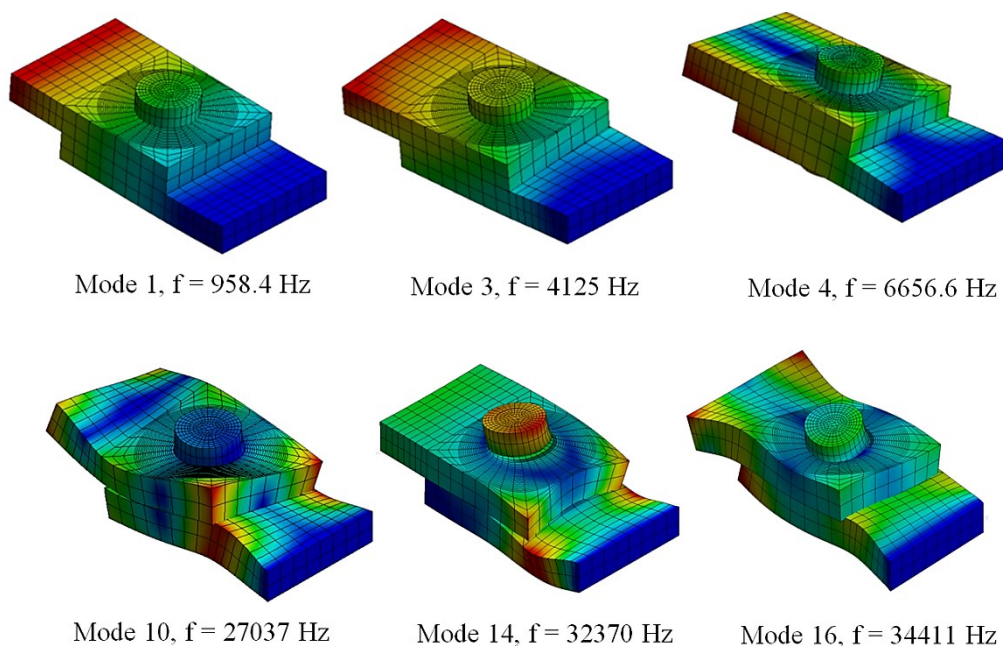


Fig. 3.11 Principal vibration mode shapes of the one-bolt joint model in the normal condition

3.4.2 Frequency response on the six-bolt joint model

To check the integrity of the modeling and to ensure the applicability of the laser excitation vibration test to more complex bolted joint, the simulation and the experiment on six-bolt joint are conducted. Fig. 3.12 shows a plot of the frequency response of the six-bolt joint in the normal condition. Frequency response for loose condition is presented in Fig. 3.13, where damage 1 and damage 5 as representation of loose condition based on damage cases on Table 3.2 are applied. The frequency response shows more resonance peaks in six-bolt joint model compared to that of one-bolt joint model in the range up to 40 kHz. The frequency response graph shows a good agreement between simulation and experiment. The results on six-bolt joint demonstrate that the proposed finite element model in this chapter can be applied well to more complex bolted joint. The frequency responses with different tightening torques (normal and several damage cases) obtained from experiments in vertical direction is presented in Fig. 3.14.

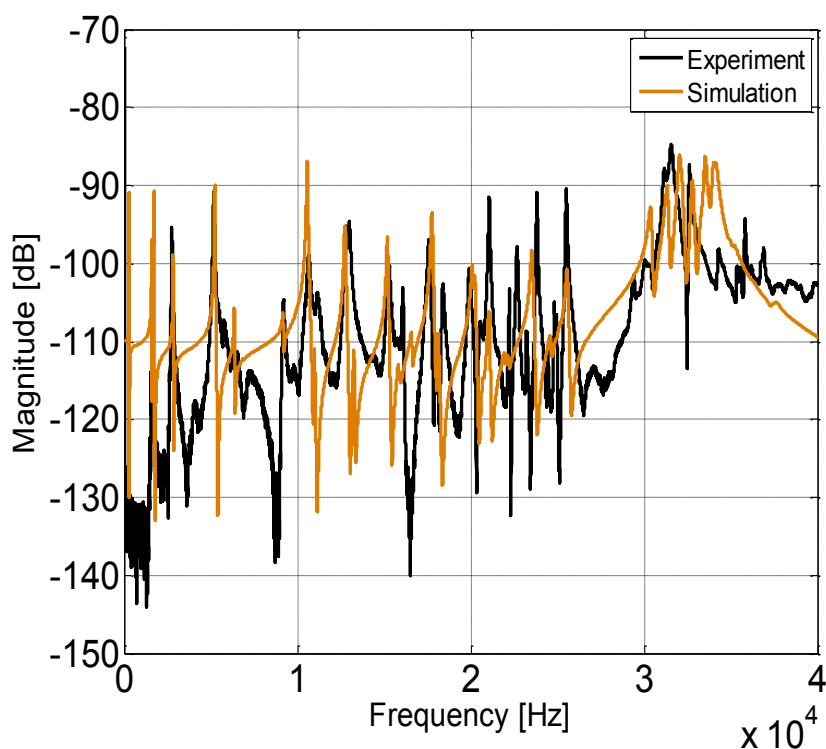


Fig. 3.12 Frequency response of the six-bolt joint in the normal condition

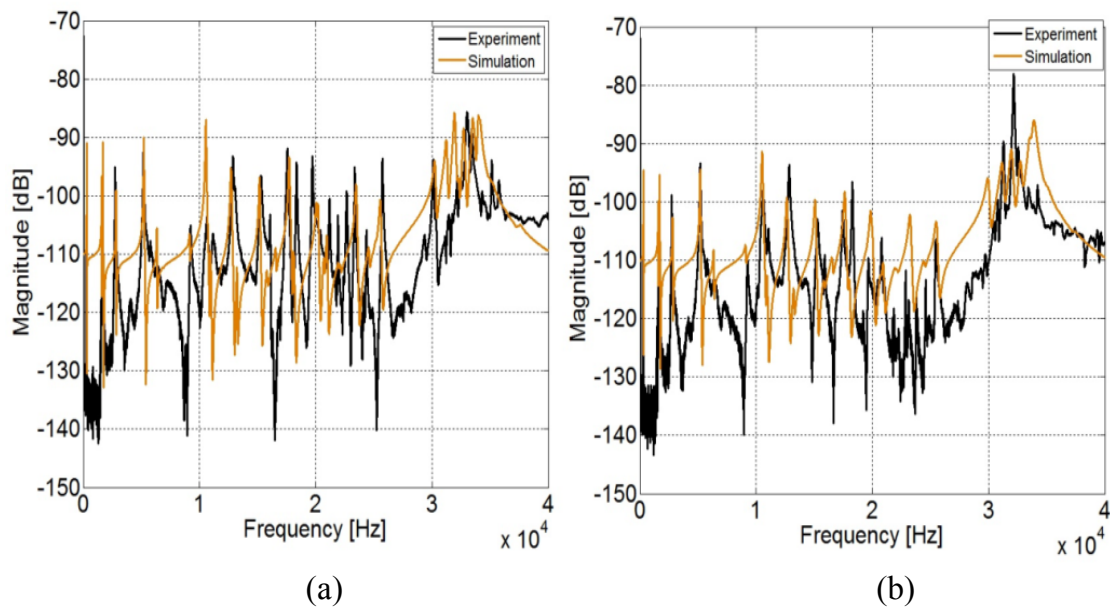


Fig. 3.13 Frequency response of the six-bolt joint in loose condition based on damage cases in Table 2 (a) damage 1, (b) damage 5

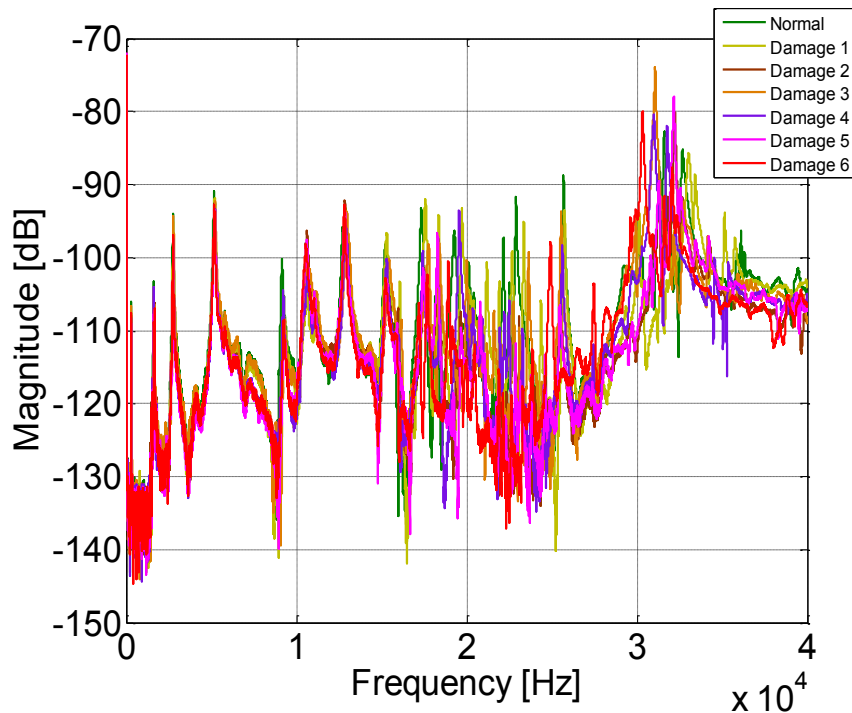


Fig. 3.14 Frequency responses of the six-bolt joint by the experiments

The graph in Fig. 3.14 shows that the frequency response changed significantly at high frequencies due to bolt loosening. This is similar to that of the one-bolt joint.

By this tendency in bolt loosening case, employing the laser excitation vibration measurement system in this dissertation is definitely an appropriate decision, because the high frequency response can be precisely measured by this excitation/measurement. Bolt loosening detection has become much easier by evaluating high frequency response, because the significant response shift in high frequency will be easy to detect.

3.5 Bolt loosening detection approach

3.5.1 Recognition-Taguchi method

The Recognition-Taguchi (RT) method is a statistical evaluation method used for detecting the loose bolts in this study. The RT method is a type of Mahalanobis-Taguchi (MT) method used in the field of quality engineering as a pattern recognition method [35]. In this method, data is measured a number of times under identical conditions, and a unit space for the condition is defined. Information that forms the unit space is called a member. For members comprising a unit space, quantities known as the standard S/N ratio η and the sensitivity β are defined based on a concept of quality engineering [35]. These are then used to define the distance in relation to the unit space using the RT method. For unknown data, distances in relation to unit spaces are calculated and compared to determine to which unit space the unknown data belongs. A value belonging to a member and used in the calculations is referred to as an item. When n is the number of members, and k is the number of items, items are expressed as X_1, X_2, \dots, X_k , and their averages are expressed as m_1, m_2, \dots, m_k . Specifically:

$$m_i = \frac{1}{n} (X_{i1} + X_{i2} + \dots + X_{in}) \quad (3.2)$$

Table 3.3 shows the relation between the items and their averages. The standard S/N ratio η and sensitivity β to each member of the unit space are obtained using the following equations. Using a linear equation L_1

$$L_1 = m_1 X_{11} + m_2 X_{21} + \dots + m_k X_{k1} \quad (3.3)$$

Table 3.3 Variables of members in a unit space

Member	X_1	X_2	...	X_k
1	X_{11}	X_{21}	...	X_{k1}
2	X_{12}	X_{22}	...	X_{k2}
\vdots	\vdots	\vdots	\vdots	\vdots
n	X_{1n}	X_{2n}	...	X_{kn}
Average	m_1	m_2	...	m_k

The sensitivity β_1 is obtained as

$$\beta_1 = \frac{L_1}{r} \quad (3.4)$$

where

$$r = m_1^2 + m_2^2 + \dots + m_k^2 \quad (3.5)$$

The total variation S_{T1} and the variation S_{β_1} of the proportional term are describe as

$$S_{T1} = X_{11}^2 + X_{21}^2 + \dots + X_{k1}^2 \quad (3.6)$$

$$S_{\beta_1} = \frac{L_1^2}{r} \quad (3.7)$$

The error variation S_{e1} and the error variance V_{e1} are obtained by

$$S_{e1} = S_{T1} - S_{\beta_1} \quad (3.8)$$

$$V_{e1} = \frac{S_{e1}}{k-1} \quad (3.9)$$

The S/N ratio η_1 is calculated as

$$\eta_1 = \frac{1}{V_{e1}} \quad (3.10)$$

Similar calculations are performed to obtain β and η for the second member, the third member, and so on until the n th member, and are listed in Table 3.4. The β and η are used to obtain the distance within the unit space. The S/N ratio η is not used directly, but is used as in the following equations and listed in Table 3.5.

$$Y_{1i} = \beta_i \quad (3.11)$$

$$Y_{2i} = \frac{1}{\sqrt{\eta_i}} \quad (3.12)$$

Table 3.4 η and β of the members in a unit space

Member	H	B
1	η_1	β_1
2	η_2	β_2
\vdots	\vdots	\vdots
n	η_n	β_n

Table 3.5 Y of the members in a unit space

Member	Y_1	Y_2
1	Y_{11}	Y_{21}
2	Y_{12}	Y_{22}
\vdots	\vdots	\vdots
n	Y_{1n}	Y_{2n}

The data of the members of a unit space is consolidated in Y_1 and Y_2 . Here, Y_1 represents sensitivity and Y_2 represents standard deviation. The RT method is applied to obtain the distance D for the unit space from the data for the n members in the unit space. A comparison is made with D to determine whether the distance in relation to the data is sufficiently large. The RT method calculates the variance and covariance of Y_1 and Y_2 , and a variance–covariance matrix. The variance of Y_1 is represented by V_{11} , the covariance of $Y_1 \cdot Y_2$ is represented by V_{12} , and the variance of Y_2 is represented by V_{22} , so that the relationship $V_{21} = V_{12}$ is valid. If \bar{Y}_1 is the average of Y_1 and \bar{Y}_2 is the average of Y_2 , then,

$$V_{11} = \frac{1}{n-1} \sum_{i=1}^n (Y_{1i} - \bar{Y}_1)^2 \quad (3.13)$$

$$V_{12} = \frac{1}{n-1} \sum_{i=1}^n (Y_{1i} - \bar{Y}_1)(Y_{2i} - \bar{Y}_2) \quad (3.14)$$

$$V_{22} = \frac{1}{n-1} \sum_{i=1}^n (Y_{2i} - \bar{Y}_2)^2 \quad (3.15)$$

Therefore, the variance–covariance matrix V is

$$V = \begin{pmatrix} V_{11} & V_{12} \\ V_{12} & V_{22} \end{pmatrix} \quad (3.16)$$

and the cofactor matrix A of the variance–covariance matrix V is

$$A = \begin{pmatrix} V_{22} & -V_{12} \\ -V_{12} & V_{11} \end{pmatrix} \quad (3.17)$$

The distance for the first member of the unit space is described by

$$D_1^2 = \frac{1}{2} [V_{22}(Y_{11} - \bar{Y}_1)^2 - 2V_{12}(Y_{11} - \bar{Y}_1)(Y_{21} - \bar{Y}_2) + V_{11}(Y_{21} - \bar{Y}_2)^2] \quad (3.18)$$

The distances $D_2^2, D_3^2, \dots,$ and D_n^2 are obtained for the remaining members of the unit space. The square root of the average of $D_1^2, D_2^2, \dots,$ and D_n^2 is the distance \bar{D} from the zero point of this unit space; i.e.,

$$\bar{D} = \left\{ \frac{1}{n} (D_1^2 + D_2^2 + \dots + D_n^2) \right\}^{1/2} \quad (3.19)$$

The above information is used to examine whether an unknown data value is included in specific unit spaces. Here, using $m_1, m_2, \dots,$ and m_k as the average of a specific unit space being examined, a linear equation

$$L = m_1X_1 + m_2X_2 + \dots + m_kX_k \quad (3.20)$$

is applied to the unknown data $X_1, X_2, \dots,$ and X_k , and the sensitivity β_o and the standard S/N ratio η_o is obtained.

$$\beta_o = \frac{L}{r} \quad (3.21)$$

$$\eta_o = \frac{1}{V_e} \quad (3.22)$$

where

$$r = m_1^2 + m_2^2 + \dots + m_k^2 \quad (3.23)$$

$$S_T = X_1^2 + X_2^2 + \dots + X_k^2 \quad (3.24)$$

$$S_\beta = \frac{L^2}{r} \quad (3.25)$$

$$S_e = S_T - S_\beta \quad (3.26)$$

$$V_e = \frac{S_e}{k-1} \quad (3.27)$$

Next, Y_{1o} and Y_{2o} for unknown data are obtained from β_o and η_o .

$$Y_{1o} = \beta_o \quad (3.28)$$

$$Y_{2o} = \frac{1}{\sqrt{\eta_o}} \quad (3.29)$$

From these relations, the distance in relation to the unknown data value is obtained using

$$D^2 = \frac{1}{2} [V_{22}(Y_{1o} - \bar{Y}_1)^2 - 2V_{12}(Y_{1o} - \bar{Y}_1)(Y_{2o} - \bar{Y}_2) + V_{11}(Y_{2o} - \bar{Y}_2)^2] \quad (3.30)$$

The D and \bar{D} are compared to determine whether the unknown data value is included in the corresponding unit space. Now, the damage index (DI) which determines the condition of bolt, normal or not, is defined by

$$\text{Damage Index (DI)} = \frac{D}{\bar{D}} \quad (3.31)$$

If $DI > 1$, the bolt is in damage condition (loosening), and if $DI \leq 1$, the bolt is in normal condition

3.5.2 The location of excitation and measurement points

The excitation conditions must be designed to excite all vibration modes of the joint in the direction of the measurement, making it necessary to select a suitable position for the excitation. The characteristic change in the measured frequency responses should be sensitive to loosening of every bolt, making it necessary to locate the measurement points close to each of the bolts. The excitation and measurement points for bolt loosening detection are shown in Fig. 3.15.

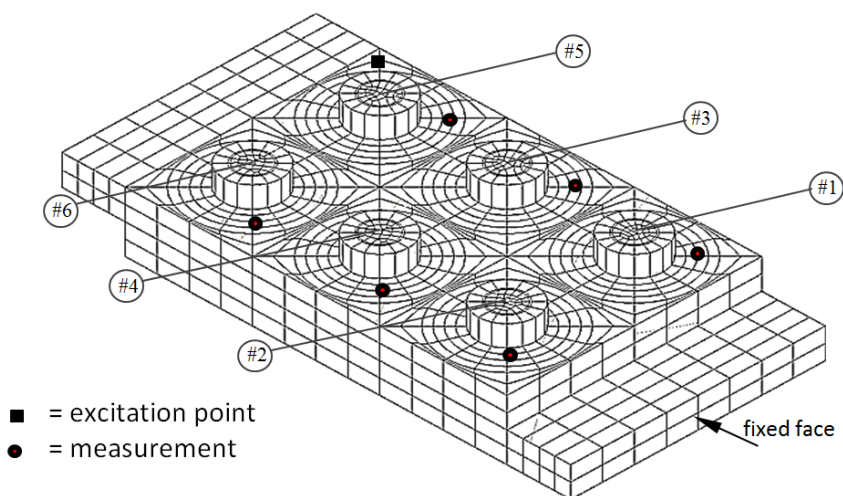


Fig. 3.15 Excitation and measurement point positions used in bolt loosening detection

3.6 Diagnosis results

By taking damage scenarios based on the damage cases on Table 3.2, vibration measurement by using laser excitation is conducted. Excitations are given on a point, and vibration measurement is conducted on several points close to the bolt which represent measurement on each bolt.

3.6.1 *Diagnosis process*

To create the unit spaces for diagnosis, the power spectra of responses in normal condition under identical conditions were measured a multiple number of times. In other words, the response varied slightly even in the same conditions due to slight differences in the actual state. For this purposes, the measurement process involved loosening all bolts after one measurement, refastening the bolts under the same tightening condition as before, and measuring the response under the same test condition. The process was repeated, and ten sets of power spectrum data for normal condition were measured. The measured data were analysed as follows with regards to data sample regions and data sample points for diagnosis:

1. A frequency range in high frequency from 12.5 kHz to 40 kHz is set within the range of interest to perform the diagnosis.
2. The range is divided into multiple sub-regions, where the frequency band of sub-regions in the data analysis was 125 Hz.
3. An average value is obtained as an item within each of the sub-regions.
4. The items are obtained within all the sub-regions.

The unit space in a member was created with the items in the member in the range of interest, and it was performed on normal condition only. This unit space was used to perform a comparison with unknown data and used for a diagnosis. The correlation between the data belonging to the unit space of normal condition and unknown data (loosening condition) in the same range of interest was evaluated with the damage index.

3.6.2 Results and discussion

To investigate the applicability of the diagnosis in this study, the power spectra of the responses were measured at six points, where each point had its position close to a bolt. Every point of measurement represents the measurement on each bolt, so there were six bolts and six points of measurement.

The measurements were conducted first for the normal condition to get the unit space that was constructed from ten sets of power spectrum data. The measurements for several damage conditions were then conducted to get one set of power spectrum data for each case of damage. By comparing the damage data with the unit space, a damage index was developed. The damage index for each bolt for the simulation and experiments is shown in Table 3.6 and Table 3.7, respectively.

Table 3.6 Damage index based on simulation

Case \ Position	Bolt 1	Bolt 2	Bolt 3	Bolt 4	Bolt 5	Bolt 6
Damage 1	36.00	14.00	14.60	11.90	18.00	6.32
Damage 2	16.86	16.82	15.08	55.68	14.08	14.27
Damage 3	15.75	15.65	15.90	16.15	17.30	16.30
Damage 4	56.70	20.74	20.05	31.20	27.80	10.30
Damage 5	25.22	19.30	25.88	40.03	16.51	18.97
Damage 6	25.73	26.05	24.54	28.90	33.10	27.70

Table 3.7 Damage index based on experiments

Case \ Position	Bolt 1	Bolt 2	Bolt 3	Bolt 4	Bolt 5	Bolt 6
Damage 1	10.40	7.00	1.60	0.67	0.45	0.41
Damage 2	0.45	2.20	0.44	5.47	1.62	0.62
Damage 3	1.80	2.20	3.11	2.38	7.76	2.56
Damage 4	29.30	9.10	5.30	3.20	2.53	2.86
Damage 5	0.58	1.88	0.32	5.93	4.70	2.39
Damage 6	3.73	3.25	7.54	0.82	11.43	3.77

Table 3.6 and Table 3.7 show that most of damage index numbers are greater than 1, which means that the damage condition (loosening) of the joint can accurately be detected in every position of measurement, and the highest value of damage index in the same damage case represents the position of the loose bolt. These results correspond to the scenario of the cases of loosening that has been designed in this dissertation.

3.7 Concluding remarks

In this dissertation, bolt loosening detection by vibration testing using non-contact laser excitation and a finite element model of bolted joint undergoing loosening were proposed to investigate modelling and detection of bolt loosening on bolted structures. In addition, through a comparison between simulations and experimental results, the effectiveness and usefulness of laser excitation by laser ablation on vibration measurement and bolt loosening detection approach were confirmed.

To model a structure with bolted joints in a loosening condition, it is necessary to change the pretension force, and contact conditions between parts from the initial conditions. The frequency response analysis by pre-stressed modal analysis has shown that the proposed modelling method works well and the experimental results show good agreement with the simulation results. The use of the laser excitation vibration measurement arrangement in this dissertation enabled a high degree of measurement reproducibility; offering the promise that the quality and reliability of the bolt loosening detection methodology can be improved. Both the simulation and experimental results for the bolt loosening detection showed that various loosening states and their positions can be effectively identified by using the Recognition-Taguchi method as a frequency response based approach, which requires excitation at a point and measurements at several points close to the bolts.

Chapter 4

Damage Detection in Membrane Structures Using Non-contact Laser Excitation and Wavelet Transformation

Membrane structures as one important application in engineering are extremely light and flexible. These properties cause damage identification in membrane structures using vibration approach is not easy, and so the damage identification requires non-contact excitation and measurement with convenient operation. To solve the problems, in this chapter author proposes damage detection in membrane structure using non-contact laser excitation generated by laser-induced breakdown.

4.1 Introduction

Membranes are widely used in a number of fields of engineering as membranes are thin, light, flexible, and translucent. There are numerous existing practical applications of membrane structure in architectural and civil engineering structures, diaphragms in switches and transducers, biomedical prosthesis such as artificial arteries and organs, and space-based applications such as radio antennas, optical reflectors and solar sails. From this background, research into membrane structures has become an important research topic in mechanical engineering contributing to ensuring the proper functioning of membrane structures, and assessment of vibration of membrane structures is important and has been investigated for at least three centuries [36].

Vibrating membranes have been investigated with different types of excitation and vibration measurement methods. Because of the extreme flexibility and lightness of membranes, the standard methods of experimental modal analysis, which involve attaching accelerometers and shaker stringers directly to a vibrating structure, cannot be used with membranes, since these techniques lead to non-negligible added mass and stiffness that influences and skews the results, making the use of non-contact measurement methods essential [36]. Chobotov investigated the non-linear vibration of membranes [37], with an experimental system using horn-acoustical excitation and employing a capacitance displacement sensor to measure the fundamental mode of circular Mylar membrane. Jenkins performed experiments using local excitation on low tensioned membranes [38,39] with loudspeaker to provide acoustic excitation and a laser vibrometer to measure the natural frequencies and mode shapes of circular Mylar polyester membrane. However, using acoustic exciters like horns and loudspeakers require attaching these exciters close to the vibrating structure. Loudspeakers may affect the characteristics of the sound field or placement may be difficult because of the shape and size of loudspeakers [18], and when producing acoustic excitation, the loudspeakers give a finite-area excitation while point excitation is required for ideal vibration measurement. Kajiwara conducted experiments on membrane structures in vacuum using non-contacting laser excitation to excite membrane structures, and used a laser Doppler vibrometer (LDV) to measure the vibration response [40]; however this method requires attaching light metal part at the point of excitation of the membrane structure to generate laser ablation adding mass and stiffness to the membrane.

Based on the above, those issues have led to research into acoustical excitation without any attachments to measured structures which permits some distance to the excited structure and gives the possibility of conducting experiments in small areas. Vibration test using laser-induced breakdown (LIB) involves no any attachments to measured structures, and offers the possibilities of applying acoustical excitation on a point with some distance between exciter and membrane structure, even in really small area.

In this dissertation, a vibration testing and health monitoring system based on an impulse response excited by laser is proposed to detect damage on membrane structures. A high power Nd: YAG pulse laser is used to generate an ideal impulse on the membrane structure by applying shock wave generated by LIB in air. A health monitoring apparatus is developed with this vibration testing set-up and a damage location detecting algorithm which only requires the vibration mode shape of the damaged membrane is developed. Artificially induced damages to membrane structure are provided by cutting and tearing the membrane. The vibration mode shapes of the membrane structure extracted from the vibration testing by LIB and LDV are analyzed by two-dimensional (2-D) continuous wavelet transformation (CWT). The effectiveness of the present approach is verified by finite element analysis (FEA) using ANSYS 14.0 and experimental results. Finally, a method for damage detection in membrane structures is proposed by applying 2-D CWT and an iso-surface concept to the membrane structure with different types of damage. The effectiveness of the present approach is verified by simulations.

4.2 Vibration testing system using LIB

4.2.1 Acoustic excitation by LIB

In this dissertation, an excitation to a membrane structure is applied in the form of acoustic excitation achieved by generating an ideal point sound source at specific location via LIB which offers the possibility of conducting experiments with acoustic excitation in small and limited space. In the vibration testing here, the acoustic excitation set-up is configured by combining a high power Nd: YAG pulse laser (Surelite III, Continuum Inc., wavelength: 1064 nm, laser beam radius: 4.75 mm, pulse width: 5 ns, maximum output: 1 J), and a convex lens which is placed on an optical table to focus the laser beam and generate the point sound source LIB. The set-up for the application of the acoustic excitation to a membrane structure by LIB is shown in Fig. 4.1, where the laser beam produced by Nd: YAG pulse laser passing through the convex lens, and the LIB then occurs at a point determined by the distance equal to the focal length of the convex lens. The LIB at the point of focus generates the sound, and the sound excites the membrane, this phenomenon is termed acoustic excitation by LIB.

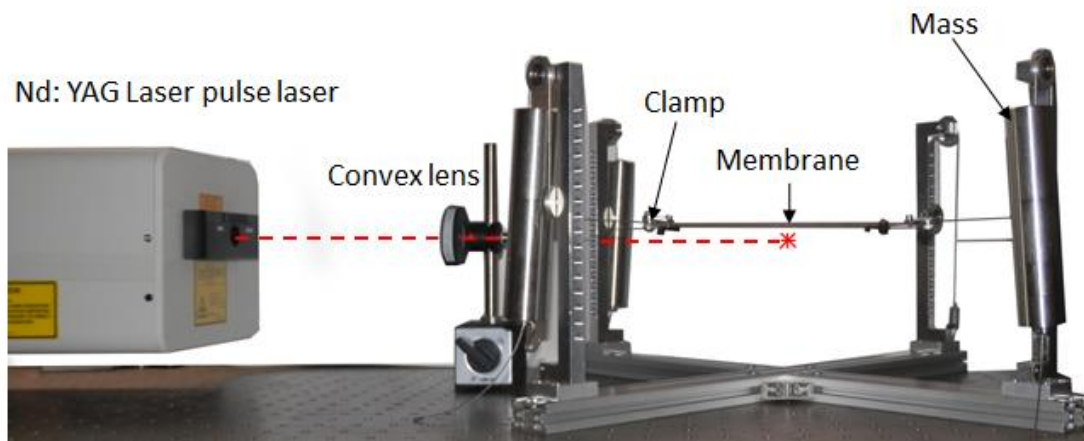


Fig. 4.1 Acoustic excitation of a membrane structure by LIB

4.2.2 Measurement and analysis of the output

To measure the output response, two LDVs are used to obtain the responses of the membrane structure. One LDV is fixed at the center of the membrane as a reference point, while the other is moved along the membrane to measure the vibration response. A spectrum analyzer (A/D; NI-4472B, Software; Catec CAT-System) is used to analyze the Fourier spectrum of the vibration of the membrane. The vibration mode shapes are extracted by analyzing the measured data on the membrane. The vibration testing apparatus and arrangement for the membrane structure are shown in Fig. 4.2.

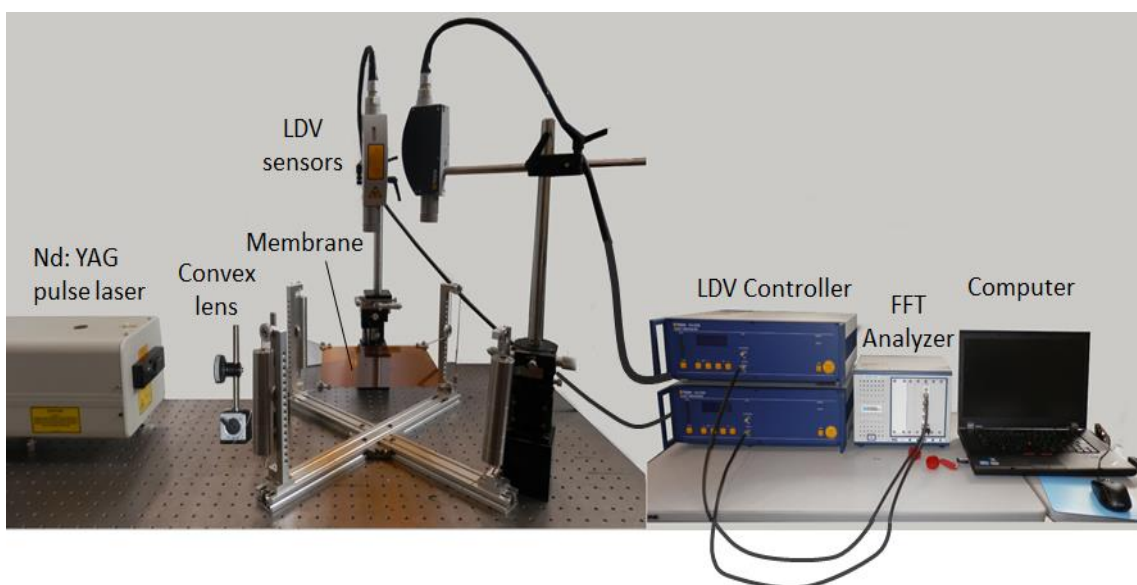


Fig. 4.2 Vibration testing apparatus and arrangement for the membrane structure

4.2.3 Membrane structure setup

The membrane material is Kapton, manufactured by Du Pont-Toray Co., Ltd. Owing to its good resistance to temperature. Kapton is often used in space applications. The membrane here is 200 mm × 200 mm and 50 μm thick, with a mass density of 1420 kg/m³, Poisson ratio 0.29, and Young's modulus 3.4 GPa.

The membrane is clamped on four sides by a metal clamps. Three sides are stretched by three 700 gram masses, and the other side is fixed. The masses and fixed sides are connected to the metal clamps by steel wires. This membrane structure is supported by a base, which is fixed to an optical table. In order to extract the mode shapes of the membrane, the responses are measured at the intersections in 20 mm interval grid lines, resulting 11 × 11 measurement points on the membrane.

4.2.4 Mode shape estimation

Any discrete system can be described by equation of motion:

$$M\ddot{x}(t) + C\dot{x}(t) + Kx(t) = F(t) \quad (4.1)$$

where M, C, K are the mass, damping and stiffness matrices, respectively. Laplace transform of equation of motion Eq. (4.1) gives:

$$(Ms^2 + Cs + K)X(s) = F(s) \quad (4.2)$$

where s is a Laplace variable. Eq. (4.2) can be rewritten as

$$B(s)X(s) = F(s) \quad (4.3)$$

where $B(s)$ known as a system matrix. Transfer function matrix is defined as follows:

$$H(s) = B(s)^{-1} \quad (4.4)$$

Evaluating the transfer function matrix along the frequency axis ($s = i\omega$) results in frequency response function (FRF) matrix given as

$$H(\omega) = X(\omega)[F(\omega)]^{-1} \quad (4.5)$$

When excitation is an impulse force, ideally the Dirac delta function, the $F(\omega) = 1$, and Eq. (4.5) will be changed to be the same as Eq. (2.5)

$$X(\omega) = H(\omega) \quad (4.6)$$

Matrix H of size $m \times m$, where m denotes a number of degrees of freedom, contains individual FRFs $H_{jk}(\omega)$ obtained by impacting point k and measuring the response at point j . To determine one column of the FRF matrix $H(\omega)$ the response signal is measured in all points whereas the excitation is applied the same one point. Mode shape is contained in each row or columns of FRF matrix.

4.3 2-D CWT for damage detection in membrane structure

The mode shape of a structure can be treated as a spatially distributed signal, allowing the 2-D CWT coefficients to be computed for this signal. Analysis of the mode shapes by a continuous wavelet transform is important to detect damage because simply looking for anomalies in the mode shapes may not identify damage. However, 2-D CWT can recognize undetected anomalies using the mode shape. Because it has an excellent performance as a singularity scanner, it is mostly used to detect features [41], and 2-D CWT can also recognize unclear anomalies in the mode shape.

The 2-D CWT considered in this dissertation is based on the formulation by Antoine [42], and wavelet computations are performed using MATLAB[®] and the YAWTb toolbox [43]. The procedure to detect the position of damage in the membrane structure is adopted from the procedure suggested by Fan [41], using the 2-D CWT derivative Gauss (Dergauss2d), which was used successfully for detecting damage on plates using mode shape data.

4.3.1 2-D CWT derivative Gauss

If there is a 2-D image/signal of $s(\vec{x}) \in L^2(\mathbb{R}^2, d^2\vec{x})$, its 2-D CWT (with respect to the wavelet ψ) $S(\vec{b}, a, \theta) \equiv T_\psi s$ is the scalar product of s with the transformed wavelet $\psi_{\vec{b}, a, \theta}$ and considered as a function of (\vec{b}, a, θ) as:

$$\begin{aligned} S(\vec{b}, a, \theta) &\equiv \langle \psi_{\vec{b}, a, \theta}, s \rangle = a^{-1} \int_{\mathbb{R}^2} \overline{\psi(a^{-1}r_{-\theta}(\vec{x} - \vec{b}))} s(\vec{x}) d^2\vec{x} \\ &= a \int_{\mathbb{R}^2} \overline{\hat{\psi}(ar_{-\theta}(\vec{k}))} e^{-i\vec{b} \cdot \vec{k}} \hat{s}(\vec{k}) d^2\vec{k} \end{aligned} \quad (4.7)$$

where,

$$\begin{aligned}
S(\vec{b}, a, \theta) &= \text{wavelet coefficient of transformed signal} \\
\psi_{\vec{b}, a, \theta} &= \text{wavelet function} \\
\hat{\psi} &= \text{Fourier transform of wavelet function} \\
\vec{b} &= \text{translation vector} \\
a &= \text{scaling factor} \\
\theta &= \text{rotation angle} \\
\vec{k} &= \text{Fourier transformation function} \\
r_{-\theta} &= \text{rotation matrix.}
\end{aligned}$$

Gaussian filtering is a widely used approach to filter out the high frequency noises. In this case, the desired signal can be obtained by convolving the differentiated mode shape $s(x,y)$ with a Gaussian $g(x,y)$ as:

$$\tilde{s} = g(x, y) * \left(\frac{\partial}{\partial x}\right)^m \left(\frac{\partial}{\partial y}\right)^n s(x, y) \quad (4.8)$$

where (*) denotes the convolution operator. The 2-D Gaussian is defined as

$$g(x, y) = \exp\left(-\frac{|\vec{x}|^2}{2\sigma^2}\right) = \exp\left(-\frac{x^2+y^2}{2\sigma^2}\right), \vec{x} = (x, y) \quad (4.9)$$

Using the well-known property of convolution, the following equation is obtained

$$\tilde{s} = g(x, y) * \left(\frac{\partial}{\partial x}\right)^m \left(\frac{\partial}{\partial y}\right)^n s(x, y) = \left(\frac{\partial}{\partial x}\right)^m \left(\frac{\partial}{\partial y}\right)^n g(x, y) * s(x, y) \quad (4.10)$$

When the derivative of a 2-D Gaussian as the mother wavelet is adopted and equation (1) is rewritten as a convolution, the equation becomes:

$$S(\vec{b}, a, \theta) \equiv (\psi_{a,\theta} * s)(\vec{b}) = \left(\left(\frac{\partial}{\partial x}\right)^m \left(\frac{\partial}{\partial y}\right)^n g_{a,\theta} * s\right)(\vec{b}) = \tilde{s}_{a,\theta}(\vec{b}) \quad (4.11)$$

where $\left(\frac{\partial}{\partial x}\right)^m \left(\frac{\partial}{\partial y}\right)^n g_{a,\theta}$ is the Gaussian filter. Hence, the desired differentiated and filtered signal can be obtained by a 2-D wavelet transform of the original mode shape with the derivative of the 2-D Gaussian (Dergauss2d) as the wavelet.

Fan [41] has suggested using $m = n = 2$ for damage detection because it gives a smoother result and is blind to the “healthy” mode shape. By not considering the healthy mode shape, the wavelet coefficients will have relatively high values when

singularity is detected. In this dissertation, the above $m = n = 2$ parameters are adopted to detect the position of damage on the membrane structure.

4.3.2 The procedure for damage detection on the membrane

The following procedure suggested by Fan [41] will be used to detect damage locations in the membrane structure:

- Step 1: Transforming the mode shape data by 2-D CWT. The 2-D CWT of the membrane mode shape is computed using the YAWTb toolbox [43] in a continuous scale variation.
- Step 2: Applying a boundary distortion treatment to wavelet coefficient. All the wavelet coefficients in the “boundary effect regions” are set to zero. With this treatment, damage at the edge of the membrane cannot be detected, and this dissertation is only concerned with detecting membrane damage in non-edge locations.
- Step 3: Calculating the threshold value. The maximum and minimum values of the updated wavelet coefficient are calculated. The largest absolute value is multiplied with a threshold ratio between 0 and 1 to generate a threshold value.
- Step 4: Generating the iso-surface graph. The points with the threshold values are connected to form an “iso-surface” connecting points of equal elevation with contour lines.

In this dissertation, the first principal mode shape of the membrane is employed to detect the position of damage, but other mode shapes at higher frequencies will be used to detect the damage if the damage cannot be detected by this first principal mode shape. This approach is based on the idea that the high amplitude at specific area of the mode shape of the damage could occur in higher frequency modes, and this mode shape shows the dominant peak of the position of the damage. Further, the present vibration testing method enables high frequency vibration measurements due to the non-contact excitation making it possible to detect the position of the damage on the membrane using higher order mode shapes. Several wavelet transformations for damage detection in membrane structures are explained in Appendix.

4.4 FEA investigation of damage detection on the membrane structure

4.4.1 Model description

The finite element analysis software ANSYS 14.0 is used to conduct the pre-stress modal analysis to generate the mode shapes of normal and damaged membrane structures. The SHELL181 element of ANSYS is used to construct the physical model of the membrane, and the SOLID186 element is employed to model the clamps at the corners of the membrane. The contact between the membrane and the clamps is presented by surface-surface contact elements, pairs of elements, the contact element CONTA174 and target element TARGE170. Bonded type contacts are applied to each contact between the membrane and a clamp. The membrane is uniformly divided into approximately 10,000 $2\text{ mm} \times 2\text{ mm}$ four node membrane elements. The mode shapes are extracted from all 11×11 node data in the model. The finite element model of the membrane structure is shown in Fig. 4.3.

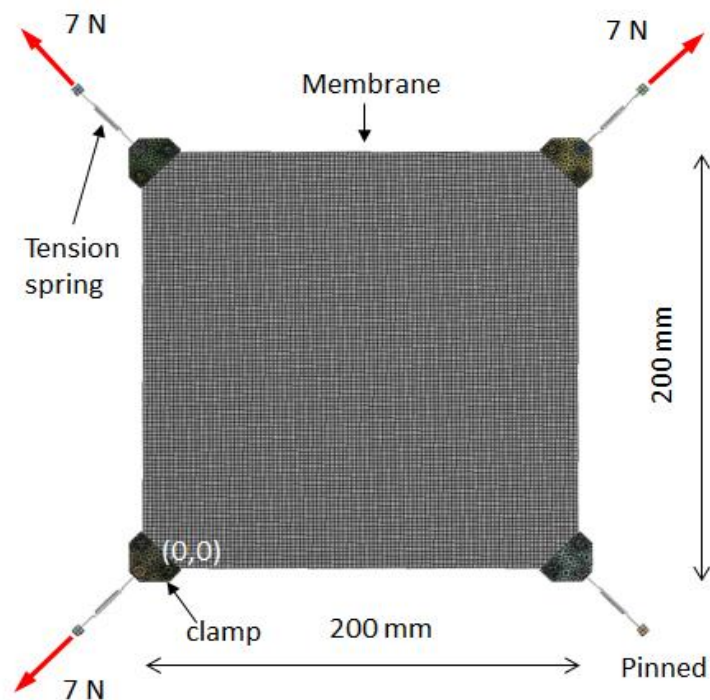


Fig. 4.3 Finite element model of the membrane structure (with forces and meshing elements)

Fig. 4.3 shows that the membrane is tightened by wires at the four corners, where each wire is modeled as a tension spring with a stiffness of 5000 N/m. Three wires are kept in tension by 700 gram masses, equivalent to 7 N of tension force, and one wire is pinned to the base.

The membrane is modeled in normal (without induced damage) and damaged conditions. The damaged conditions are achieved by cutting or tearing the membrane in specified forms and positions. The static structural analysis is conducted first, followed by the modal analysis. The results of static structural analysis are plotted as the initial condition of the modal analysis, and this is termed the pre-stress modal analysis. The mode shapes of the membrane structure are then calculated from the results of this analysis.

4.4.2 Analysis of the normal condition by simulation

To apply the damage detection approach to simulations, the normal condition of the membrane must first be established to validate the finite element model, without exposing the membrane to any type of imposed damage. Simulation results of the normal membrane vibration are presented in Fig. 4.4. The first principal modeshape (Fig. 4.4 (a)) is interpolated by cubic spline interpolation to get more data along the membrane (Fig. 3.4(b)), and then processed by 2-D CWT, with scale $a = 2$ (Fig. 4.4(c)). To get a clearer view of the state of the 2-D wavelet coefficient, the boundary treatment, removing large irregularities at the boundaries, needs to be applied (Fig. 4.4(d)).

From wavelet coefficient with the boundary treatment obtained from the simulation data, it can be seen that there are peaks at the corners caused by the clamps; these do not arise from damage to membrane. The overall wavelet coefficient does not show any dominant peak for the wavelet coefficient, making it unnecessary for the next process to employ iso-surface generation.

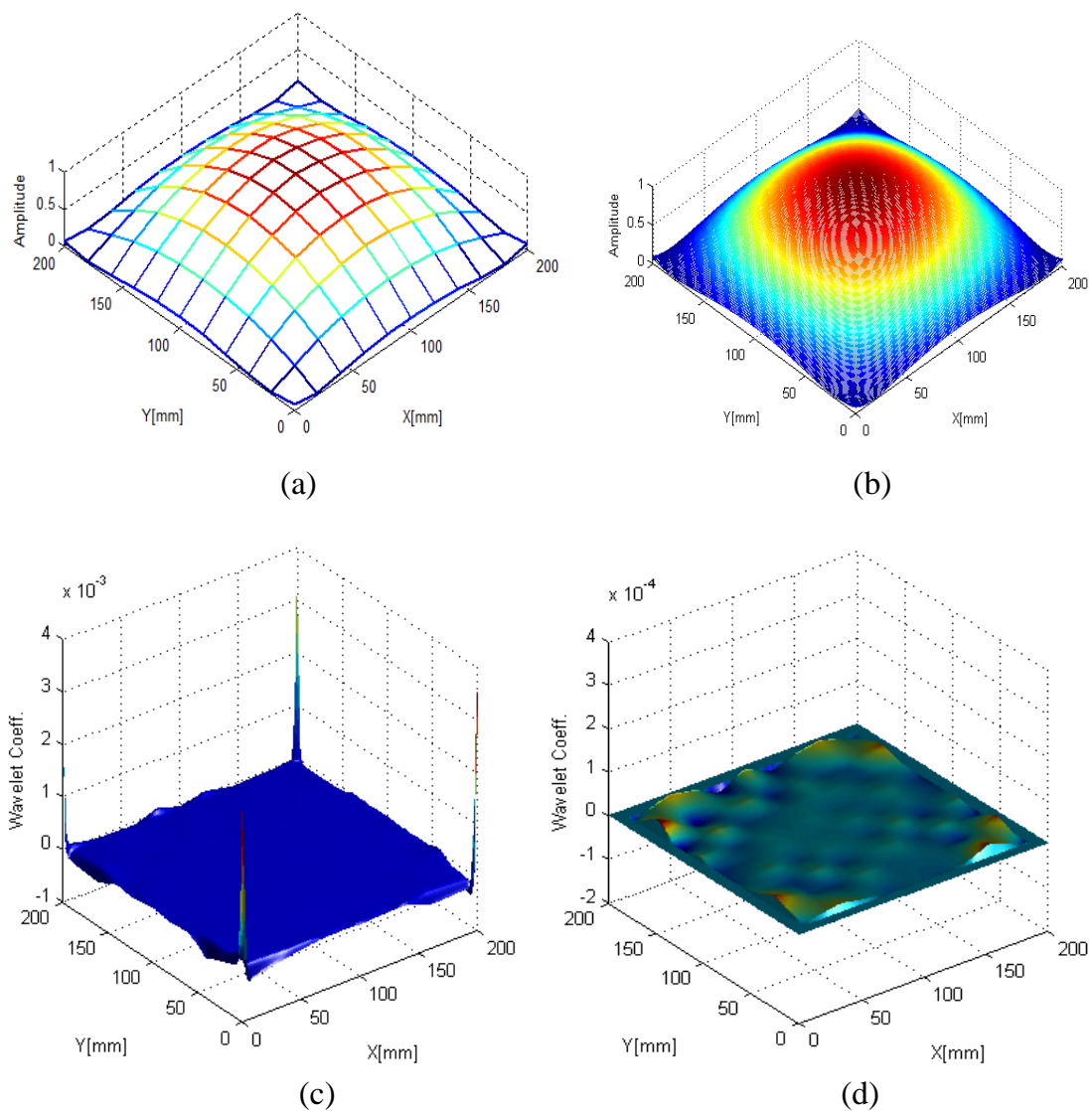


Fig. 4.4 Simulation results of the normal membrane vibration (a) first principal mode shape (41.8 Hz), (b) interpolated first principal mode shape, (c) wavelet coefficient, (d) wavelet coefficient with boundary treatments

4.4.3 Application of damage detection

To examine details of the results generated by the damage detection approach by 2-D CWT and FEM simulation, three different damage conditions were induced in the membrane finite element models. The Finite element model of the membrane with three damage scenarios is presented in Fig. 4.5, and details of the three damage cases are listed in Table 4.1.

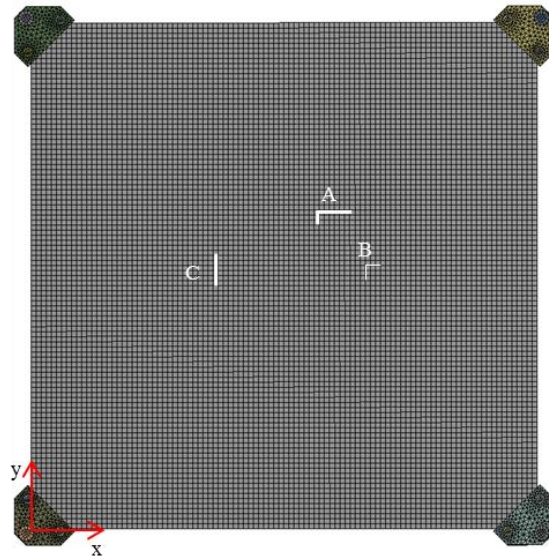
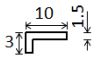
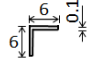
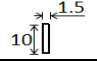


Fig. 4.5 Finite element model of membrane with damage scenario detailed in Table 4.1

Table 4.1 Details of the damage induced on the membrane

Item	Damage type	Damage size (mm)	Closest measurement point (x,y) in mm
A	L-cut		(120,120)
B	L-tear		(140,100)
C	I-cut		(80,100)

In industry, the shape and dimensions of membrane damage depend on the product. For example, a solar sail that sustains damage due to the impact load from a micrometeorite could tear or have an area completely removed. It is assumed that the types of damage introduced in this dissertation adequately represent ideal damage from the field. Although the damage areas in this dissertation can be observed up close, the damage size compared to the overall size of actual membranes makes damage detection difficult. Hence, a damaging detection method is necessary to monitor structural health. The effect of damage size on damage detection should be evaluated in the future.

There are two types of damage: cut and tear. The difference between cut and tear is that a cut requires removing some mass part of the membrane, while a tear does not remove any mass part of the membrane. The damage is simulated by pre-stress modal analysis and then the mode shapes are calculated from this analysis.

The first principal mode shape of the membrane is employed to detect the position of the damage by applying the 2-D CWT and the iso-surface concept. When the position of the damage cannot be established by the first principal mode shape, higher order mode shapes that may appear at high frequency will be employed. This will be possible, because laser excitation offers the possibility of measurements at high frequency. Simulation results for detecting the L-cut damage (A in Table 4.1) on the membrane are shown in Fig. 4.6.

To detect the L-cut damage on the membrane, the first principal mode shape data (Fig. 4.6 (a)) is used. The mode shape is then interpolated to obtain more data for the mode shape of the membrane (Fig. 4.6 (b)). The interpolated data of the mode shape is then analyzed using 2-D CWT, but the result still does not show the signature of the damage, because the results of the transformation have very high values on the corners and the edges of the 2-D wavelet coefficient (Fig. 4.6(c)), this condition overwhelms the damage signature.

To remove the effect of the high boundary values induced by the anchoring, the boundary treatment on wavelet coefficient data is implemented. From 2-D wavelet coefficient with the boundary treatment, scale $a = 2$, a dominant peak can be seen, and this may assumed to be the damage position (Fig. 4.6 (d)). The exact position of the damage can be verified by applying the iso-surface concept, where some of the treated 2-D wavelet coefficients from different scales (1-20) which have the same value range are connected to form surfaces, and the appearance becomes pointlike (Fig. 4.6 (e) and Fig. 4.6 (f)). The iso-surface for detecting L-cut position shows the damage position accurately similar to the damage scenario, where the closest measurement point is (120,120). These results allow the assumption that the FEA and damage detection approach using 2-D CWT works well in determining damage position on a membrane structure.

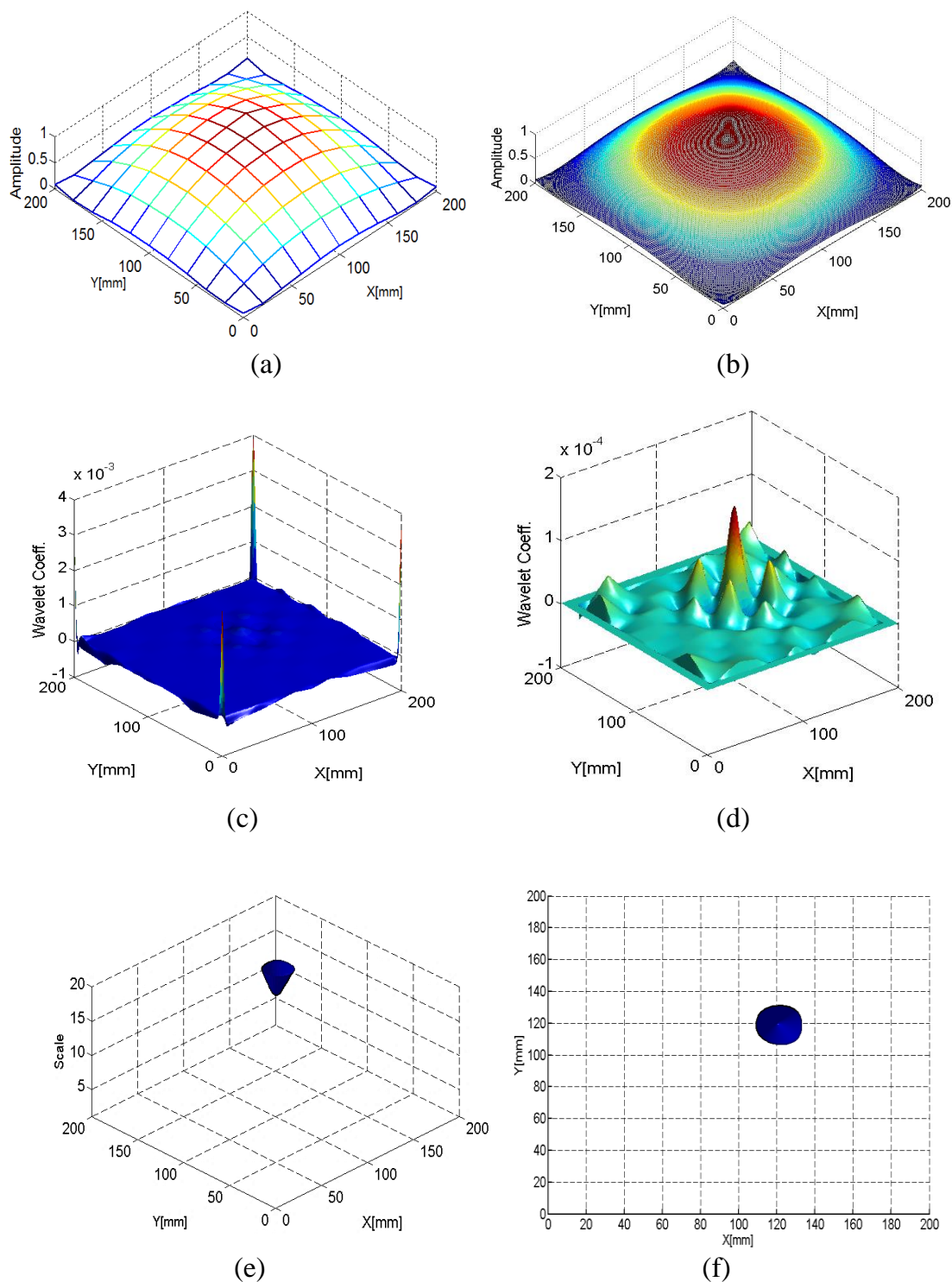


Fig. 4.6 Simulation results for detecting the L-cut damage (A in Table 4.1) on the membrane (a) first principal mode shape (41.78 Hz), (b) interpolated first principal mode shape, (c) wavelet coefficient, (d) wavelet coefficient with boundary treatment, (e) 3-D view of iso-surface, (f) top view of iso-surface

The same procedure as for detecting the L-cut is used to determine the position of the damage with L-tear (B in Table 4.1). The first principal mode shape is analyzed to detect the damage. The iso-surface view of the detected L-tear damage on the membrane by simulation data is shown in Fig. 4.7. The iso-surface result detects the position (140,100) matching that of the damage scenario (Table 4.1).

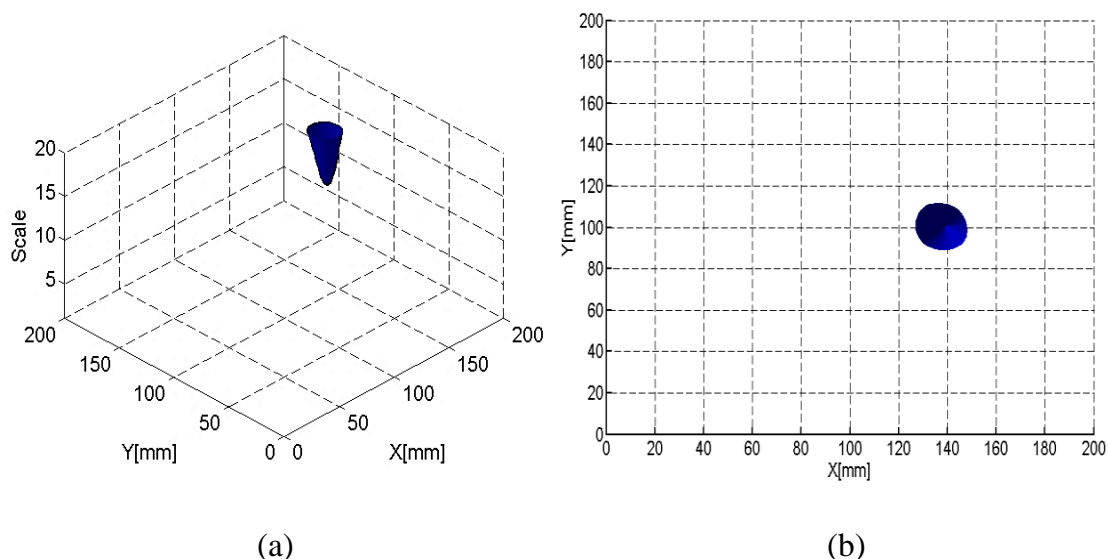


Fig. 4.7 Iso-surface view of the detected L-tear damage (B in Table 4.1) on the membrane by simulation data (a) 3-D view of iso-surface, (b) top view of iso-surface

For I-cut damage (C in Table 4.1), the first principal mode shape cannot be used to detect the damaged location because the change in membrane stiffness at the measurement point closest to this damage scenario is negligible, and consequently, the mode shape is similar to the normal condition. Simulation results of first principal mode shape for detecting the I-cut damage on the membrane is shown in Fig. 4.8. The results indicate that analyzing the first principal mode shape does not reveal anomalies (Fig. 4.8(a)), but transforming the mode shape using 2-D CWT reveals several peaks (Fig. 4.8(b)), suggesting that the membrane is affected even though a dominant peak is not present. Thus, the 2-D CWT is a powerful tool to detect a small anomaly, but higher order modes must be evaluated to fully understand the membrane condition.

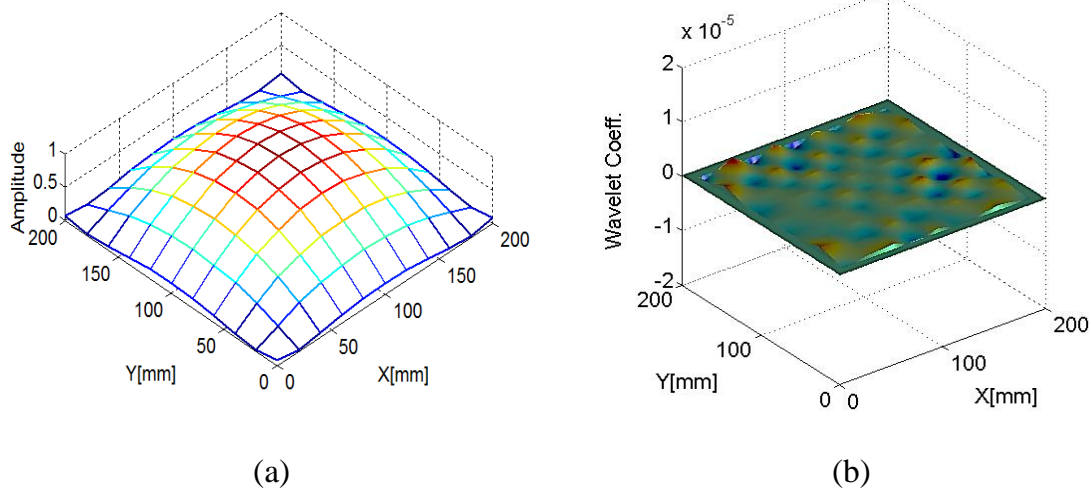


Fig. 4.8 Simulation results of first principal mode shape for detecting the I-cut damage (C in Table 4.1) on the membrane (a) first principal mode shape (41.79 Hz), (b) wavelet coefficient with boundary treatment

The higher order mode shapes can be used to determine the position of the damage, and Fan used the fifth principal mode shape to establish the damage position on a plate [41]. Investigating higher frequency mode shapes, it is found that there is a mode shape which shows the existence of the dominant peak at frequency of 851 Hz. The mode shape at this frequency can be used to establish the position of the damage on the membrane structure. Simulation results of higher order mode shape for detecting the I-cut damage (C in Table 4.1) on the membrane are presented in Fig. 4.9. The iso-surface views show the position of the damage of the I-cut damage corresponding to the damage scenario.

The simulation results indicate that if damage (cut, tear, hole, etc.) exists in the membrane structure, the stiffness of the membrane, especially at the point that is damaged, degrades. The lower stiffness causes a relatively higher vibration response, producing a peak where the damage is located in the vibration mode shape. If this mode shape is transformed by 2-D CWT, the peak is detected as a singularity, and the 2-D wavelet coefficients have high peaks at the singularity (damage) position. These results are consistent with the FEA predictions and the experiments on the membrane structure using laser excitation by LIB.

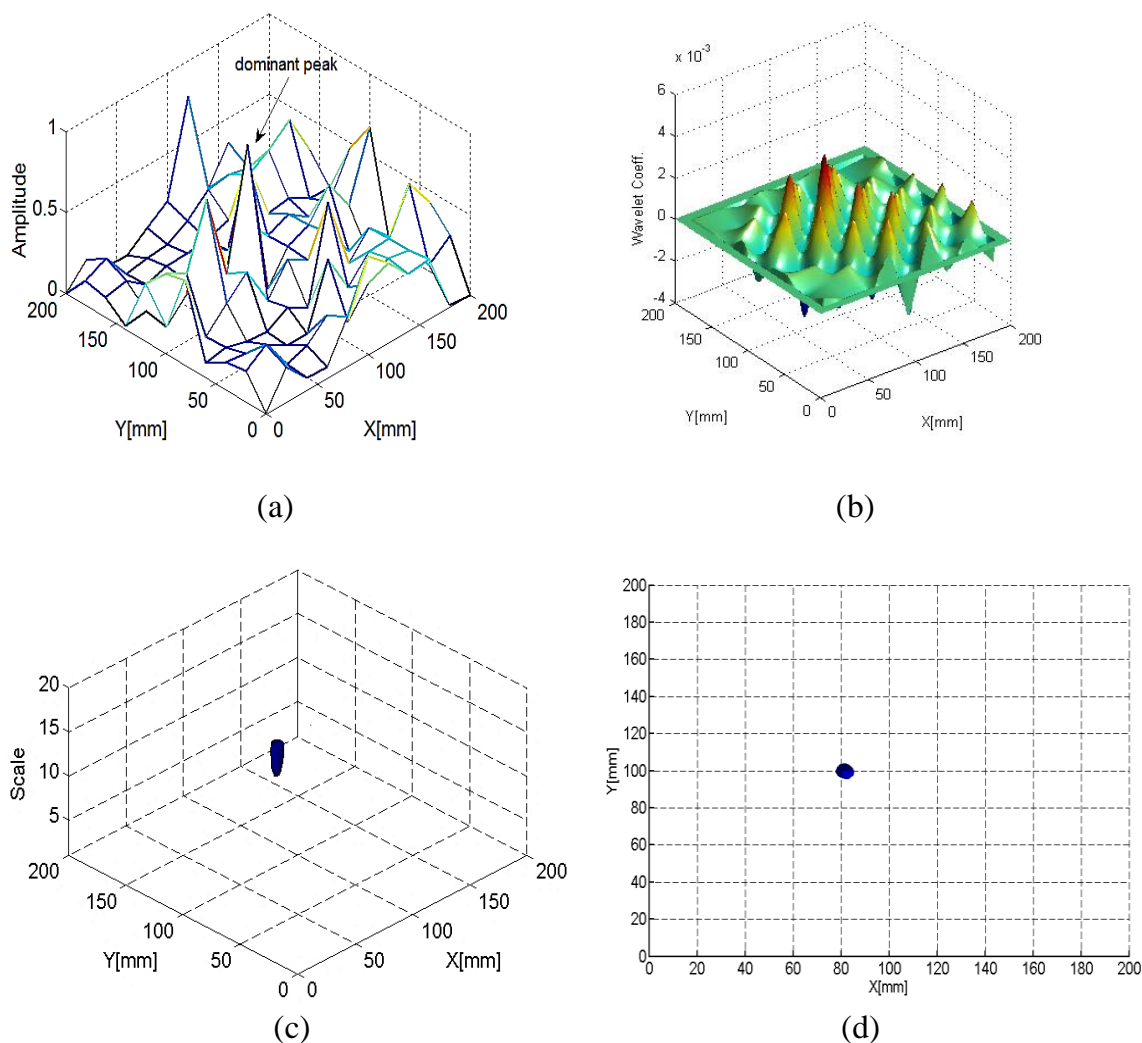


Fig. 4.9 Simulation results of higher order mode shape for detecting the I-cut damage (C in Table 4.1) on the membrane (a) mode shape (851 Hz), (b) wavelet coefficient with boundary treatment, (c) 3-D view of iso-surface, (d) top view of iso-surface

4.5 Damage detection in membrane structure by experiment

4.5.1 Damage detection for single damage on membrane

To verify the applicability of damage detection using laser excitation and wavelet transformation on a membrane by experiment, vibration testing on the membrane structure employed here using impulse excitation by LIB was conducted. The membrane structure was excited by acoustic excitation using the LIB, and the vibration responses were measured at the 11×11 points across the membrane. The

frequency responses at all points of measurements were processed to show the mode shapes of the membrane by using MATLAB[®]. An example of the frequency response of the membrane in the normal (undamaged) condition at the center point of the membrane is presented on Fig. 4.10.

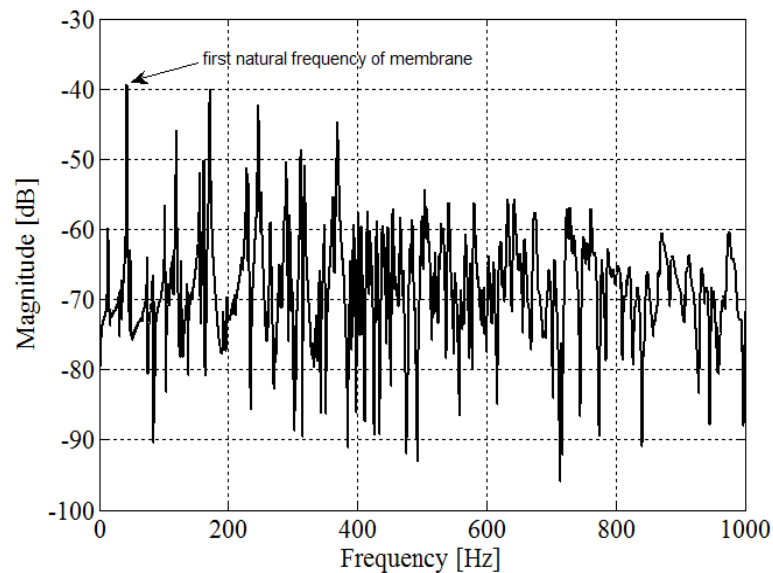


Fig. 4.10 Frequency response of the membrane in the normal condition at centre of membrane

As Fig. 4.10 shows, there are a large number of resonance peaks which explain the number of mode shapes of the membrane structure. The first natural frequency of the membrane is not the peak at the lowest frequency, but the peak with high amplitude response that is marked in Fig. 4.10. By further investigating the mode shapes of the membrane for these two peaks (the first and the marked peak), the first peak involves the deformation on tightening wires and clamps which means that it is not the proper membrane mode shape (rigid body of the membrane). The second peak as pointed in Fig. 4.10 does not reflect deformation of the wires and the clamps. The marked peak is the mode shape of the membrane alone, and will be used as the first principal mode shape of the membrane.

As the first step, the experiments are conducted by following the damage scenario (Table 4.1), single damage, as explained in section of 4.3. The experimental results for detecting the L-cut damage (A in Table 4.1) on the membrane are presented in Fig. 4.11.

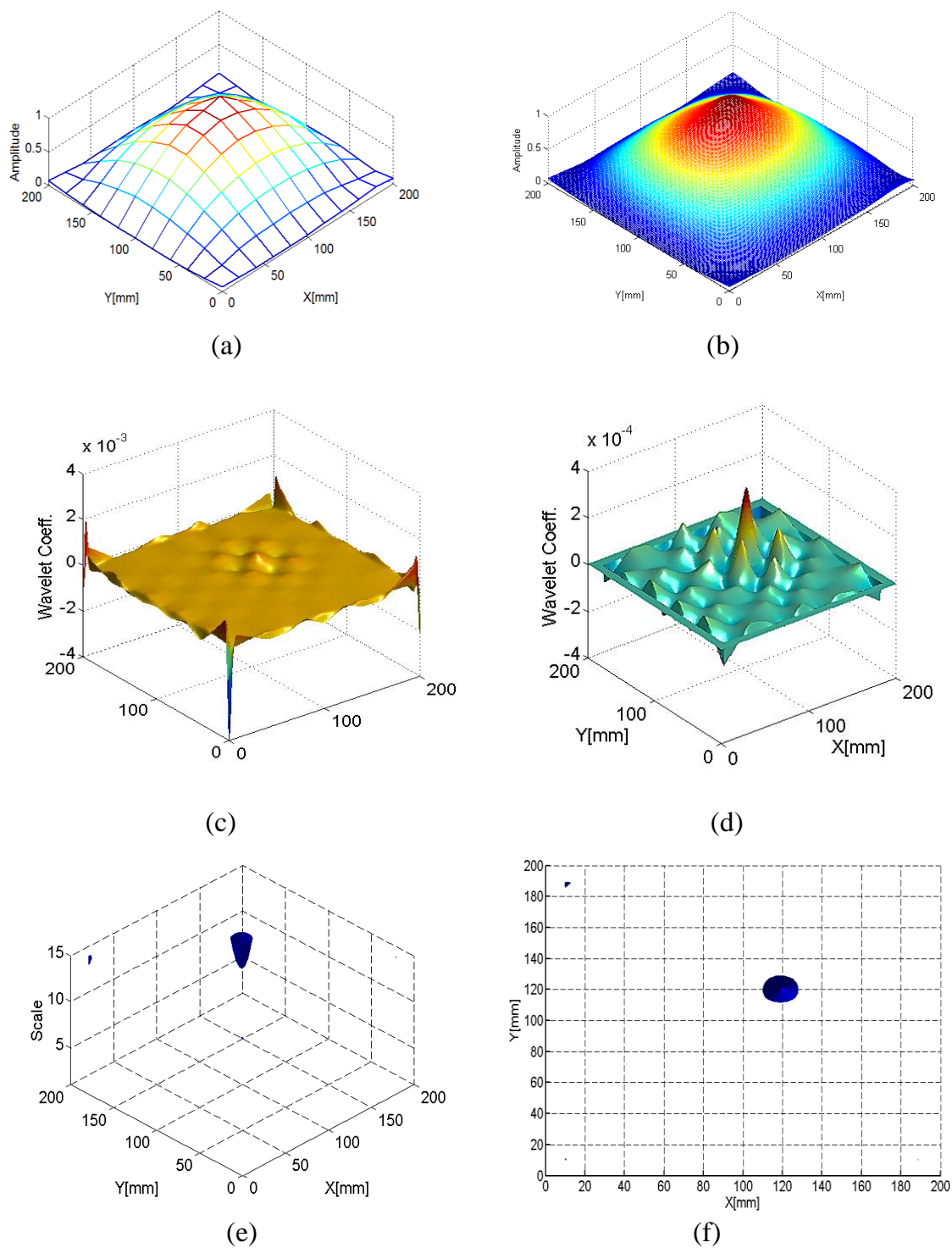


Fig. 4.11 Experimental results for detecting the L-cut damage (A in Table 4.1) on the membrane (a) first principal mode shape (40.63 Hz), (b) interpolated first principal mode shape, (c) wavelet coefficient, (d) wavelet coefficient with boundary treatment, (e) 3-D view of iso-surface, (f) top view of iso-surface

The procedure used for detecting the damage location using simulation data (detailed above) is implemented for the experimental data. Fig. 4.11 shows that the analysis employs the first principal mode shape of the membrane (Fig. 4.11(a)). To get more point of data, the mode shape is interpolated (Fig. 4.11(b)), which are then transformed by 2-D CWT to get wavelet coefficient (Fig. 4.11(c)), and wavelet coefficients are then treated by the boundary treatment to get clearer contour of the wavelet coefficient (Fig. 4.11(d)) on the membrane. The position of the L-cut damage can be seen on the iso-surface view in 3-D ((Fig. 4.11(e)) and top view (Fig. 4.11(f)). The L-cut damage location on the membrane can be accurately detected, with good agreement between the experiment and simulation results. The location of the L-cut damage is shown at the position of (120,120) in Fig. 4.11.

The L-tear damage (B in Table 4.1) determination also uses the first principal mode shape, the iso-surface view of the detected L-tear damage on the membrane by experimental data are presented in Fig. 4.12, which agrees with the simulation. Here, the noise additional to the point of the damage appearing as a small point (right panel in Fig. 4.12) can be ignored, because it is much smaller than the point at the damage position.

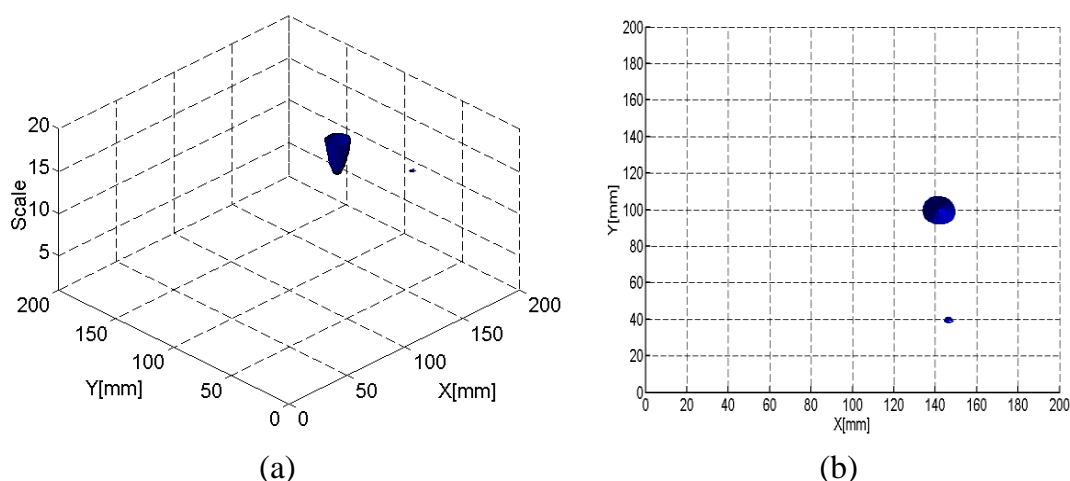


Fig. 4.12 Iso-surface view of the detected L-tear damage (B in Table 4.1) on the membrane by experimental data (a) 3-D view of iso-surface, (b) top view of iso-surface

The I-cut damage type (C in Table 4.1), can not be determined by only the analysis with the first principal mode shape. This condition requires the use of higher frequency mode shapes, and it was found that in the higher frequency modes the damaged part appears as a high amplitude in the mode shape. By determining the mode shape at higher frequency, the damage position can be established. To detect a case with I-cut damage, a higher order mode shape with high local amplitude appears at frequency of 843.8 Hz (similar to FEM simulation). The experimental results of higher order mode shape for detecting the I-cut damage (C in Table 4.1) on the membrane are presented in Fig. 4.13.

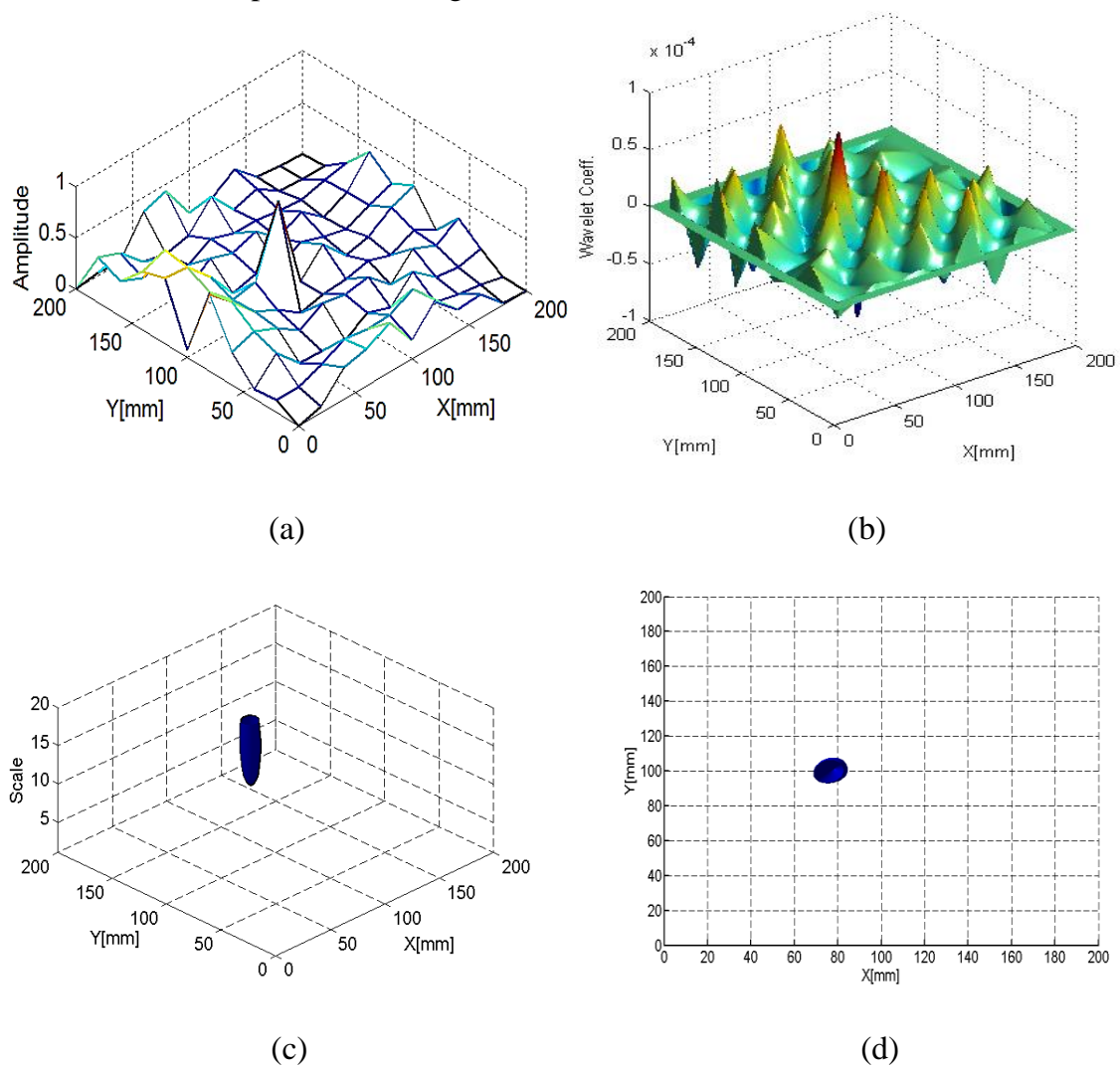


Fig. 4.13 Experimental results of higher order mode shape for detecting the I-cut damage (C in Table 4.1) on the membrane (a) mode shape (843.8 Hz), (b) wavelet coefficient with boundary treatment, (c) 3-D view of iso-surface, (d) top view of iso-surface

From Fig. 4.13, it can be seen that there is a dominant peak in the mode shape (Fig. 4.13(a)). This peak can also be seen clearly on the wavelet coefficient with boundary treatment by the scale $a = 2$ (Fig. 4.13(b)). Finally, on the iso-surface view (Fig. 4.13(c) and (d)), the exact position can be determined, and it corresponds to the damage scenario.

From the damage detection on the membrane structure involving the higher frequency mode shape, it can be assumed that using the higher frequency mode is effective to detect damage positions on the membrane structure. This allows the conclusion that using laser excitation to excite membrane structure in vibration testing is appropriate, because vibration testing using laser excitation provides the high frequency vibration data [6,13,14,17,44].

4.5.2 Damage detection for two damages on membrane

The damage detection method for membrane structures was also attempted with two places of damage on the membrane. Here, an I-cut and a square-hole were introduced in the membrane. The I-cut damage was $10 \text{ mm} \times 1.5 \text{ mm}$, and the square-hole was $10 \text{ mm} \times 10 \text{ mm}$. These positions of the damage on the membrane are shown in Fig. 4.14. These types of damages in these dimensions cannot be determined well using the first principal mode shape and the higher order mode approach will be used.

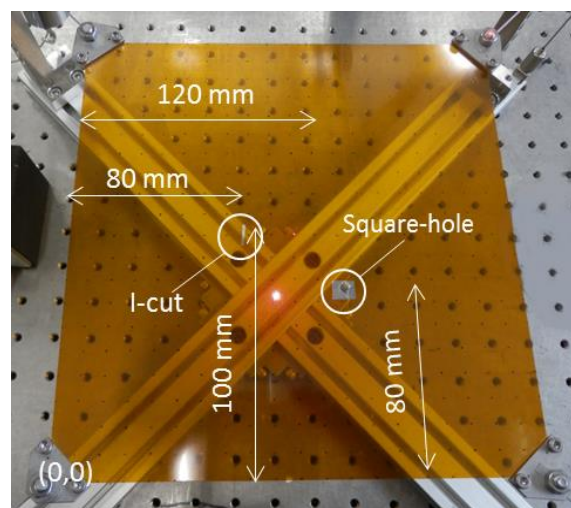


Fig. 4.14 Membrane with I-cut and square-hole damage

Vibration testing using laser excitation was performed on the membrane, and the mode shape containing dominant peaks caused by the two types of damage was found at the natural frequency of 799.1 Hz. The experimental results for detecting I-cut and square-hole damage on the membrane are presented in Fig. 4.15.

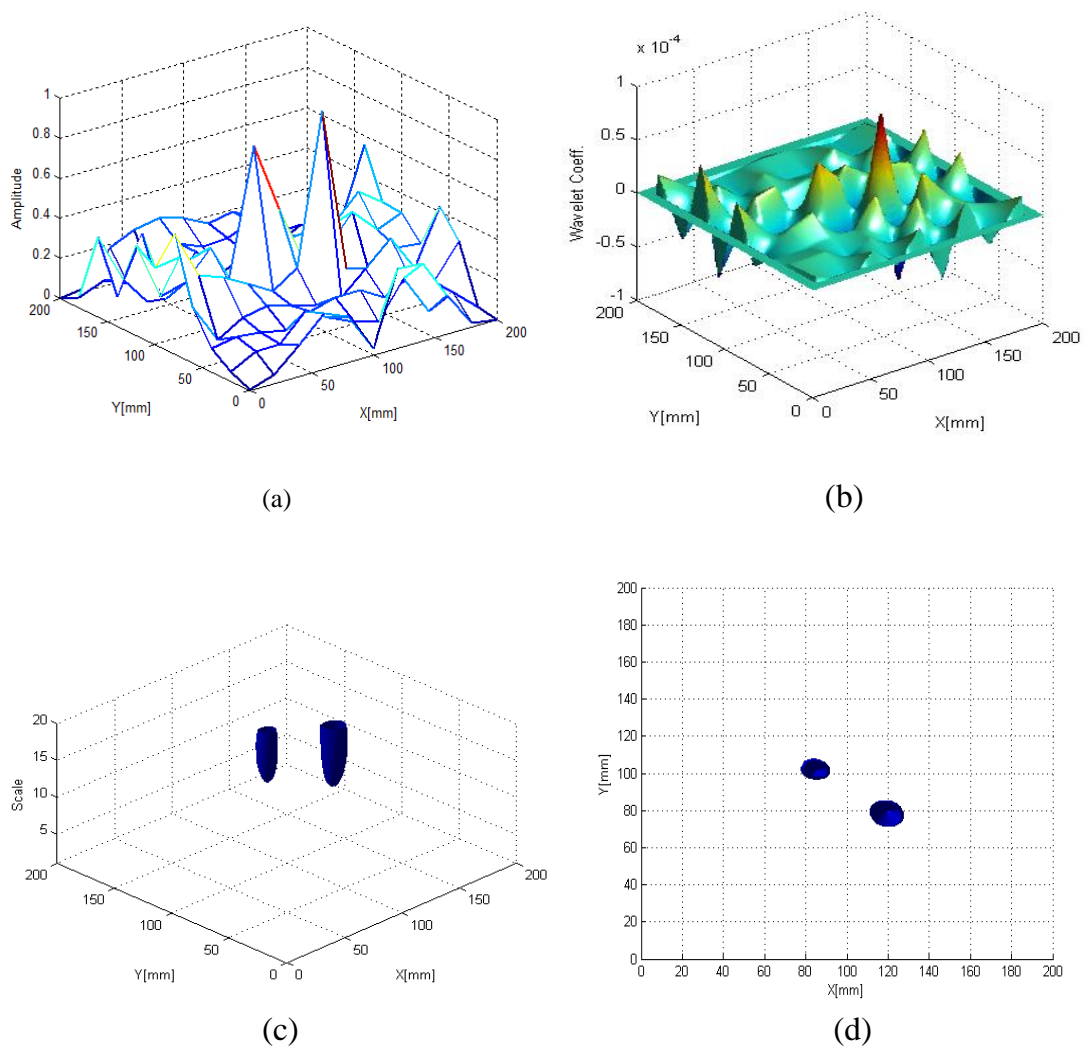


Fig. 4.15 Experimental results for detecting I-cut and square-hole damage on the membrane (a) mode shape (799.1 Hz), (b) wavelet coefficient with boundary treatment, (c) 3-D view of iso-surface, (d) top view of iso-surface

The mode shape at high frequency of 799.1 Hz shows two dominant peaks which may be predicted to be the position of damage (Fig. 4.15(a)). The wavelet coefficient with the boundary treatment (Fig. 4.15(b)) also shows the same situation with the

peaks. Finally, the iso-surface views (Fig. 4.15(c) and (d)) determine the two positions of damage which correspond to the positions of the induced damages.

When the mode shape change is evaluated by the frequency response of the membrane, it shows the corresponding resonance peak in the normal membrane condition. The frequency response without induced damage and condition with damage in two places (by the I-cut and square-hole, Fig. 4.14) is shown in Fig. 4.16. Here, the resonance peaks for the normal and damaged conditions show that the peak in the frequency response of the normal condition corresponds to a resonance peak used in damage detection. In the normal condition, the initial resonance peak is at 801.6 Hz, and after introducing the two points of damage to the membrane, the resonance peak has shifted to 799.1 Hz. The mode shape at this frequency is used for detecting the position of the two locations of damage. It is commonly observed in structures, that damage which removes some part of the mass of the structure also reduces the stiffness, and the stiffness reduction shifts the resonance peaks to the lower frequencies. To verify that these two resonance peaks correspond to each other, the mode shape of the two conditions were compared, and the plots are shown in Fig.4.17.

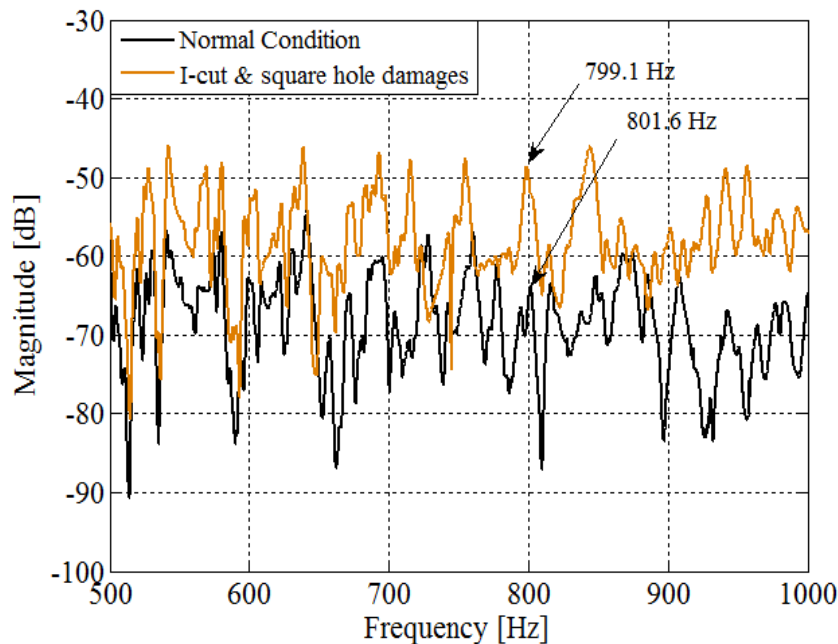


Fig. 4.16 Frequency response of membrane without induced damage and condition with damage in two places

Fig. 4.17 shows that the mode shape in the normal condition (Fig. 14.17(a)) has no dominant peak, but has contours which appear to have a similar appearance as those of the damaged membrane (Fig. 4.17(b)). The mode shape in the damaged condition has two dominant peaks, and these two dominant peaks were used to determine the damage positions.

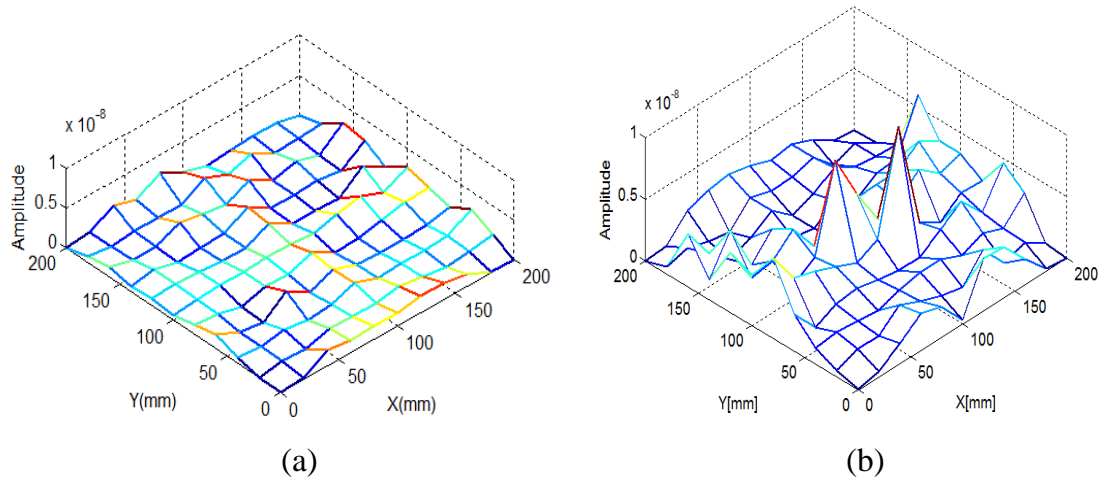


Fig. 4.17 Plots of the two mode shapes (a) mode shape w/o induced damage (801.6 Hz), (b) mode shape with damage in two places (799.1 Hz)

The above discussion demonstrates that unlike damage detection based on resonance peak shifting, which requires both comparison of the normal and current conditional data and complex analysis, 2-D CWT can easily detect the location of damage in the membrane structure using the mode shapes. 2-D CWT requires only data about the current membrane structure to estimate the damaged location.

4.6 Concluding remarks

In this dissertation, membrane structure damage determination by vibration testing using non-contact laser excitation and a finite element model of the membrane structure were proposed to investigate modelling and damage detection of membrane structures. In addition, a comparison between the simulations and the experimental results confirmed the effectiveness and usefulness of the measurement method and damage detection approach.

The use of the laser excitation vibration measurement arrangement for LIB in this dissertation enabled a high degree of measurement reproducibility, and experiments with very small extents of damage; offering the promise that the quality and reliability of membrane structure damage detection methodology can be improved with the proposed approach. Both the simulations and experimental results for the membrane structure damage detection showed that different types and positions of damage in the membrane can be effectively identified by using the 2-D CWT and the iso-surface concept, which requires only mode shapes of membrane in the application they are used. Vibration testing using acoustic excitation by LIB offers the possibility of detecting the position of damage in membrane structure using both low frequency data (first principal mode shape) and high frequency data (high order mode shape).

Chapter 5

Conclusions and Future Works

5.1 Conclusions

The concluding remarks about each chapter of this dissertation are summarized as follows;

In chapter 2, “Laser excitation”, two mechanism of high power laser effect that can be used as excitation to structure to generate vibration; laser ablation and laser-induced breakdown (LIB) were explained. Excitation by laser ablation to metal structure occurs when laser beam is focused and directed to metal and then absorbed by metal causes releasing the particle at a velocity from the metal which represents the laser-induced impulse that generates the vibration of structure. Excitation by LIB occurs when laser beam is focused, and plasma is then generated, and a portion of this plasma energy is transformed to a shock wave, which is the source of the sound generated by LIB, and it can be used as a source of acoustic excitation. In addition, these excitation methods have high reproducibility, can apply ideal impulse excitation to structure and have the big potency to be implemented to vibration testing without measuring the input, cause the easiness of combining them to structural health monitoring (SHM).

In chapter 3, “Bolt loosening analysis and diagnosis by non-contact laser excitation vibration test”, bolt loosening detection by vibration testing using non-contact laser

excitation and a finite element model of bolted joint undergoing loosening was explained in detail to investigate modelling and detecting bolt loosening on bolted structures. To model a structure with bolted joints in a loosening condition, changing the pretension force, and contact conditions between parts from the initial conditions are really significant. The frequency response analysis by pre-stressed modal analysis has shown that the proposed modelling method works well and the experimental results show good agreement with the simulation results. The use of the laser excitation vibration measurement arrangement in this research enabled a high degree of measurement reproducibility; offering the promise that the quality and reliability of the bolt loosening detection methodology can be improved. Finite element analysis validated vibration measurement by laser ablation and damage detection method, both the simulation and experimental results for the bolt loosening detection showed that various loosening states and their positions can be effectively identified by damage sensitivity feature, the Recognition-Taguchi method, as a frequency response based approach, which requires excitation at a point and measurements at several points close to the bolts.

In chapter 4, “Damage detection in membrane structures using non-contact laser excitation and wavelet transformation”, the finite element model of the membrane structure was elaborated to validate vibration measurement by laser excitation with LIB and damage detection approach to detect damages in membrane structures. The use of the laser excitation vibration measurement arrangement for LIB in this research enabled a high degree of measurement reproducibility, and experiments with small extents of damage; offering the promise that the quality and reliability of membrane structure damage detection methodology can be improved with the proposed approach. Both the simulations and experimental results for the membrane structure damage detection showed that different types and positions of damage in the membrane can be effectively identified by using the 2-D CWT and the iso-surface concept, which requires only mode shapes of membrane in the application they are used. Vibration testing using acoustic excitation by LIB offers the possibility of detecting the position of damage in membrane structure using both low frequency data (first principal mode shape) and high frequency data (high order mode shape).

5.2 Future works

As the continuation of this research, the following future work can be considered;

1. Two non-contact vibration excitation methods were explained and implemented to SHM in this dissertation. The other non-contact vibration method based on high power laser effects is really possible to be discovered and then implemented in damage identification.
2. The contact between flange in bolted joint and behavior of membrane are non-linear. The model of bolted joint and membrane structure are possible to be more optimized by considering non-linear analysis in modelling the structures.
3. The other types of damage in mechanical structures are really possible to be detected using proposed methods in this dissertation.

List of Publications

Journal papers

1. Feblil Huda, Itsuro Kajiwara, Naoki Hosoya and Shozo Kawamura, "Bolt loosening analysis and diagnosis by non-contact laser excitation vibration tests", *Mechanical System and Signal Processing*, Vol.40, pp.589-604, 2013.
2. Feblil Huda, Itsuro Kajiwara and Naoki Hosoya, "Damage detection in membrane structures using non-contact laser excitation and wavelet transformation", *Journal of Sound and Vibrations*, Vol. 333, pp.3609-3624, 2014.

Conference proceedings

1. Feblil Huda, Itsuro Kajiwara, Naoki Hosoya and Shozo Kawamura, "Bolted joint loosening detection by using laser excitation", *Proceedings of SPIE Smart Structures/NDE 2013*, CD-ROM (No. 8695-109), 2013.
2. Feblil Huda and Itsuro Kajiwara, "Bolted joint health monitoring using non-contact laser excitation", *Proceedings of The second International workshop on intelligent convergence 2013*, page 124, 2013.
3. Jun Shinzato, Itsuro Kajiwara, Naoki Hosoya and Feblil Huda, "Health monitoring of membrane structures using non-contact laser excitation", *Proceedings on JSME Dynamics and Design Conference 2013*, Paper No. 530, 2013.
4. Yoshiaki Ito, Feblil Huda, Itsuro Kajiwara and Naoki Hosoya, "Detective method of the loosening bolt based on the vibration measurement using laser excitation", *JSME Symposium on Evaluation and Diagnosis 2013*, No.13-24, pp. 125-129, 2013.
5. Feblil Huda, Itsuro Kajiwara and Naoki Hosoya, "Vibration test and health monitoring of membrane structure using non-contact laser excitation", *Proceedings of SPIE Smart Structures/NDE 2014*, 90640U, 2014.

Bibliography

- [1] A. Deraemaeker, K. Worden, *New trends in vibration based structural health monitoring*, Springer Wien New York, Italy, 2010.
- [2] V. Giurgiutiu, A. Zagrai, and J. Bao, "Damage identification in aging aircraft structures with piezoelectric wafer active sensors." *Journal of Intelligent Material Systems and Structures*, 15, 673-687, 2004.
- [3] W. J. Staszewski, B. C. Lee and R. Traynor, "Fatigue crack detection in metallic structures with Lamb waves and 3D laser vibrometry." *Measurement Science & Technology*, 18(3), 727-739, 2007.
- [4] E. B. Shell, R. G. Buchheit and B. Zoofan, "Correlation of residual fatigue life with quantified NDE measurements," *International Journal of Fatigue*, 27(2), 105-112, 2005.
- [5] J. M. Papazian, J. Nardiello, R. P. Silberstein, G. Welsh, D. Grundy, C. Craven, L. Evans, N. Goldfine, J.E. Michaels, T.E. Michaels, Y.F. Li, and C. Laird, "Sensors for monitoring early stage fatigue cracking," *Elsevier Sci. Ltd*, 1668-1680, 2007.
- [6] H. Xue, D. Wagner, N. Ranc and E. Bayraktar, "Thermographic analysis in ultrasonic fatigue tests," *Fatigue & Fracture of Engineering Materials & Structures*, 29(7), 573-580, 2006.
- [7] B. Yang, "Thermographic detection of fatigue damage of reactor pressure vessel steels," *Journal of Materials Engineering and Performance*, 12(3), 345-353, 2003.
- [8] D. Shang, M.E. Barkey, Y. Wang, T.C. Lim, "Fatigue damage and dynamic natural frequency response of spot-welded joints," *Proceedings of 2003 SAE World Congress*, No. 2003-01-0695, 2003.
- [9] PCB International Corp., *Electric Impact Hammer Operating Guide*, Model 086 C.
- [10] M. Iwahara, et al., "Improvement of accuracy and reliability of experimental modal analysis (invention on impact testing and decrease of measurement error)," *Transactions of the Japan Society of Mechanical Engineers Series C*, 64 (618), 538-545, 1998.
- [11] L.L. Koss, R.C. Tobin, "Laser induced structural vibration," *Journal of Sound and Vibration*, 86 (1), 1-7, 1983.
- [12] W.R. Philp, et al., "Single pulse laser excitation of structural vibration using power densities below the surface ablation threshold," *Journal of Sound and Vibration*, 185 (4), 643-654, 1995.

- [13] I. Kajiwara, D. Miyamoto, N. Hosoya, C. Nishidome, Structural health monitoring by high frequency vibration measurement with non-contact laser excitation, *Proceedings of SPIE Smart Structures/NDE 2011*, No. 7984-54, 2011.
- [14] I. Kajiwara, and N. Hosoya, Vibration testing based on impulse response excited by laser ablation, *Journal of Sound and Vibration*, 330, 5045 – 5057, 2011.
- [15] The institute of Electrical Engineers of Japan (Ed.), *Laser ablation and applications*, corona publishing Co., Ltd, 1999.
- [16] J.F. Ready, *Effects of high-power laser radiation*, Academic Press Inc., New York, 1971.
- [17] N. Hosoya, M. Nagata, I. Kajiwara, Acoustic testing in a very small space based on a point sound source generated by laser-induced breakdown: stabilization of plasma formation, *Journal of Sound and Vibration*, 332, 4572 – 4583, 2013.
- [18] N. Hosoya, I. Kajiwara, T. Hosokawa, Vibration testing based on impulse response excited by pulsed-laser ablation: measurement of frequency response function with detection-free input, *Journal of Sound and Vibration*, 331, 1355-1365, 2012.
- [19] Q. Qin , K. Attenborough, Characteristics and application of laser-generated acoustic shock waves in air, *Applied Acoustics*, 65, 325-340, 2004.
- [20] M. Oksanen, J Hietanen, Photo acoustic breakdown sound source in air, *Journal of Ultrasonics*, 32, 327-333, 1994.
- [21] V.B. Georgiev, V.V. Krylov, Q. Qin, K. Attenborough, Generation of flexural waves in plates by laser-initiated air borne shock waves, *Journal of Sound and Vibration*, 330, 217-228, 2011.
- [22] S. Nemoto, *Laser Engineering*, Baifukan Co. Ltd., 2001.
- [23] D.M. Peairs, G. Park, D.J. Inman, Practical issues of activating self-repairing bolted joints, *Smart Material and Structure*, 13, 1414-1423, 2004.
- [24] T. Yokoyama, M. Olsson, S. Izumi, S. Sakai, Investigation into the self-loosening behavior of bolted joint subjected to rotational loading, *Engineering Failure Analysis*, 23, 35-43, 2012.
- [25] J. Kim, C. J. Yoon, S. B. Kang, Finite element analysis and modeling of structure with bolted joints, *Applied Mathematical Modeling*, 31, 895-911, (2007).
- [26] H. Ahmadian, H. Jalali, Generic element formulation for modeling bolted lap joints, *Mechanical Systems and Signal Processing*, 21, 2318-2334, 2007.
- [27] S. Bograd, P. Reuss, A. Schmidt, L. Gaul, M. Mayer, Modeling the dynamics of mechanical joints, *Mechanical Systems and Signal Processing*, 25, 2801-2826, 2011.

- [28] C.R. Farrar, K. Worden, An introduction to structural health monitoring, *Philos. Trans. R. Soc., A* 365, 303-315, 2007.
- [29] D.M. Peairs, G. Park, D.J. Inman, Improving accessibility of the impedance-based structural health monitoring method, *Intelligent Material System and Structure*, 15, 129-139, 2004.
- [30] S. Ritdumrongkul, M. Abe, Y. Fujino, T. Miyashita, Quantitative health monitoring of bolted joints using a piezoceramic actuator sensor, *Smart Material and Structure*, 13, 20-29, 2004.
- [31] I. Argatov, I. Sevostianov, Health monitoring of bolted joints via electrical conductivity measurements, *International Journal of Engineering Science*, 48, 874 – 887, 2010.
- [32] M.D. Todd, J.M. Nichols, C.J. Nichols, L.N. Virgin, An assessment of modal property effectiveness in detecting bolted joint degradation: theory and experiment, *Journal of Sound and Vibration*, 275, 1113 – 1126, 2004.
- [33] J. E. Shigley, *Mechanical Engineering Design Eight Edition*, McGraw-Hill, 2006.
- [34] S. Kawamura, Y. Nagao, R. Katae, H. Minamoto, Construction of finite element model of a bolt jointed structure with high accuracy, *Proceedings of Dynamics and Design Conference 2011*, No. 409, 2011.
- [35] G. Taguchi, S. Chowdhury, and Y. Wu, *The Mahalanobis-Taguchi system*, McGraw-Hill, 2001.
- [36] C.H. Jenkins, Membrane vibration experiments: An historical review and recent results, *Journal of Sound and Vibration*, 295, 602-613, 2006.
- [37] V.A. Chobotov, R.C. Binder, Nonlinear response of a circular membrane to sinusoidal acoustic excitation, *Journal of Acoustical Society of America*, 36, 59-73, 1964.
- [38] C.H. Jenkins, Membrane vibrations: a review and new experimental results, in: *ASME Joint Applied Mechanics and Materials Summer Conference*, Blacksburg, VA, 1999.
- [39] C.H. Jenkins, M. Tampi, Local membrane vibrations and inflatable space structures, in: S.W. Johnson, K.M. Chua, R.G. Galloway, P.I. Richler (Eds.), *Space 2000*, Albuquerque, NM, 2000.
- [40] I. Kajiwara, K. Obara, Laser excitation vibration test for membrane structures in vacuum environment, *The Sixth Japan-Taiwan Workshop on Mechanical and Aerospace Engineering*, Sapporo, Hokkaido, Japan, 2011.
- [41] W. Fan, P. Qiao, A 2-D continuous wavelet transform of mode shape data for damage detection of plate structures, *International Journal of Solids and Structures*, 46, 4379-4395, 2009.
- [42] J.P. Antoine, R. Murenzi, P. Vandergheynst, *Two-dimensional wavelets and their relatives*, Cambridge University Press, Cambridge, 2004.

- [43] L. Jacques, A. Coron, P. Vandergheynst, A. Rivoldini, The YAWTb Toolbox: Yet another Wavelet Toolbox, web page: (<http://sites.uclouvain.be/ispgroup/yawtb>).
- [44] F. Huda, I. Kajiwara, N. Hosoya, S. Kawamura, Bolt loosening analysis and diagnosis by non-contact laser excitation vibration tests, *Journal of Mechanical Systems and Signal Processing*, 40, 589-604, 2013.

Appendix

Several Wavelet Transformations for Damage Detection in Membrane Structures

If there is a 2-D image/signal of $s(\vec{x}) \in L^2(\mathbb{R}^2, d^2\vec{x})$, its two dimensional continuous wavelet transformation (2-D CWT) with respect to the wavelet ψ , $S(\vec{b}, a, \theta) \equiv T_\psi s$ is the scalar product of s with the transformed wavelet $\psi_{\vec{b}, a, \theta}$ and considered as a function of (\vec{b}, a, θ) as:

$$\begin{aligned} S(\vec{b}, a, \theta) &\equiv \langle \psi_{\vec{b}, a, \theta}, s \rangle = a^{-1} \int_{\mathbb{R}^2} \overline{\psi(a^{-1}r_{-\theta}(\vec{x} - \vec{b}))} s(\vec{x}) d^2\vec{x} \\ &= a \int_{\mathbb{R}^2} \widehat{\psi}(ar_{-\theta}(\vec{k})) e^{-i\vec{b} \cdot \vec{k}} \widehat{s}(\vec{k}) d^2\vec{k} \end{aligned} \quad (\text{A.1})$$

where,

$$\begin{aligned} S(\vec{b}, a, \theta) &= \text{wavelet coefficient of transformed signal} \\ \psi_{\vec{b}, a, \theta} &= \text{wavelet function} \\ \widehat{\psi} &= \text{Fourier transform of wavelet function} \\ \vec{b} &= \text{translation vector} \\ a &= \text{scaling factor} \\ \theta &= \text{rotation angle} \\ \vec{k} &= \text{Fourier transformation function} \\ r_{-\theta} &= \text{rotation matrix.} \end{aligned}$$

To choose an analyzing wavelet ψ , there are two possibilities, depending on whether one is interested or not in detecting oriented features in an image, i.e., regions where the amplitude is regular along one direction and has a sharp variation along the perpendicular direction. There are two classifications of wavelet ;

a. *Isotropic wavelets*

If a point-wise analysis needs to be performed, i.e., when no oriented features are present or relevant in the signal, one may choose an analyzing wavelet ψ which is invariant under rotation. Then the θ dependence drops out. Some familiar examples

of isotropic wavelets are; Mexican hat, Pet hat, different of Gaussian, and derivative of Gaussian wavelets.

b. *Anisotropic wavelets*

When the aim is to detect oriented features in an image (for instance, in the classical problem of edge detection or in directional filtering), one has to use a wavelet which is *not* rotation invariant. The best angular selectivity will be obtained if ψ is *directional*, which means that the (essential) support of $\hat{\psi}$ in spatial frequency space is contained in a convex cone with apex at the origin (by which we mean that the wavelet is numerically negligible outside the cone).

In this dissertation, an isotropic wavelet will be appropriate, because membrane structure damage effects on mode shape have no specific orientation, and finding singularity in membrane seems like finding some peaks without orientation. To select an appropriate mother wavelet, some isotropic mother wavelets are examined in finding the singularity in membrane structure. Some of the isotropic 2-D CWT wavelets with their functions are expressed as following:

1. Mexican hat:

The Mexican hat wavelet is expressed by the following function:

$$\psi(\vec{x}) = (2 - |\vec{x}|^2) \exp\left(-\frac{1}{2}|\vec{x}|^2\right) \quad (\text{A.2})$$

and in the form of Fourier function:

$$\hat{\psi}(\vec{k}) = |\vec{k}|^2 \exp\left(-\frac{1}{2}|\vec{k}|^2\right) \quad (\text{A.3})$$

2. Pet hat

The Pet hat wavelet is expressed by the following Fourier function:

$$\begin{aligned} \hat{\psi}(\vec{k}) &= \cos^2\left(\frac{\pi}{2} \log_2 \frac{|\vec{k}|}{\pi}\right) |\vec{k}|^2, \text{ for } \pi < |\vec{k}| < 4\pi \\ &= 0, \text{ for } |\vec{k}| < \pi \text{ and } |\vec{k}| > 4\pi \end{aligned} \quad (\text{A.4})$$

3. Different of Gaussian (DOG)

The DOG wavelet is expressed by the following function:

$$\psi(\vec{x}) = \frac{1}{2\alpha^2} \exp\left(-\frac{1}{2\alpha^2}|\vec{x}|^2\right) - \exp\left(-\frac{1}{2}|\vec{x}|^2\right) \quad (0 < \alpha < 1) \quad (\text{A.5})$$

4. Derivative of Gaussian (DerGauss)

To explain DerGauss wavelet, because it involves convolution operator, this wavelet needs to be explained by complete equation to determine wavelet coefficient:

$$S(\vec{b}, a, \theta) \equiv (\psi_{a,\theta} * s)(\vec{b}) = \left(\left(\frac{\partial}{\partial x} \right)^m \left(\frac{\partial}{\partial y} \right)^n g_{a,\theta} * s \right)(\vec{b}) \quad (\text{A.6})$$

and the 2-D Gaussian is defined as:

$$g(x, y) = \exp\left(-\frac{|\vec{x}|^2}{2\sigma^2}\right) = \exp\left(-\frac{x^2+y^2}{2\sigma^2}\right), \vec{x} = (x, y) \quad (\text{A.7})$$

In order to determine the ability of each wavelet function to recognize damage in membrane structure, the first principal mode shape of a damaged membrane structure that gotten from experiment by laser-induced breakdown is employed. The damaged membrane with L-cut damage position is presented in Fig. A.1, and the first principal mode shape is shown in Fig. A.2.

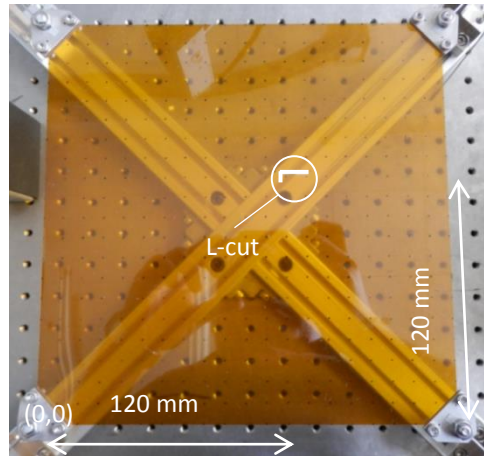


Fig. A.1 Membrane structure L-cut damage

In Fig. A.1 can be seen that the position of L-cut damage on coordinate of (120,120). To get the mode shape of membrane, laser excitation by LIB is used to generate vibration on membrane, and vibration responses are measured on 121 of measurement points on membrane. To get more points on membrane mode shape, interpolation is applied. The basic mode shape and interpolated mode shape are presented in Fig A.2(a) and Fig. A.2(b) respectively.

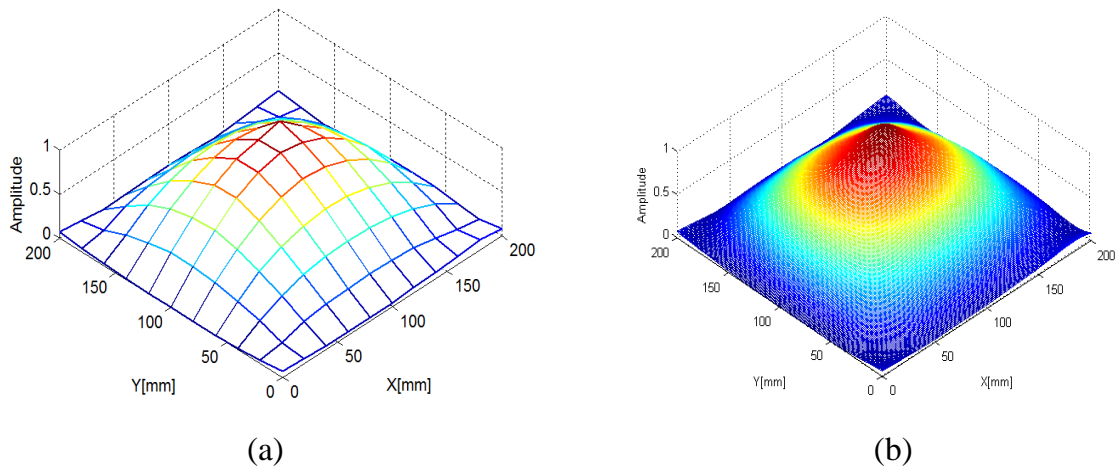


Fig. A.2 First principal mode shape of membrane (a) basic mode shape,
(b) interpolated mode shape

To detect the position of damage, the mode shape is transformed by 2D continuous wavelet transformation (2-D CWT). The wavelet coefficients with several chosen scales got from transformation by 2-D CWT of Mexican hat, Pet hat, DOG, and DerGauss mother wavelets are presented in Fig. A.3 to Fig. A.6 respectively.

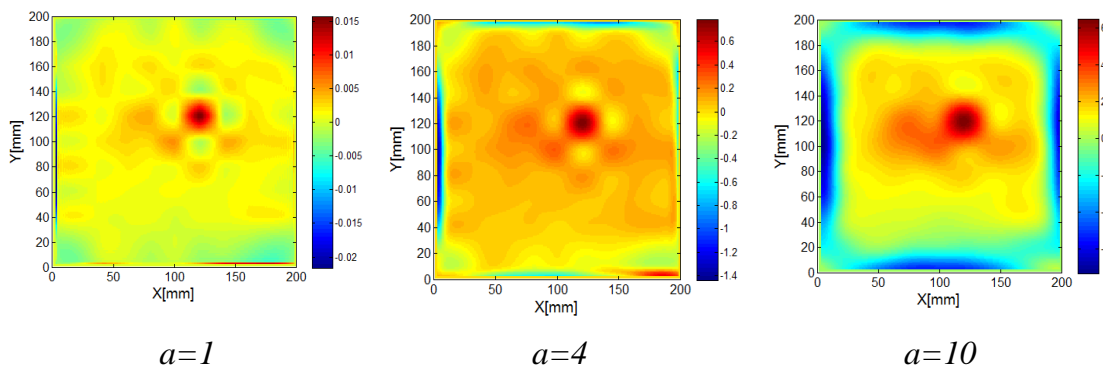


Fig. A.3 Wavelet coefficient by Mexican hat

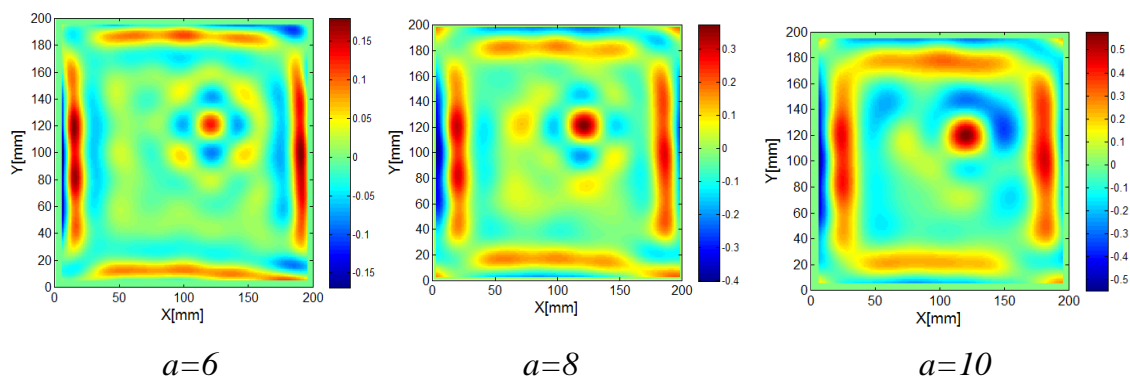


Fig. A.4 Wavelet coefficient by Pet hat

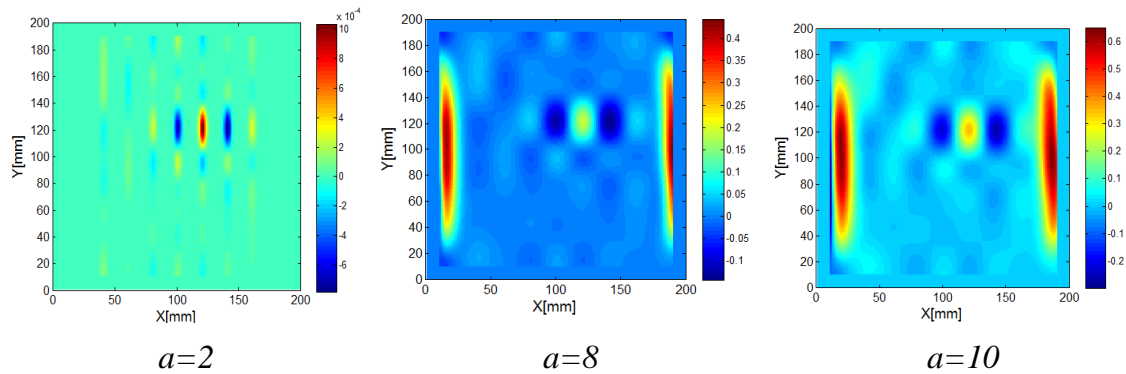


Fig. A.5 Wavelet coefficient by DOG

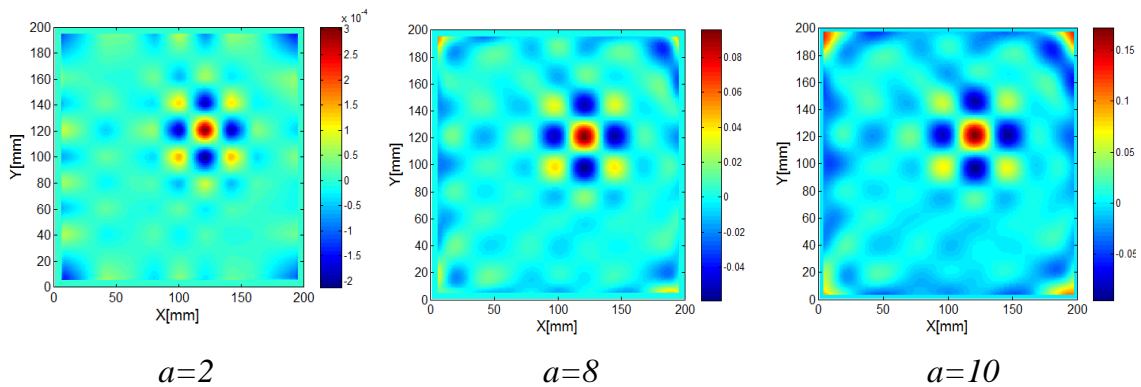


Fig. A.6 Wavelet coefficient by Dergauss

The chosen scales are varying to show the clearer result for detecting the damage. Generally, it can be seen in Fig. A.3 to Fig. A.6 that all of mentioned mother wavelet can detect the position of damage, but Pet hat and DOG wavelet (Fig A.4 and Fig. A.5) show the distortion in some areas with peak values close to damage peak (red contour). This distortion is raise up by the increasing of scale. This condition could overwhelm the damage peak in advance analysis. Wavelet coefficients do not show the consistency of clear view of damage position. Wavelet coefficient by Mexican hat wavelet show a little bit clearer view contour (Fig. A.3), but the red contour around damage position becomes closer to damage position by the increasing of scale. The blue contour on the edge is also become larger as the increasing of scale. This condition could give bad effect in advance analysis.

Wavelet coefficient by DerGauss wavelet show the consistency of damage position (Fig. A.6), where the red contour as the highest coefficients values is only exist on

damage position. There is no enlargement of red contour in other area of membrane except on the corners. The red contours on the corners appear as the clear effect of membrane clamps on the corners. Even though blue contour is scattered, but this condition still show the consistency of wavelet coefficient in different scale values. So, 2-D DerGauss wavelet would be used to transform the mode shape of membrane and to detect damage location.

To get clearer position of damage in membrane, an advance process is employed by generating the iso-surface graph. Wavelet coefficients by several scales are managed, and the points with the threshold values are connected to form an “iso-surface” connecting points of equal elevation with contour lines. Fig. A.7 shows L-cut damage detection by DerGauss wavelet, where the position of L-cut damage can be detected well. Author try to employ this method to detect the shape of damage, but in this L-cut damage the displacement of a point on the corner of the damage is really high compare with the other along the damage, so this dominant peak could overwhelm the other peak, so that one point appears as a dominant peak which can be seen in Fig. A.7.

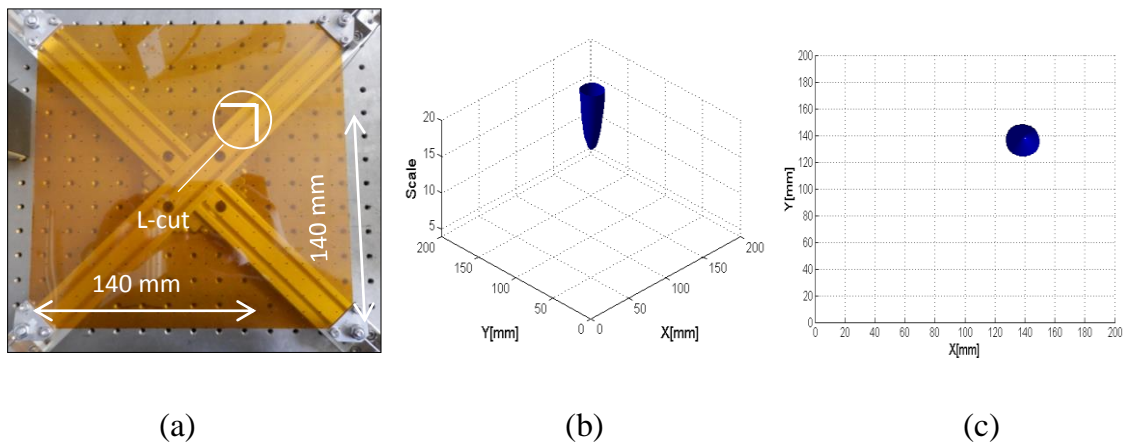
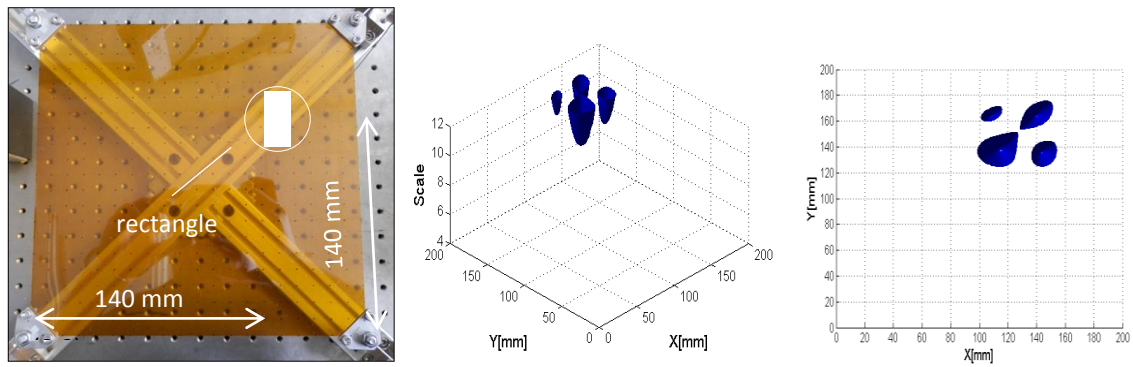


Fig. A.7 L-cut damage detection by DerGauss wavelet (a) damage position, (b) 3-D iso-surface view, (c) 2-D iso-surface view

The other type damage is also induced to membrane to check the ability of proposed method. The process to detect rectangular damage is presented in Fig. A.8. It can be seen that the damage shape is almost determined by iso-surface, but it still does not reflect the real shape of damage, but it shows the tendency to be similar shape. This

condition caused by the density of measurement data on damage is still not so good. More measurement points on membrane will be better to show the shape of damage.



(a)

(b)

(c)

Fig. A.8 Rectangle damage detection by DerGauss wavelet (a) damage position, (b) 3-D iso-surface view, (c) 2-D iso-surface view